



**HAL**  
open science

## Enabling future nanomanufacturing through block copolymer self-assembly: A review

Cian Cummins, Ross Lundy, James Walsh, Virginie Ponsinet, Guillaume Fleury, Michael Morris

### ► To cite this version:

Cian Cummins, Ross Lundy, James Walsh, Virginie Ponsinet, Guillaume Fleury, et al.. Enabling future nanomanufacturing through block copolymer self-assembly: A review. *Nano Today*, 2020, 35, pp.100936. 10.1016/j.nantod.2020.100936 . hal-02924083

**HAL Id: hal-02924083**

**<https://hal.science/hal-02924083v1>**

Submitted on 22 Aug 2022

**HAL** is a multi-disciplinary open access archive for the deposit and dissemination of scientific research documents, whether they are published or not. The documents may come from teaching and research institutions in France or abroad, or from public or private research centers.

L'archive ouverte pluridisciplinaire **HAL**, est destinée au dépôt et à la diffusion de documents scientifiques de niveau recherche, publiés ou non, émanant des établissements d'enseignement et de recherche français ou étrangers, des laboratoires publics ou privés.



Distributed under a Creative Commons Attribution - NonCommercial 4.0 International License

## Enabling future nanomanufacturing through block copolymer self-assembly: A review

Cian Cummins,<sup>1,2\*</sup> Ross Lundy,<sup>3</sup> James J. Walsh,<sup>4,5</sup> Virginie Ponsinet,<sup>2</sup> Guillaume Fleury,<sup>1,2</sup> Michael A. Morris<sup>3\*</sup>.

1. Laboratoire de Chimie des Polymères Organiques (LCPO), CNRS UMR 5629, ENSCPB, Université de Bordeaux, 16 Avenue Pey-Berland, F-33607 Pessac Cedex, France.

2. Université de Bordeaux, CNRS, Centre de Recherche Paul Pascal (CRPP), UMR 5031, 33600, Pessac, France.

3. AMBER Research Centre and School of Chemistry, Trinity College Dublin, Dublin, Ireland

4. School of Chemical Sciences, Dublin City University, Glasnevin, Dublin 9, Ireland.

5. National Centre for Sensor Research, Dublin City University, Glasnevin, Dublin 9, Ireland.

\* C.C: [cian.a.cummins@gmail.com](mailto:cian.a.cummins@gmail.com)

\* M.A.M: [morrism2@tcd.ie](mailto:morrism2@tcd.ie)

### Abstract:

Self-assembly approaches, *e.g.* colloidal, emulsion and polymer phase separation, provide scientists with an exotic yet direct platform to access technologically desired nanostructures at competitive costs. In particular, soft nanomaterial systems such as block copolymer (BCP) materials present a powerful means to tailor templates and spatially controlled systems that are amenable to large scale manufacturing practices. BCP nanoarchitectures in bulk, solution and thin film form can act as structural motifs to template foreign materials and pave the way towards important applications across industry and society. While extensive literature and research efforts exist on electronic device uses using BCPs, we look at nascent applications outside the integrated circuit realm. Recent reports are discussed including for example; light-harvesting (energy – section 2), metasurfaces (photonics – section 3), nanofiltration membranes (environmental – section 4) and antibacterial activity (biological – section 5). We endeavour to illustrate the window of opportunity presented through BCP self-assembly for nanomanufacturing. We believe the highlights discussed will aid in directing new research initiatives and facilitate the large-scale integration of BCP materials with broad societal impact.

## Contents

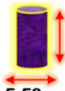






Introduction.....	3
BCP thin film self-assembly .....	5
BCP solution self-assembly .....	7
Review Outline .....	9
Energy.....	10
Background .....	10
Photocatalysis .....	11
Electrocatalysis .....	16
Summary .....	20
Photonics.....	20
Background .....	20
Photonic crystals and metamaterials .....	21
Metasurfaces .....	28
Summary .....	32
Environmental .....	33
Background .....	33
Surfactant separation .....	33
BCP rigid membranes .....	35
Summary .....	43
Biological.....	44
Background .....	44
Biorelated solution based BCPs .....	45
Biorelated BCP thin film features .....	48
Summary .....	53
Conclusions.....	53
Perspective .....	55
Acknowledgements.....	58
References.....	58

## 1. Introduction

Bottom-up fabrication methods are becoming indispensable for progressing nanomanufacturing. The concept of nanomanufacturing relies on innovative approaches to fabricate functional devices that are both societally and economically attractive, *i.e.* low-cost consumer devices that are power efficient while accommodating extra functionality. The progression of nanomanufacturing to produce useful everyday devices relies on our understanding of fabrication strategies at the nanoscale. Although silicon manufacturing for semiconductor processing is traditionally at the forefront of nanomanufacturing discussion, this article addresses other emerging areas where nanostructured and nanopatterned surfaces can be exploited for novel applications as *e.g.* nanostructured biocompatible devices for health monitoring, nanotextured surfaces as displays, nanoporous membranes for ultra-filtration and nanosensors for environmental analysis. Determining factors of nanomanufacturing nanomaterials, nanostructures, and nanodevices centre on cost, throughput and time-to-market as described in a recent perspective by Liddle and Gallatin.[1] Possible avenues to fabricate nanostructures are now plentiful, *e.g.* laser direct writing, interference lithography, scanning probe lithography, e-beam lithography, nanoimprint lithography,[2] however, only a few methods offer a true means to develop nanofeatures in a low-cost, timely, and large-scale way.

Block copolymer (BCP) patterning may be the best example of an approach that satisfies the criteria above in relation to nanomanufacturing (see table 1 below). In this regard, the large-scale manufacturing of nanomaterials and nanodevices beyond silicon integrated circuit manufacturing is appealing as time-to-market in some instances may be shortened.

**Table 1.** Outline of key nanomanufacturing requirements and BCP material characteristics.

 ~ 5-50 nm	<b>Nanomanufacturing Requirements</b>	 <b>Block Copolymer Methodologies</b>	
	Defined geometries	Intricate architectures ✓	
	Access to ultra-small features	Nanoscale precision ✓	
	Reduced time for efficiency	Rapid processing ✓	
	Access to raw materials	Scalable synthesis ✓	
	Cost	Low cost of ownership ✓	

This is feasible as logic based semiconductor processing require defect free patterns but BCP

accessible technologies *e.g.* membranes, solar-cells, batteries, anti-reflective surfaces to name a few[3] have some defect tolerance (defects may actually augment performance in certain applications). The aim in this piece is to outline key BCP self-assembly approaches that have been utilized hitherto with applications in energy, photonic, environmental and biorelated nanodevices as shown in Fig. 1.

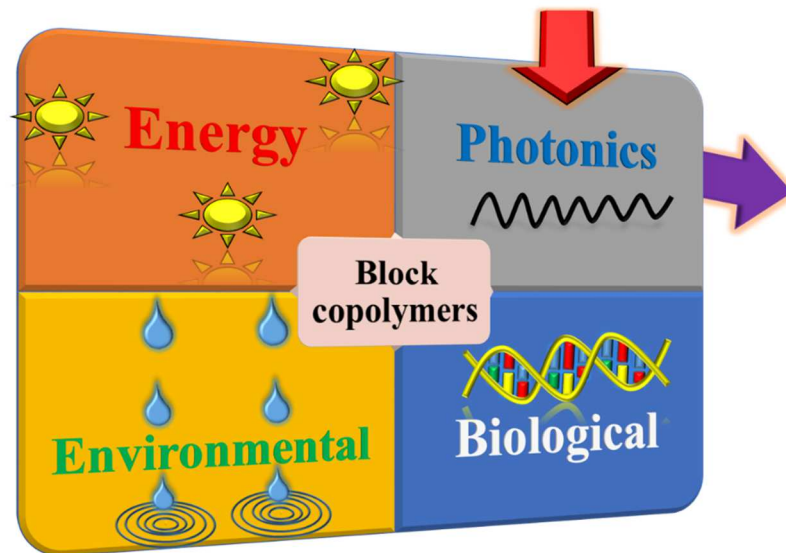


**Figure 1.** Areas of emerging interest for nanomanufacturing based upon block copolymer self-assembly which are reviewed in this article.

Self-assembly is a process that defines the spontaneous organization in soft condensed matter. Based on intermolecular interactions of energy close to  $kT$ , it produces resilient structures, easily distorted by external fields. Self-assembly also underpins various intricate structural formations in biological systems, in particular hierarchical features, which are ever-present in Nature. Such phenomena have continually intrigued material scientists and replicating Nature's exquisite designs could lead to significant progress for future nanomanufacturing. Among self-assembling systems, BCPs present fascinating spontaneous spatial organization as well as complex properties, combining those of the individual blocks. The composition of BCP materials enables advantageous chemical properties, *e.g.* water resistant, flame retardant *etc.* and physical properties *e.g.* ductility, durability, flexibility *etc.* and has provided a fascinating means to develop novel applications.[4],[5],[6] Since the 1950's, research on bulk BCPs has led to industrial production in sectors including food packaging,[7] automotive[8] and drug delivery[9] amongst others.[10],[11] Today, we can

choose from a collection of BCPs with varying compositions and diverse chemistries as a result of innovative synthesis strategies including ring-opening polymerization, atom transfer radical polymerization, reversible addition-fragmentation chain transfer, nitroxide-mediated polymerization and ring-opening metathesis polymerization.[12],[13],[14] The choice of various commercial suppliers of BCPs is also a critical element to consider for potential nanomanufacturing. With the option of commercial BCPs, prohibitive raw material costs hypothetically will not impede progress of prototype development to real products. **While some polymerization induced self-assembly (PISA) reports are detailed later, it has been well reviewed recently [15], [16], and thus we focus more specifically in this review on thin film and solution based assembly.**

### **1.1 BCP thin film self-assembly**

The advent of nanotechnology over the past two decades has also allowed us to characterize nanometre thin films with exquisite precision and encoding nanochemistry with such films has enabled new research areas to blossom. In this respect, fabricating thin films of BCPs, typically less than 100 nm in thickness,[17] have garnered intense study since their identification (*ca.* 1995) as potential etch masks for nanolithography.[18],[19] A key enabler for future BCP applications in thin film form has emanated from “directed self-assembly” (DSA) research.[20],[21],[22],[23],[24],[25] The thrust of DSA research over the past decade advanced our understanding to control BCP thin films and extensive DSA reviews are available for interested readers.[26],[27]

The most basic type of BCP is a linear A-B di-BCP (containing two polymer blocks only), as shown in Fig. 2 below. Linear tri-BCPs (containing three polymer blocks), *i.e.* ABA and ABC type BCPs are also of interest in this review since they offer more complex structural arrangements and chemistry. BCP self-assembly is intrinsically driven by three distinct parameters for a BCP: i) Flory-Huggins interaction parameter ( $\chi_{AB}$  for AB di-BCP, and  $\chi_{AB}$ ,  $\chi_{AC}$ , and  $\chi_{BC}$  for an ABC tri-BCP) ii) degree of polymerization (N), and iii) volume fraction ( $f$ ).  $\chi$  is a measure of the dissimilarity between the two constituent polymer blocks. Polystyrene-*block*-poly(methyl methacrylate) (PS-*b*-PMMA) is considered a first generation material and is well documented in the literature.[28],[29],[30] However, due to the low  $\chi$  value ( $\sim 0.03$  @ 150°C) of PS-*b*-PMMA which limits period size reduction, a range of high  $\chi$  BCPs (favoring ultra-low period sizes) have been designed by careful synthesis.[31] N defines the period size of BCPs, and can be tuned to desired periods that are generally in the

sub-100 nm regime, but more recently can be used to exceed 100 nm.[32] Recent advances in synthetic strategies have also paved the way to formulate novel BCPs that can possess a crosslinkable component,[33],[34] a metal moiety,[35],[36] or a biodegradable block.[37],[38] Volume fraction is critical in regard to BCP morphologies. In bulk BCPs, used as a reference for thin film BCPs, the volume fraction can be modified to dictate morphologies for di-BCPs; spherical, cylindrical, gyroidal and lamellar phases are realizable conformations, as shown graphically in Fig. 2 a and in the microscopy images in Fig. 2 b-e.

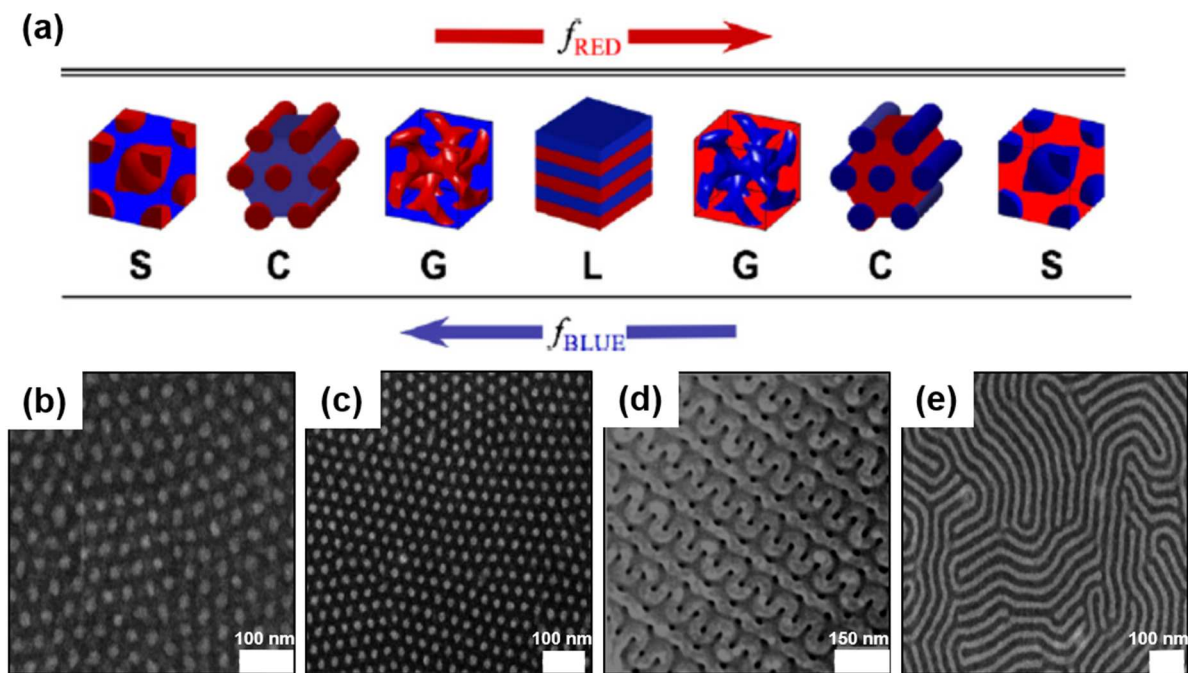


**Figure 2.** (a) Di-BCP morphologies based upon respective volume fraction change between two constituent polymer blocks. Reproduced with permission from Elsevier.[39] (b)-(e) SEM images of corresponding BCP morphologies. (f)-(i) Reproduced with permission from American Chemical Society.[40],[41]

**Processing:** Critical parameters concerning BCP thin film formation at substrate surfaces are outlined in Fig. 3. As mentioned above, BCP characteristics, *e.g.* block chemistry,  $\chi$ ,  $N$ , and  $f$  (Fig. 3 a) are initially evaluated with respect to intended application. Prior to deposition, one must consider the substrate chemistry and its potential effect on BCP formation, *i.e.* polymer-substrate interface interactions. For example, substrate surface modification with end-functionalized polymers is well documented to mitigate surface dewetting and control feature orientation.[42],[43],[44] Typically, a BCP film is spun cast in appropriate solvents to form a thin film. Thereafter, the BCP film is subjected to an annealing technique, *e.g.* thermal, solvent vapor, laser, microwave *etc.* to enable microphase segregation of the polymer blocks.[45],[46],[47],[48] Balancing the polymer-air interface is also critical to define

orientation. Likewise, the BCP film thickness must be controlled/monitored in order to avoid dewetted structures as well as mixed orientation (see Fig. 3 d).[49],[50] A myriad of organic/inorganic/metallic structures can then be realized by exploiting the block chemistry (Fig. 3e,f) with well-established fabrication processes.[51]

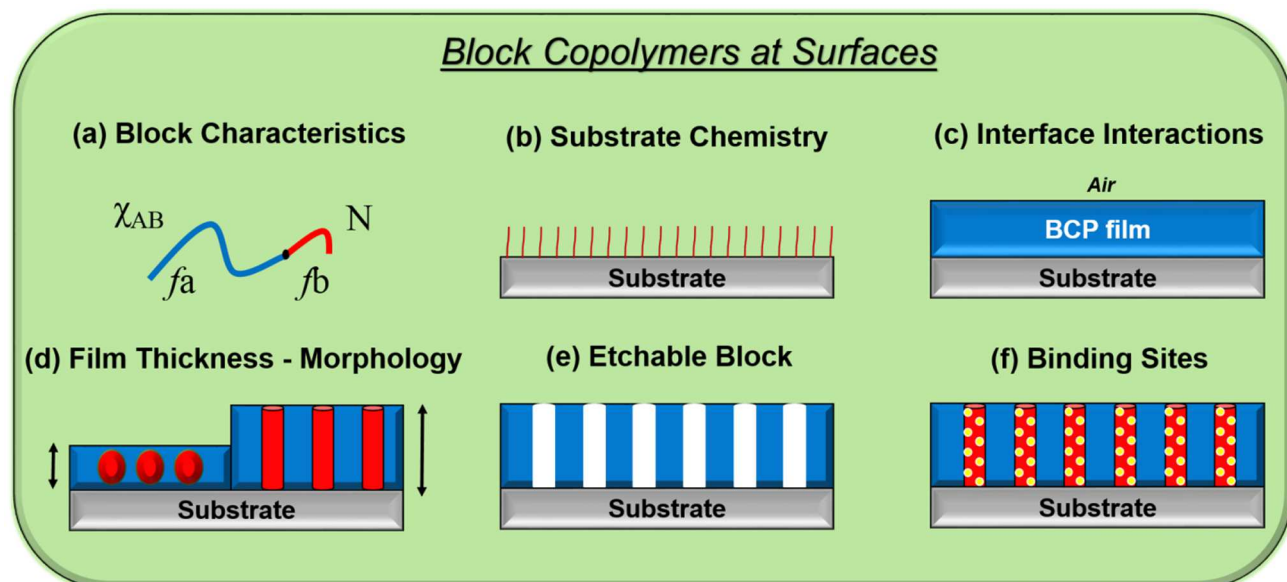


**Figure 3.** Key factors for consideration of BCP thin film formation at substrate surfaces.

## 1.2. BCP solution self-assembly

Whilst BCPs in solution are not as well researched fundamentally as their bulk counterparts, we have witnessed a remarkable playground for tailoring nano-objects endowing photosensitive, biological and chemical characteristics. Thus, BCP solutions have appreciable applications in medicine as nanoreactors,[52] photonics for display technologies[53] and environmental use for remediation purposes.[54] BCPs in aqueous solutions form various stable morphologies depending on the length of hydrophobic and hydrophilic blocks.[55] These morphologies are extremely complex in nature with minor deviations producing vastly contrasting structures. A di-BCP in a solvent-nonsolvent mixture is dependent on six  $\chi$  parameters,  $\chi_{AB}$ ,  $\chi_{AS}$ ,  $\chi_{AN}$ ,  $\chi_{BS}$ ,  $\chi_{BN}$ ,  $\chi_{SN}$ , where S denotes a good solvent for both blocks and N denotes a nonsolvent for one block, illustrating the extreme complexity of BCP self-assembly in solution even in the simplest version of a BCP. Classic morphologies (see Fig. 4) include spherical micelles, rods (cylindrical or wormlike micelles), small and large lamellae, hexagonally packed hollow hoops, and large compound micelles. An excellent tutorial review is available by Mai and Eisenberg which examines criteria leading to such systems.[11]



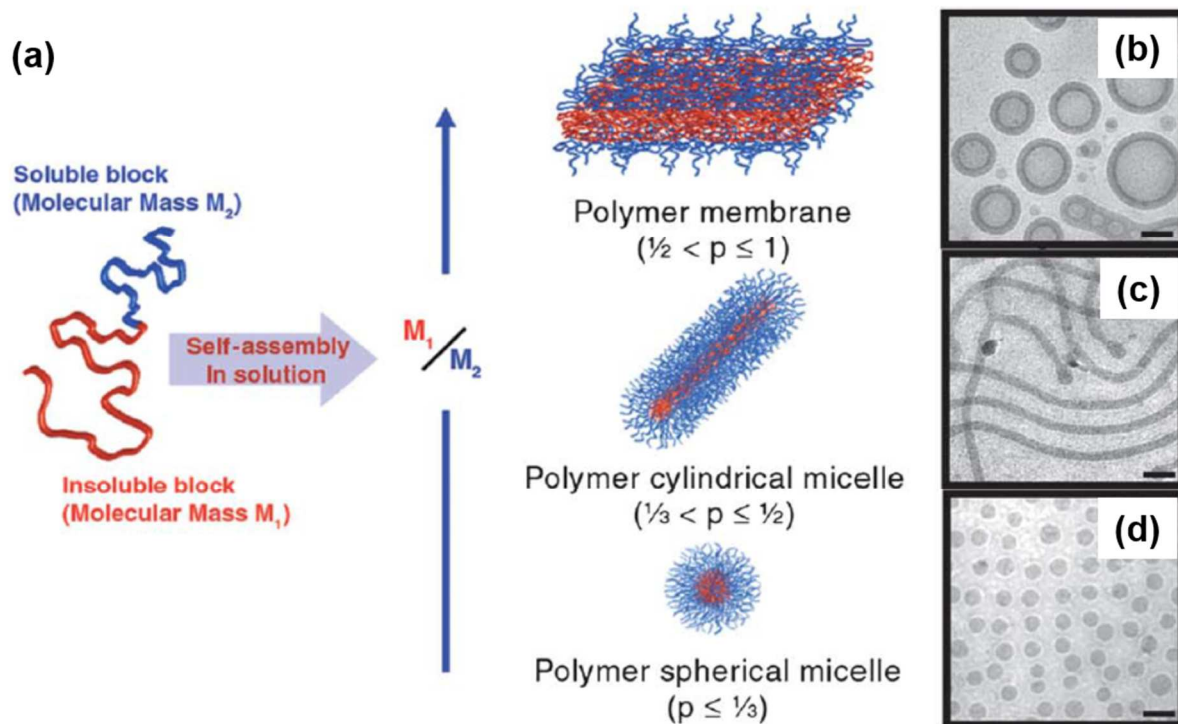


**Figure 4.** (a) Resultant micelle features depending on BCP volume fraction. (b)-(d) TEM images of respective micelle features. Reproduced with permission from Royal Society of Chemistry.[56]

Di-BCPs in solution are broadly categorized into amphiphilic, double hydrophobic and double hydrophilic systems (based on block water solubility). Symmetric amphiphilic BCPs have been investigated[57],[58] but the most extensively studied are asymmetric amphiphilic BCP systems where the hydrophobic regions are much longer than the hydrophilic block with over 20 diverse morphologies obtained following self-assembly in solution (*e.g.* spheres, rods, bilayers, tubules *etc.*) Typically, spherical micelles are the first aggregates to form and are considered as the starting morphology for the growth of more complex self-assembled structures. They consist of a spheroidal hydrophobic core surrounded by a corona of hydrophilic polymer chains.

**Processing:** For preparation, an amphiphilic BCP is dissolved in a good solvent for both blocks, *e.g.* THF, dioxane *etc.* Adding a selective solvent (Fig 5. a and b) (to one block) such as water induces micellar self-assembly, but it has also been reported that strong amphiphilicity may lead to out-of-equilibrium and process-dependent lyotropic behavior.[59] Each morphology is governed by three components of the system free energy; the surface energy between micelle core and the solvent, the degree of stretching of the core-forming block and the repulsive interaction of the coronal chains. Altering these three contributions

can induce a particular morphology. One must consider that shifts in copolymer concentration and composition (block ratio and chemistry), water concentration of solvent solution, surface energy of solvent, addition of ions *etc.* will affect the system free energy. For example, a spherical formed PS-*b*-poly(acrylic acid) (PS-*b*-PAA) micelle in a DMF-water solution will have some PS blocks stretched from the core center to the core-corona interface. For micelles formed with a constant PS block length, stretching of the PS chains increases with core size. As the PAA block length reduces, the repulsion along the corona chains decreases, resulting in increased stretching in the PS chains and consequently larger core size. This trend will continue until the entropy of the PS chains drop to a critical point and the aggregates evolve from sphere through cylinder and lamella to reduce the PS stretching by minimizing free energy of the system (Fig. 5 c). BCP derived spherical micelles are a promising candidate for drug delivery *i.e.* a hydrophobic drug encapsulated by the core with the hydrophilic corona affording solubility in water (Fig. 5 d).[60].

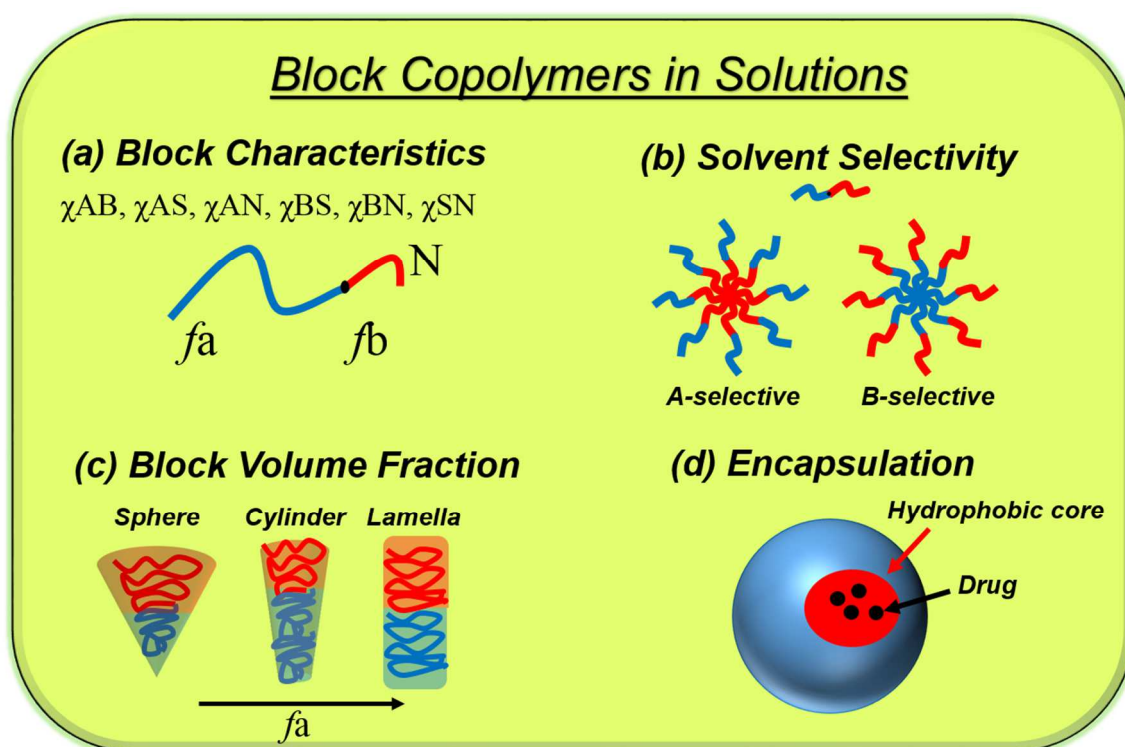


**Figure 5.** Key factors for consideration of BCP formation in solutions.

**1.3. Review Outline:** BCPs provide a robust path to produce functional nanomaterials in solution and can also be utilized to coat large-scale areas ( $> \text{cm}^2$ ) of nanoscale patterns in thin film form. Although BCP thin film and solution methodologies can contrast vastly, the comprehensive paths now available have demonstrated relatively simple processing schemes

that are attractive for nanomanufacturing of nanodevices.[61],[62] Hence, BCP materials present a versatile manner in which to tune solution based chemistry or nanoscale thin film patterns. We exemplify the alternative BCP routes hitherto as opposed to expensive top-down optical lithography techniques. BCP systems present an interesting space for new functions and we now examine salient BCP work under the following areas: energy, photonics, environmental, and biological.

Readers should be aware of the vastly different roles that BCPs play in these following sections. Some BCPs are used as host templates while other BCPs are required for engineering nanomaterials that are specifically related to BCP block chemistry. For example, is a BCP solely required for templating purposes of an active material? This is typically the case required for thin film uses. Or perhaps, is the BCP required to behave as a stabilising agent? This is particularly evident in the energy and biological sections here. Or, one must consider if a BCP is chosen because its chemistry endows specific surface properties and is used to engineer functionality or response? Researchers rationale for choice of certain BCPs is aligned with the desired application as will become apparent to readers.

## **2. Energy**

### **2.1 Background**

The ability of BCPs to precisely modify surface morphologies is extremely useful in fields requiring roughened and textured surfaces that provide high surface area, such as in catalysis. To encompass advances spanning the range of potential catalytic applications, the energy section is split into several sub-sections providing a broad scope of energy related applications. Of particular interest is the use of BCPs in the synthesis of photocatalysts since deposited films can drastically change surface properties and can also include metal precursors that significantly affect structure-relationship interactions.[63] Readers are referred to recent articles by the Deng group on synthetic strategies for templating mesoporous semiconducting metal oxides[64] as well as the progress of ABC type BCPs for templating mesoporous metal materials.[65] In heterogeneous photocatalysis, the substrate of interest is typically dissolved in solution and catalysis occurs on the surface of suspended particles of catalyst *i.e.*, substrate and catalyst are not present in the same phase.[66] The general mechanism of action for most substrates consists of initial adsorption or diffusion of substrate to the interface prior to heterogeneous electron transfer, and this process is partially

dependent on the number of active surface sites available.[67] Control of nanoparticle (NP) size and geometry can optimize the surface area to volume ratio for catalysis, or promote the growth of certain crystal facets with known photocatalytic activity (*vide infra*). Thus, homo- and heterogeneous BCP templating is an attractive route to design NPs for nanomanufacturing purposes.

## 2.2 Photocatalysis

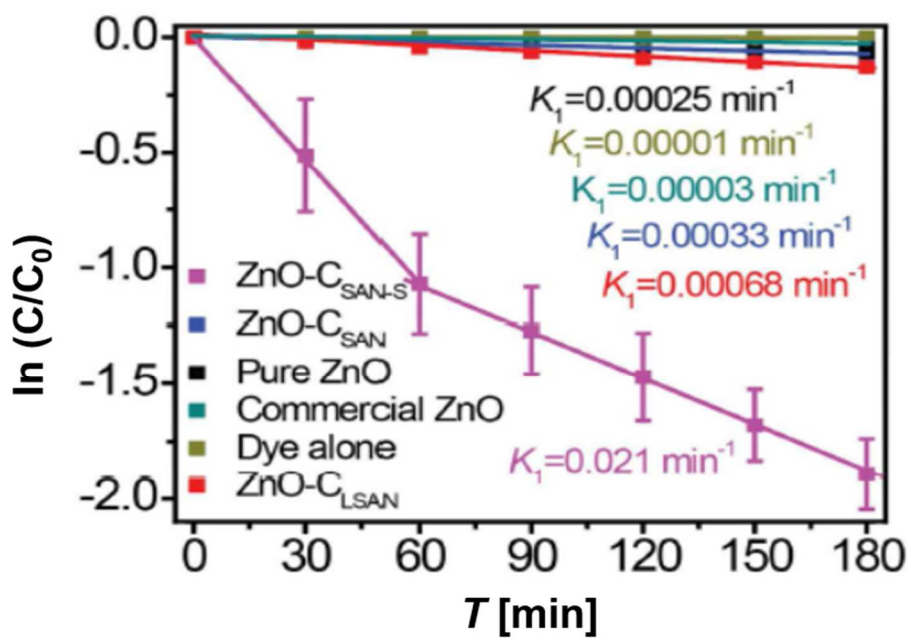
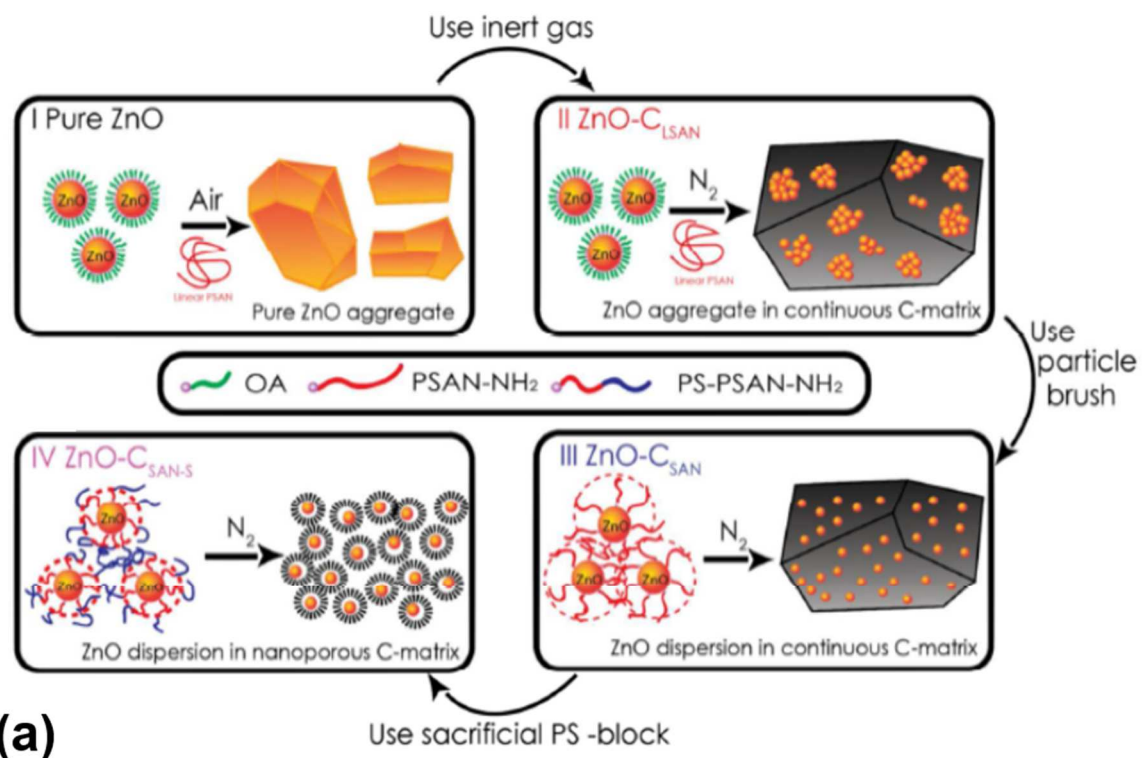
TiO<sub>2</sub> is a widely-employed nanomaterial in a range of applications including suncreams,[68] foodstuffs,[69] self-cleaning window coatings,[70] as an electrode support,[71] as a dielectric medium,[72] and in photocatalysis.[73],[74] As a wide bandgap semiconductor photocatalyst, its activity towards a huge range of photochemical reactions under UV irradiation remains unsurpassed. These reactions can mainly be broken down into model compounds (*i.e.*, dyes, pesticides), photo-oxidation, both water splitting half reactions and solar disinfection.[75] BCPs have been employed extensively in the patterning and growth of various TiO<sub>2</sub> structures for a range of photocatalytic applications; however, BCPs in this context have primarily been reported for materials synthesis as opposed to state of the art catalytic performance. Some examples include the use of Pluronic P123 (poly(ethylene oxide)-*b*-(propylene oxide)-*b*-(ethylene oxide) [PEO-*b*-PPO-*b*-PEO] to template TiO<sub>2</sub> nanoparticles for use in hydrogen evolution[76] and for dye degradation photocatalysis,[77] while F108 [(poly(ethylene glycol)-*b*-poly(propylene glycol)-*b*-poly(ethylene glycol)] (PEG-*b*-PPG-*b*-PEG) has been used to template TiO<sub>2</sub> for H<sub>2</sub> evolution.[78] Indeed, NPs of the BCP-templated anatase TiO<sub>2</sub> phase showed improved activity in the absence of an added co-catalyst, in comparison to commercially available material. This was attributed to the formation of defect states in the BCP-templated titania. This shows the potential for BCPs in templating defective NPs materials which provide trap sites (usually oxygen vacancies) which retard electron-hole recombination kinetics, leading to intrinsically high photocatalytic activity.[79] More recently, Li *et al.* reported the use of carbon and nitrogen doping (derived from a PS-*b*-P4VP BCP template) to fabricate bowl-like TiO<sub>2</sub> nanostructures decorated with Au nanoparticles (~ 5 nm in diameter).[80] The resulting tuneable template was used towards visible light degradation of Rhodamine B, with degradation of 90% attained within 150 mins, which is five times faster than commercially available TiO<sub>2</sub> nanoparticles (P25) that were also loaded with Au nanoparticles. In parallel, Zhao *et al.* utilized Pluronic P123 to make 3D interconnected ordered macro/mesoporous TiO<sub>2</sub> possessing a crystalline framework, ~ 420 nm cavities, mesopores of 3.7 nm and high surface area (177 m<sup>2</sup> g<sup>-1</sup>) for the degradation of

Rhodamine B.[81] They showed the reaction rate to be three times higher than commercially available P25 TiO<sub>2</sub>. Trapalis *et al.* have reported a similar strategy using Pluronic F127 to synthesize TiO<sub>2</sub>/graphene (and reduced graphene oxide) composites to remove NO<sub>x</sub> under UV and visible light.[82] The above mentioned work in this section exemplify the diversity of using BCPs to design a wide range of useful hierarchical features with controlled dimensions to address specific photocatalytic uses. Indeed, of late, studies have elucidated efficient practices to pattern thin film TiO<sub>2</sub> structures derived using BCPs from solution[83],[84] and vapor[85] deposition phases. While powders are still traditionally studied for their performance and well-known synthesis, thin films represent a scalable platform for nanomanufacturing since they can be developed on large surface areas. Thus, they could potentially be utilized for photocatalysis with the added benefits of reusability without the need for purification as required in homogenous reactions.

While TiO<sub>2</sub> studies tend to dominate the photocatalysis literature, it is severely limited by its optical properties, absorbing only in the UV region corresponding to *ca.* 5 % of incident solar light and its relatively positive conduction band edge renders it of somewhat limited use for reduction reactions. Other materials with similar UV and near-visible absorption properties have been templated using BCPs - for example ZnO NPs synthesized using PS-*co*-acrylonitrile-*b*-PS) as shown in Fig. 6 a and b,[86] and WO<sub>3</sub> NPs synthesized using PEO-*b*-PS have been used in dye degradation and water oxidation photocatalysis (see Fig. 6 c-e)[87], respectively. The use of other semiconductors with various valence and conduction band potentials, and a wide range of optical properties is, therefore, an ongoing area of research. Amphiphilic poly(alkylene oxide) BCPs have been employed as structure-directing agents for templating NPs of a range of mesoporous oxide materials including TiO<sub>2</sub>, ZrO<sub>2</sub>, Nb<sub>2</sub>O<sub>5</sub>, Ta<sub>2</sub>O<sub>5</sub>, Al<sub>2</sub>O<sub>3</sub>, SiO<sub>2</sub>, SnO<sub>2</sub>, WO<sub>3</sub>, HfO<sub>2</sub>, and mixed oxides SiAlO<sub>y</sub>, Al<sub>2</sub>TiO<sub>y</sub>, ZrTiO<sub>y</sub>, SiTiO<sub>y</sub> and ZrW<sub>2</sub>O<sub>y</sub>. [88] The above series of nanomaterials were synthesized using various metal chloride salts and modest aging conditions (*e.g.* 40 - 60°C for 1-30 days in air before calcining) and displayed high BET surface areas of between *ca.* 100 and 800 m<sup>2</sup> g<sup>-1</sup>. While none of these materials were used photocatalytically, the mesoporous morphology demonstrated shows the versatility of BCP NP templating and potential applications using a large range of oxide NPs. More recently, a CoO porous 3D network was synthesized by calcining colloidal CoO NPs with Pluronic F127 (PEO-*b*-PPO-*b*-PEO) for 4 hours.[89] The network consisted of 18 nm diameter CoO NPs with *ca.* 4 nm diameter pores bound tightly in a crystalline lattice, with a BET surface area of 134 m<sup>2</sup> g<sup>-1</sup>. Unlike TiO<sub>2</sub>, CoO appears green

and can, therefore, be driven with visible light. Suspension photocatalysis was performed using a  $> 360$  nm light source for the removal of toxic Cr(VI) from aqueous solution. Concomitant reduction of Cr(VI) to Cr(III) with water oxidation was measured, as evidenced by  $O_2$  evolution measurements,[90] showing the great promise of using BCPs in templating nanoparticulate photoreduction catalysts. Finally, non-oxide NPs have also been templated using BCPs; for example 20 nm diameter  $MoS_2$  nanowires using PS-*b*-P2VP BCPs.[91] Graphitic carbon nitride ( $g-C_3N_4$ ) is an emerging photocatalyst material which has been reported for use in overall water splitting[92] and  $CO_2$  reduction.[93] Using Pluronic F68, it was shown that particles of  $g-C_3N_4$  exhibited superior photocatalytic efficiency for both oxidation (dye degradation) and reduction ( $H_2$  evolution) reactions than bulk  $g-C_3N_4$ , which was attributed to improved crystallinity on the basis of X-ray diffraction and gas sorption measurements.[94]

Additionally, other photocatalysts have been synthesized through covalent bonding to BCPs. These systems have been used for homogeneous photocatalysis in solution,[95] whereby the BCP structure prevents aggregation of the molecular catalyst centres, and so exhibit similarities to the function of BCPs in catalyst NP synthesis. They can also be used to stabilize photocatalyst molecules as emulsions; for example, Zn phthalocyanine emulsions using poly(arylene ether nitriles). CdS NP photocatalysts have been immobilized on the surface of exfoliated graphene sheets using the amphiphilic poly(isoprene)-*b*-PAA (PI-*b*-PAA) BCP and used for visible light-driven  $H_2$  evolution.[96] Moreover, BCPs have also been employed to co-aggregate donor-acceptor pairs in micelles illustrating their broad applicability.[97]



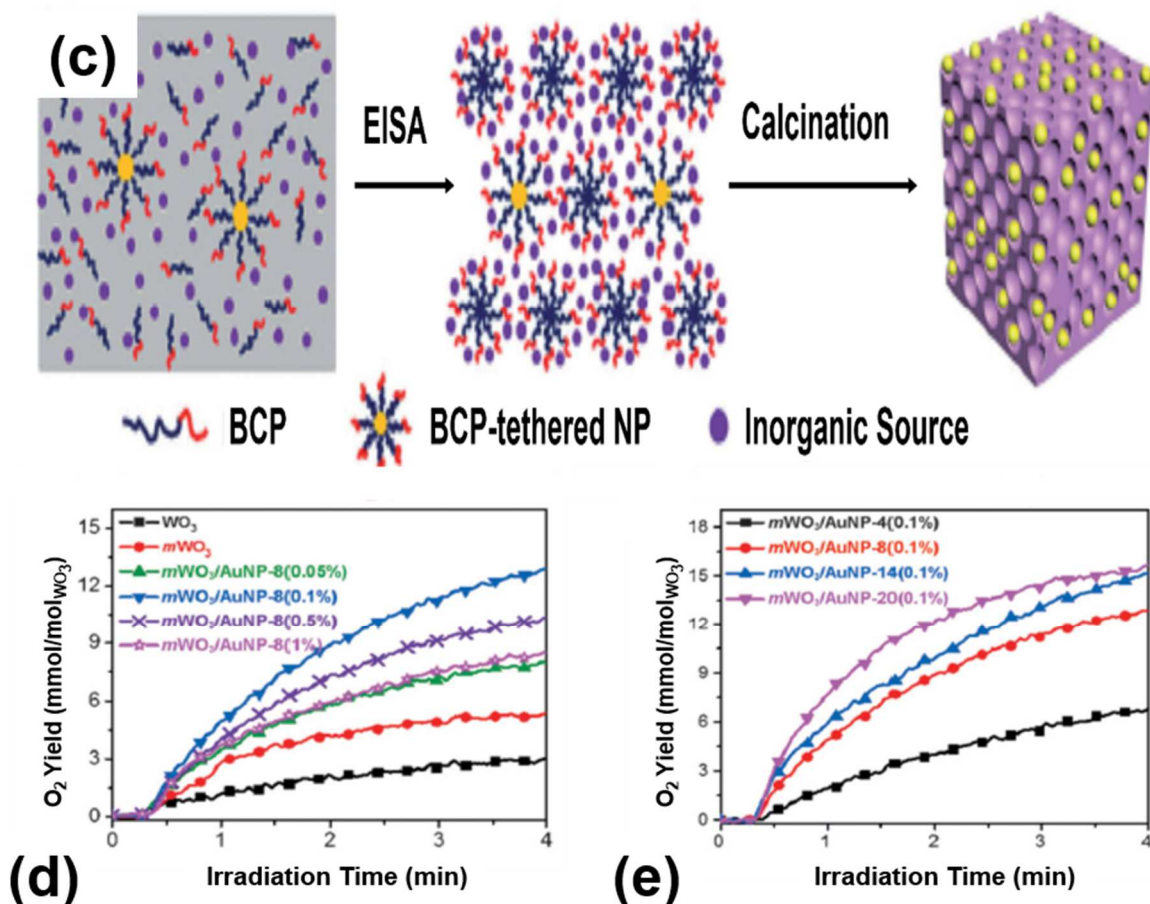


**Figure 6.** (a) Scheme illustrating different routes to photocatalytic active ZnO/C hybrid materials using BCPs. (b) Graph of methylene blue degradation under visible light for different ZnO/C materials from fabrication routes in (a). Reproduced with permission from American Chemical Society.[86] (c) Synthesis route using EISA (Evaporation Induced Self-Assembly) of  $m\text{WO}_3/\text{Au NP}$  hybrid catalysts.  $m\text{WO}_3$  refers to mesoporous  $\text{WO}_3$ . (d, e) Graphs showing photocatalytic activity in water oxidation reactions of  $\text{WO}_3/\text{Au NPs}$  with various loadings of Au NPs in (d) and with varying Au NP sizes in (e). Reproduced with permission from Wiley.[87]

As highlighted in the introduction, exploiting the specific nature of selected amphiphilic BCPs, judicious selection of physical parameters (*e.g.* concentration, solvent polarity, solution pH, and material electrostatics) enables precise morphology control in solution and thin films, which is advantageous for nanomanufacturing. This applies to the formation of both novel homogeneous and heterogeneous photocatalysts for a wide range of reactions. To date, the approaches outlined herein have largely focused on the self-assembly and analysis of new materials, so there is considerable scope for further work in this space focusing on catalytic performance and new breakthroughs.

### 2.3 Electrocatalysis

Early work from Kim and co-workers introduced the catalytic potential of using BCP thin films as hosts to realise monodisperse nanoparticle arrays to prepare highly organized carbon



nanotube arrays.[98],[99] More recently, as will be discussed in this section, BCPs have served as a useful methodology in electrocatalysis. Electrocatalytic reactions are most commonly monitored in analytical chemistry such as blood glucose sensing (*e.g.* Therasense Freestyle) and ethanol detection (*e.g.* in a breathalyser). Electrocatalytic reactions are also employed in a variety of energy conversion and storage applications relevant to electrolyser technologies such as hydrogen and oxygen evolution reactions (HER, OER) via water electrolysis;[100] and also to fuel cell technologies through oxygen reduction reaction (ORR) and the electro-oxidation of methanol.[101] The breath of this section is broad, as will become clear, reflecting the complexity of material requirements for electrocatalysis. With this in mind, we note that surface structures or overall morphology can vary drastically, *e.g.* BCPs have been used to template NPs on graphene as well as pattern silicon nanostructures. As we will evaluate, intended application has determined the route employed leading to such contrasting surface structures/morphology.

**Heterogeneous Electrocatalysis:** BCPs have been employed extensively in the synthesis of catalytic electrode materials for use in electrolyzers *i.e.* both of the water splitting half reactions. For the reduction of water (HER), platinum (Pt) is the most widely studied material possessing an extremely high efficiency for hydrogen evolution at overpotentials below even 100 mV.[102] PS-*b*-PMMA has been used to pattern the surface of chemically modified graphene (CMG) with Pt NPs for HER. This was achieved through reduction of spin-coated layers of reduced graphene oxide to give a 15 nm thick CMG substrate onto which 80 nm of the BCP was spin coated, followed by annealing at 250°C and selective reactive ion etching of the PMMA microdomains, before Pt was evaporated onto the patterned substrate.[103] The authors also reported the patterning of the surfaces with Pd nanowires and Au nanodots, indicating the potential versatility of this approach, as shown in SEM images in Fig. 7 a and b. The electrocatalytic efficiency of these substrate towards HER was impressive (see Fig. 7 c), with onset potentials and Tafel slopes for HER comparable with commercially available Pt/C materials.

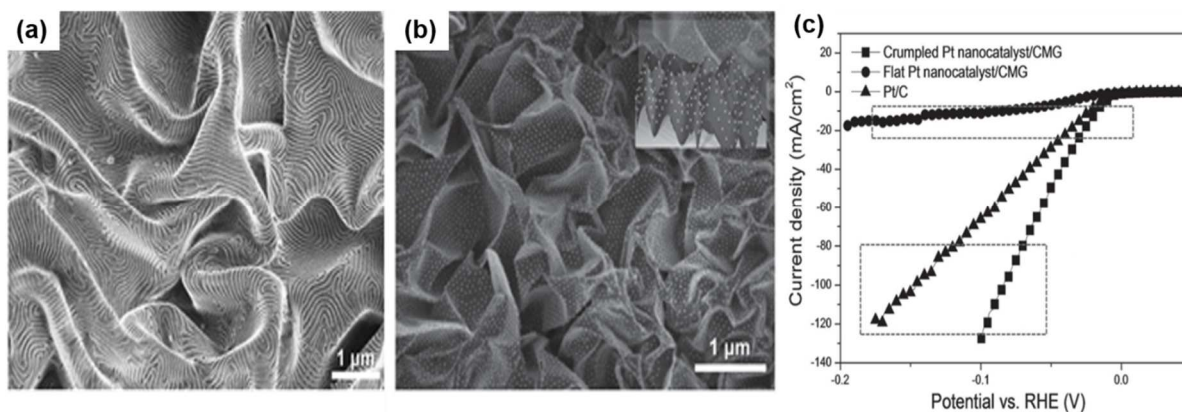


**Figure 7.** (a) SEM of an isotropically crumpled CMG fabricated from BCP nanotemplates. (b) Surface modified with Au nanodot arrays. (c) The HER onset overpotential is lower than for commercial Pt/C. Reproduced with permission from Wiley.[103]

However, the scarcity of Pt makes it very expensive so the search for non-Pt HER electrode materials is a field of intense research efforts; one example utilised BCPs in the synthesis of spinel  $\text{ZnFe}_2\text{O}_4$  with Pluronic P123, which showed HER activity superior to a commercial Pt/C standard.[104] Additionally, a range of materials have been templated using BCPs for complementary OER. Although a rare and expensive material,  $\text{IrO}_2$  is recognized as a leading OER catalyst and has been synthesized using  $[\text{Ir}(\text{OH})_6]^{2-}$  and Pluronic F127 (PEO-*b*-PPO-*b*-PEO) at  $400^\circ\text{C}$  to yield a NP film with over  $500 \text{ m}^2 \text{ g}^{-1}$  surface area. Water oxidation electrocatalysis at + 1.2 V vs. Ag/AgCl showed that the templated materials were more than twice as active for  $\text{O}_2$  evolution than an equivalent untemplated  $\text{IrO}_2$  catalyst.[105] Due to the high cost of Ir, other materials have also been investigated – for example, Pluronic F127 (PEO-*b*-PPO-*b*-PEO) has been used to template heterostructured  $\text{Ni}_3\text{S}_2/\text{VS}_2$  on Ni foil electrodes, which showed slightly superior linear sweep and Tafel characteristics than  $\text{IrO}_2$ . [106] Research to move beyond Ir and Pt is paramount to reduce the cost of electrode materials in commercial electrolyzers, and possible future studies will focus on lower cost OER materials such as  $\text{MnO}_2$ .

In direct methanol fuel cells (DMFCs), the electro-oxidation of methanol occurs concomitantly with ORR to generate electrical power with  $\text{H}_2\text{O}$  and  $\text{CO}_2$  as the by-products. As with electrolyzer technologies, many of the best performing catalysts for fuel cell electrodes consist of expensive and rare elements, and research into new electrode materials is intensive. BCPs have been used to template catalysts for ORR. For example, 2D dendritic Pt NPs have been synthesized in solution using oleic acid and Pluronic F127 (PEO-*b*-PPO-*b*-PEO) templates and transferred to carbon electrodes for ORR studies,[107] and Mo-doped

PdPt NPs have been templated on graphene using poly(dimethylaminoethyl methacrylate)-*b*-poly [(ethylene glycol) methyl ether methacrylate], showing superior activity to Pt/C for ORR.[108] Additionally, BCPs have also been used to template Rh NPs for use in solid oxide fuel cells, the first report of using BCPs in such a fashion.[109] The NPs remained stable after SOFC operation at 650°C, and BCPs will potentially find further use in patterning defined electrodes in such devices with lower-cost metals. PS-*b*-PAA BCP micellar features have also been employed to develop mesoporous transition metal sulfide structures, a material class of increasing interest for energy storage and conversion.[110] The PS-*b*-PAA system was used to template mesoporous MoS<sub>2</sub>/CoMo<sub>2</sub>S<sub>4</sub>, and these materials were further doped with Fe exhibiting excellent electrochemical activities for both hydrogen and oxygen evolution reactions. Moreover, a very recent report has answered key questions related to metal nanoparticles and high temperature electrocatalysis of oxide electrodes. Choi *et al.* detailed a design to pattern 10 nm monodisperse particle particles (Pt, Pd, Au or Co were used), which were fabricated at a mixed-conducting oxide electrode for high-temperature (> 600°C) electrocatalytic reactions.[111] The report elucidated how Pt metal catalysts are best suited to activate hydrogen electrooxidation, while Au nanoparticles were observed to be inactive.

**Li-ion and Li-O<sub>2</sub> batteries:** Templating of nanostructured materials, often oxides, is of high importance in Li-ion battery anode design as it can be used to synthesize porous or nanostructured materials suitable for Li-ion intercalation, and BCPs have been employed in this field. For example, In 2018, Wiesner and co-workers took advantage of a gyrodial forming tri-BCP system, poly(isoprene)-*b*-poly(styrene)-*b*-poly(ethylene oxide) (PS-*b*-PI-*b*-PEO), to fabricate thin film device layers in the fabrication of a fully functional 3D Li-ion/sulfur battery.[112] Importantly, the footprint area of their 3D battery design was orders of magnitude lower than traditional 2D designs, which make it quite appealing for future nanomanufacturing. Fischer *et al.* have synthesized mesoporous TiO<sub>2</sub> microspheres as anode materials for Li-ion batteries generated from mixing TiO<sub>2</sub> and PEO-*b*-PPO-*b*-PEO (with PMMA homopolymer) or PS-*b*-PEO (with PI homopolymer).[113] The work illustrated the use of BCPs as a powerful means to control mesopore structure and pore size, key device characteristics. PEO-*b*-PS has been employed to synthesize (using evaporation-induced self-assembly) mesostructured TiNb<sub>2</sub>O<sub>7</sub> with 40 nm pore diameters as an anode material for Li-ion batteries.[114] The mesoporous TiNb<sub>2</sub>O<sub>7</sub> (346 mAh g<sup>-1</sup>) outperformed its bulk counterpart (266 mAh g<sup>-1</sup>) in galvanostatic charge-discharge tests, due to its higher surface

area. PEO-*b*-PS has also been used to template TiN with 30 nm hexagonal pores for Li-O<sub>2</sub> battery anodes.[115] Other examples include mesoporous Ge/GeO<sub>2</sub>/carbon templated using PEO-*b*-PS for Li-ion batteries;[116] carbonized inverse-opal Co<sub>3</sub>O<sub>4</sub>[117] and mesoporous WC[118] templated using Pluronic P123 for Li-O<sub>2</sub> batteries. The range of metals used in mixed oxide anode materials, and the selection of methods, BCPs and potential applications, suggests a myriad of further developments in this field are possible. In particular, promotion of material growth exhibiting specific crystal facets is a complex field and BCPs offer significant potential in this space given their tunable chemistry.

**Photoelectrochemistry and photovoltaics:** The best performing electrocatalytic systems such as IrO<sub>2</sub> for OER and Pt for HER operate at overpotentials due to kinetic limitations, which are especially pronounced for OER. Photoelectrochemical (PEC) systems offer the possibility of running electrocatalytic reactions at potentials lower than their formal reaction potentials by using light to provide the extra voltage. As described earlier, TiO<sub>2</sub> is the most widely used material for photocatalysis and also for PEC, usually grown using a sol-gel or CVD approach.[119],[120] BCPs have been used to template electrodes for various PEC reactions; for example, TiO<sub>2</sub> photoanodes for overall PEC water splitting have been templated using the BCP PIB3000;[121] ZnO has been templated using PS-*b*-P2VP and employed in water oxidation PEC;[122] and a Si photocathode was etched using PS-*b*-PMMA to give a random lamellar surface structure with improved HER activity under AM1.5 (simulated solar) irradiation, as evidenced by higher photocurrent densities as shown in Fig. 8 below.[123]

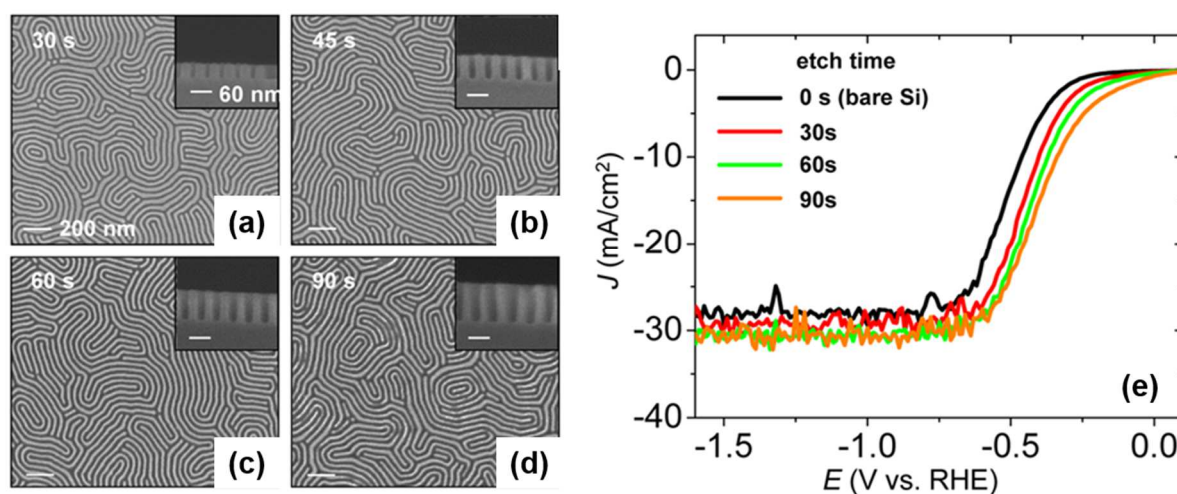


**Figure 8.** A lamellar PS-*b*-PMMA structure was self-assembled at 190°C for 24 hours. After exposure to 254 nm irradiation, 10 nm of Cr was evaporated and the remaining polymer removed by sonication. The patterned Cr was then used as an etch mask to form nanostructured Si. Si nanostructures are shown after 30 secs (a), 45

secs (b) 60 secs (c), and 90 secs (d) respectively. (e) Si structures were then applied as a HER photocathode in 0.1 M H<sub>2</sub>SO<sub>4</sub> electrolyte. Reproduced with permission from the American Chemical Society.[123]

Photoelectrodes can also be employed as solar photovoltaic cells. The sensitization of mesoporous TiO<sub>2</sub> electrodes using surface adsorbed dye molecules (dye-sensitized solar cells, DSSCs) and a redox electrolyte based on the I<sup>-</sup>/I<sup>3-</sup> couple was a major breakthrough in a seminal 1991 paper,[124] and DSSCs have attracted enormous academic and commercial (Dyesol, Solaronix) attention since. Several notable examples of solar cells templated using BCPs have been reported, including 15 nm TiO<sub>2</sub> templated using Pluronic F127 in CH<sub>3</sub>NH<sub>3</sub>Pb(I<sub>0.9</sub>Br<sub>0.1</sub>)<sub>3</sub> perovskite-based cells;[125] 7 nm TiO<sub>2</sub> photoanodes templated using Pluronic P123 for use in DSSCs;[126] and porous NiO has been templated using PS-*b*-P2VP and sensitized using “push-pull” organic chromophores for photocurrent generation.[127]

Finally, BCP templating has found use in the patterning of oxide films for heterogeneous photocatalysis. For example, TiO<sub>2</sub> mesoporous films have been templated using Pluronic F127 and Ti(OBu)<sub>4</sub> spin-coated onto glass surfaces and plasma treated.[128] The TiO<sub>2</sub> films were under 100 nm thick and exhibited photocatalytic activity towards the degradation of various pollutants. The films are therefore of interest when constructed directly onto solar cells for cleaning of dirt from the surface and hence ensuring light reaches the underlying semiconductor to generate photocurrent. The combination of BCP templating and plasma treatment produced films of high mechanical robustness and excellent optical transparency, ensuring durability and minimal competitive light absorption with the solar cell beneath.

## 2.4 Summary

For most energy applications involving interfacial electron transfer, surface catalysis, ion intercalation, *etc.*, the structuring of the surface plays a major role in nanodevice performance. Therefore, morphology control of nanoparticles and other hierarchical structures is critical in optimizing device performances. The emergent use of BCPs in directing structuring has already played a considerable role in photo- and electrocatalytic systems, batteries, fuel cells and photovoltaics, as well as other surface applications such as electrochemical sensors. There is now high commercial potential for such energy related materials since power efficient and clean technologies are called for. The continued development of structured electrodes for photovoltaic and battery applications using precise lithography is likely to expand the utility of BCPs in future nanodevices and nanomanufacturing. Additionally, the synthesis of non-oxide nanoparticulate photocatalysts

such as metal sulfides, nitrides and oxynitrides could benefit greatly from the relatively mild conditions employed in BCP-templated particle synthesis, to prevent oxidation. For example, a solvent (*i.e.* acetone) lift-off of a nanoporous BCP derived PS template can be applied after material deposition (*e.g.* sputtering, electrochemical, sol-gel infiltration) of a photocatalytically active material such as CdS[129] to produce a patterned surface of CdS not oxidized to CdO. The potential range of BCP/material/structure combinations suggests that the BCP-templated approach will have enormous impact on energy materials synthesis in the coming years for nanomanufacturing.

## **Section 3. Photonics**

### **3.1 Background**

Photonics is an open-ended description to characterize light-matter interactions, but more specifically the interaction of photons with matter primarily in the visible and near-infrared range. The capacity to precisely engineer light-matter interactions through nanostructured features (also called *nanophotonics*) opens up a myriad of possible uses for advanced computing, medical imaging, optics technology and healthcare sensors.[130] Noticeably, silicon based nanophotonic systems have gained momentum in the research community to augment computing speeds due to scaling limitations of optical lithography.[131],[132],[133],[134],[135],[136] Moreover, the demand to drive structure directing materials like BCPs towards nanophotonics devices is clear, as excellent strategies now exist to build 1D, 2D, and 3D architectures.[137],[138] The periodic nature of features and their nanoscale dimensions imbibed by BCP geometries allows us to explore photon interactions with matter that could have significant appeal for nanomanufacturing purposes. The scope of BCP photonic reports is broad and thus is reflected in this section.

### **3.2 Photonic crystals and metamaterials**

Periodic nanostructures with characteristic sizes close to the visible wavelength are at the basis of the fabrication of photonic bandgap materials. Arranged nanostructures forbid the propagation of light in all directions within a certain wavelength range, and promise both rich fundamental physics and many technological applications including structural colors. On the other hand, the ability to engineer complex nanostructures of characteristic sizes smaller than the visible light wavelengths opens opportunities for nano-antenna and metamaterial research.

Nature has inspired scientists to replicate the striking structural color transformations observed in certain creatures whose textured skin surfaces endow color changes. Specific wildlife exhibit intense static structural colors (butterflies, beetles) or drastic color transformations for camouflage including fish (*e.g.* cuttlefish), reptiles (*e.g.* panther chameleon) and amphibians (*e.g.* salamanders) for survival from predators or to aid opportunities for capturing prey. Such creatures naturally possess a micro- or nano-structured skin that changes to manipulate light and, hence, their structural color. Likewise in material science laboratories, photonic-bandgap materials in one, two, or three dimensions can be fabricated with alternating layers or periodic organization of materials with different optical parameters to intentionally change film colors, *e.g.* a dielectric (or Bragg) mirror[139] or opals.[140] Such fabrication strategies are of particular interest for sensing and display technologies[141],[142],[143],[144] and can avoid toxic dyes and bleachable pigments. Here, reports based upon BCPs and also from brush and dendritic BCPs for photonic crystal (PhC) uses are overviewed. Readers should note that only key contributions on brush BCPs are examined here as Grubbs and co-workers have recently published an excellent review on this topic[145] while a more comprehensive overview on general brush BCP applications has been outlined by Stein and co-workers.[146] The versatility of BCPs to define nanotextures from thin films, typically *ca.* 10-100 nm, to thick films *i.e.* greater than 1 micron, offers the prospect to define similar color modulations as witnessed in Nature. Moreover, the means to modify a BCPs domain spacing and refractive index via chemical interactions or functionalization makes them appealing over photolithography, where traditional resists are typically chemically unreactive limiting further property alteration.

For example, in 2007 Thomas and co-workers reported on the quaternization of lamellar PS-*b*-P2VP (total  $M_n \sim 380$  kg/mol) BCPs showing the flexibility of such polyelectrolyte based BCPs to form responsive photonic gels.[147] The authors described a concept to manipulate PS-*b*-P2VP domain spacing and, therefore, refractive index that could reflect light from the visible-UV region to the NIR region. Later, Thomas' group demonstrated another versatile route to tuning colors via counterion exchange in a lamellar PS-*b*-P2VP BCP.[148] 1D photonic gels with a dry thickness of  $\sim 1$  micron were developed following spin-casting of a 57 kg/mol – *b* – 57 kg/mol (period  $\sim 50$  nm) PS-*b*-P2VP with microdomains oriented parallel to the substrate after chloroform vapor annealing. Following quaternization of the P2VP layers with a hexane solution of 1-bromoethane, the Br<sup>-</sup> counteranions were then replaced

with various ions. Ions with higher hydration energy than  $\text{ClO}_4^-$ , *e.g.*  $\text{SCN}^-$ ,  $\text{I}^-$ ,  $\text{NO}_3^-$ , and  $\text{Cl}^-$ , led to red shifting of the photonic band gap. This work highlighted that with judicious choice of anions and counteranions, full-color tunability could be achieved in an amphiphilic polyelectrolyte BCP. The usefulness of quaternization has also been shown with BCP micelles to form PhCs in BCP micelles[149], PS-*b*-QP2VP hydrogels that possess photoresponsivity leading to wide tunability in the visible range,[150] and a novel process for structural color displays utilizing ink-jet printed BCP PhCs that can be written and erased up to 50 times (see Fig. 9).[151] High molecular weight neat BCPs have been reported for PS-*b*-PI photonic gels, up to 1 M kg/mol in molecular weight, where blue or red shifting was observed depending on polymer concentration.[152]

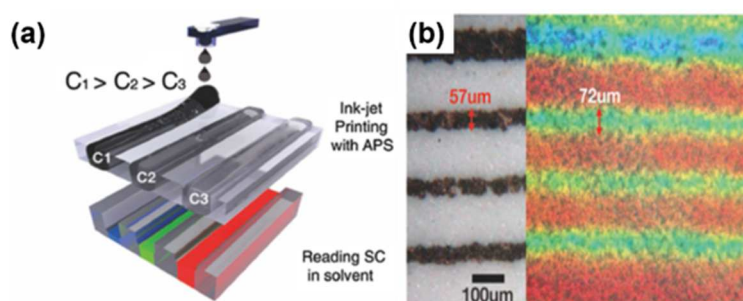


**Figure 9.** (a) Schematic of programmable printing of bottlebrush BCP PhC using a commercial office printer. (b) Optical image of inkjet printed black lines on white paper (left), while the colored image shows the pattern after swelling with ethanol. Image reproduced with permission from Wiley.[151]

A neat demonstration of PhCs was more recently reported by Park and co-workers where they fabricated a 1D PhC based architecture to realize a color responsive strain sensor (see Fig. 10).[153] The elastomeric component of the fabricated sensor changes capacitance under strain. With increased strain the original red color turned blue and the device impressively performed for over 1000 cycles. As outlined above, the stability and reliability of emerging photonic structures is now all-important for nanomanufacturing. In this regard, Noro *et al.* reported the use of mixed ionic liquids [imidazole and imidazolium bis(trifluoromethanesulfonyl)imide] to swell PS-*b*-P2VP lamellar phases, which reflect in the visible range.[154] Critically, the films maintained their photonic behavior even after a duration beyond 100 days, owing to the non-volatility of the constituent ionic liquids.



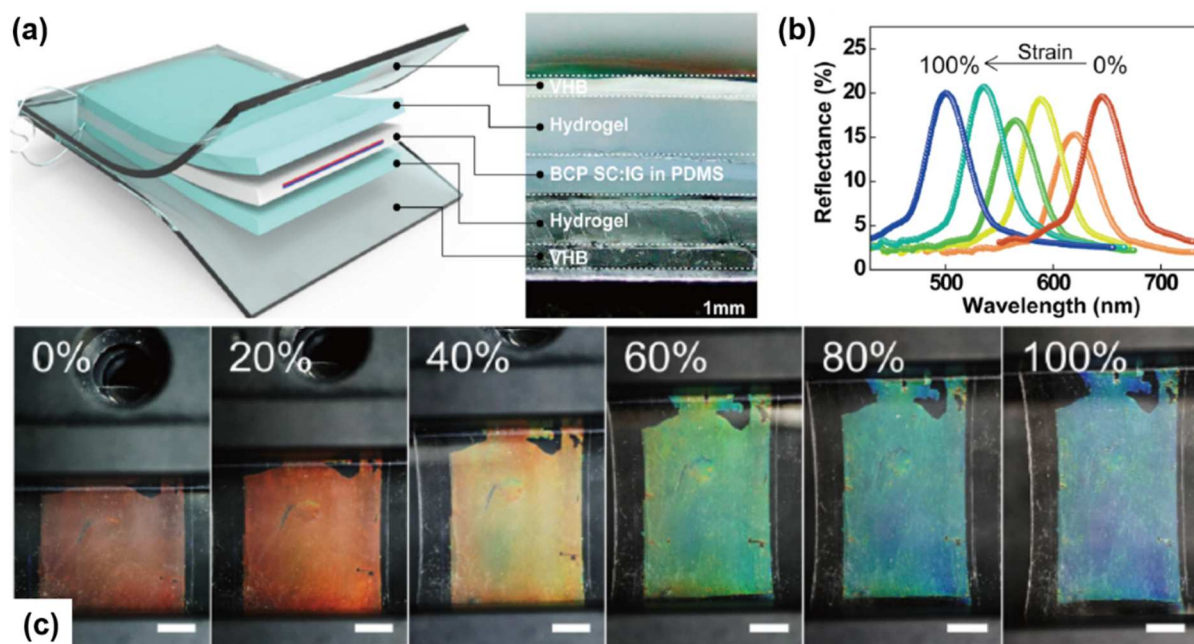


**Figure 10.** (a) Schematic representation of the PhC sensor layers consisting of elastomeric VHB, followed by a BCP structural color: ionic gel (SC:IG) atop another hydrogel and VHB layer. (b) Reflectance spectra showing the blueshift of the device under strain. (c) Photographs of the sensor with applied strain, scale bars are 1 cm. Images reproduced with permission from Nature Publishing Group.[153]

Considering the perceived kinetic barriers of large molecular weight BCPs (discussed further below), brush BCPs have proven an attractive class of macromolecule as side chain modification with bulky components limits chain entanglement thus ensuring both fast self-assembly and large periods. For example, brush BCPs have been utilized to pattern PhC dimensions with respect to visible and near-IR spectrum. Sveinbjörnsson *et al.* reported an effective route to near-IR PhCs via thermal annealing of compressed brush BCPs composed of lactide and styrene macromonomers.[155] The process and experimental approach used are attractive for nanomanufacturing as all materials are commercially available. Moreover, impressive tuning of maximum peak wavelength in near-IR was demonstrated with larger molecular weights (see Fig. 11).

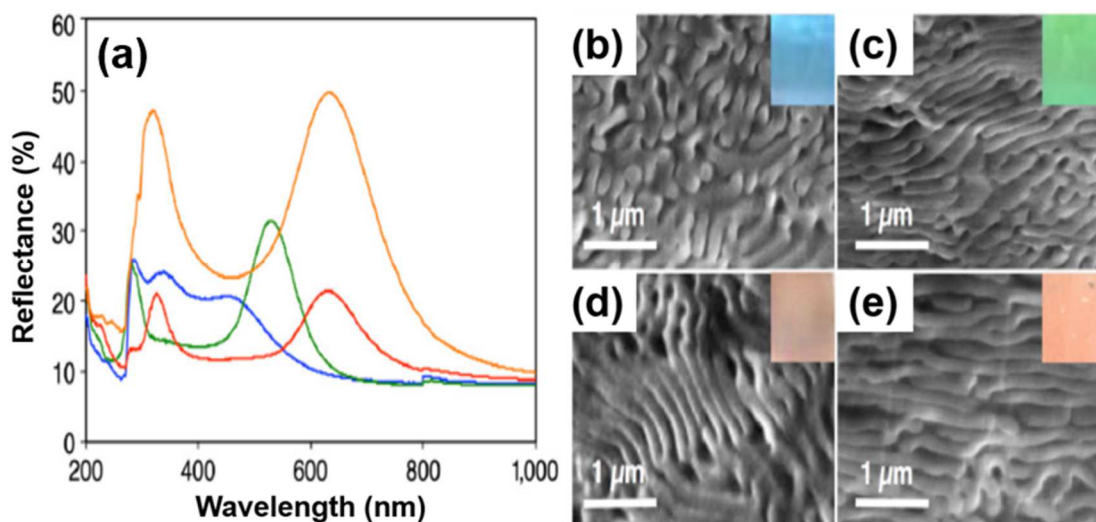


**Figure 11.** (a) Reflection spectra of high molecular weight lactide/styrene bottlebrush BCP ( $2.94 \times 10^6$  g/mol) after controlled evaporation from DCM or THF (blue curve), before (green curve) and after (red curve) thermal annealing, and after thermal annealing under compression. (b-e) Corresponding SEM images are shown for films. Colors of films in images correspond to anneal conditions indicated in (a). Images reproduced with permission from PNAS.[156]

Other notable brush BCP-PhC reports have used rapid evaporative self-assembly (*i.e.* on a scale of minutes) of isocyanate-based brush BCPs to reflect light in the UV, visible and near-IR range,[157] highly-disperse brush BCPs with wide PhC reflectance from 280 to 620 nm due to increasing dispersity and molecular weight,[158] hierarchical PhC pigments with brush BCPs (see Fig. 12 a and b),[159] while  $ZrO_2$  nanoparticles have been infiltrated in PEO based brush BCPs to enhance refractive index contrast.[160]

Moreover, researchers have also reported the fabrication of PhC resins with excellent mechanical properties (*e.g.* hardness as high as 172 MPa and Young's modulus greater than 2.9 GPa) using brush BCPs and phenol formaldehyde resins exhibiting drastically different optical appearances,[161] and more recently handwritable PhCs have been demonstrated using dendronized brush BCPs composed of decyl and benzyl groups.[162]

With regard to nanomanufacturing of nanodevices, speed and throughput are imperative as outlined in the introduction. Thus the key to forming PhCs for large scale use relies on manipulating lamellar sheet domain spacing, thereby changing optical behavior in a rapid manner. While demonstrations have been shown using solvent evaporation techniques as discussed above, these are typically based on a complex interplay between polymer/solvent, substrate surface interactions, humidity, and other environmental parameters. Controlled

strategies to tune domain spacing are therefore very appealing. In this regard, Miyake and co-workers very recently detailed a highly innovative approach introducing the concept of additive manufacturing to 3D print PhCs with BCPs (containing benzyl and alkyl wedge type monomers). Their approach thus endowed structural color changes without the need for commonly employed toxic dyes and pigments (see Fig. 12 c and d).[163] The authors reported a truly sustainable process utilizing rigid-rod dendritic BCPs that were printed using fused deposition modeling to produce PhCs for visible light applications. Readers should note that some of the PhC examples given herein constitute stimuli responsive PhCs, *e.g.* see reference [148],[153]. This is an emerging area that may be applicable for sensing pH, temperature, pressure *etc.* and is discussed in-depth in reference [164].

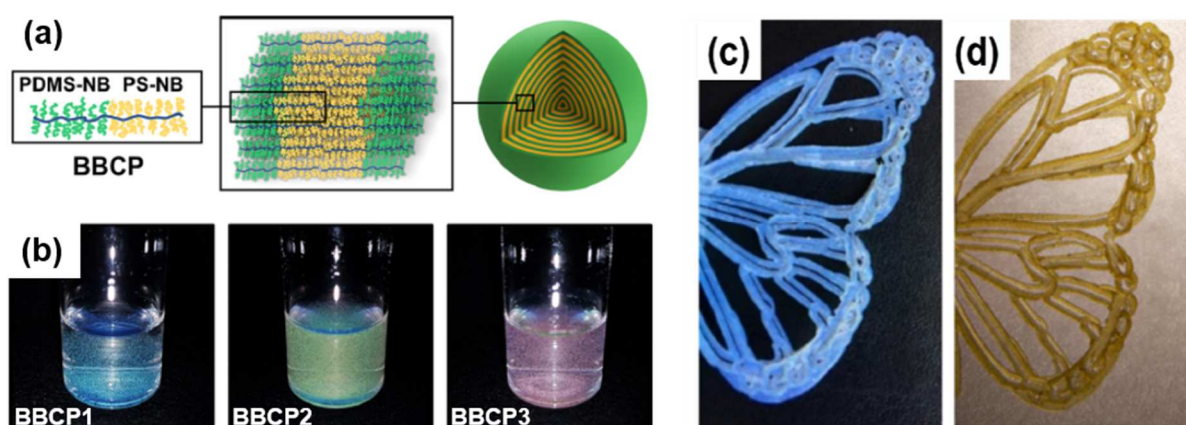


**Figure 12.** (a) Schematic illustration of concentric lamellar structure formed inside a BCP (composed of poly(norbornene)-graft-poly(styrene))-*b*-(poly-(norbornene)-graft-poly(dimethylsiloxane)) microsphere, while (b) Variation of number-average MWs ( $M_n$ ) of BCP with different colors in water suspension of BBCP1 (blue,  $M_n = 3.3$  MDa), BBCP2 (green,  $M_n = 4.1$  MDa) and BBCP3 (red,  $M_n = 7.1$  MDa). Images reproduced with permission from American Chemical Society.[159] Photograph of 3D printed butterfly wing from BCPs in reflection (c) and transmission (d). Images reproduced with permission from American Chemical Society.[163]

Gyroid forming BCPs have intriguing 3D architectures and have also been explored as PhCs. Interested readers are directed to general reviews by Hsueh *et al.*[165] and Wu *et al.*[166] on gyroid BCPs, and their applications, as well as Dolan, Wilkinson and co-workers for a more focused review on optical applications.[167] The unit cell size, symmetry as well as the refractive index contrast all influence gyroidal optical properties. Although the iridescent colors of butterflies' wings are the most commonly used example of the gyroidal morphology,[168],[169] the structural properties were first observed in strontium soaps in 1967 by Luzzati and Spetg.[170] From their initial observation, intense research has revealed the gyroidal morphologies' intricate characteristics, namely their inherent chirality and triply body centered cubic structure. Such characteristics made by gyroidal BCP self-assembly have

led to PhCs exhibiting intriguing optical phenomena. It is also worth highlighting that aside from gyroidal BCPs, Atwater and co-workers have reported the use of two-photon lithography to create gyroid materials using sacrificial polymer templates to examine PhC optical behavior.[171]

With regard to gyroidal BCPs, an early demonstration from 2002 by Urbas *et al.* revealed the ability to form a PhC from a BCP self-assembly strategy.[172] A PS-*b*-PI BCP was employed to form a double gyroid PhC interacting in the visible range based on the difference between the PS/PI blocks and the dielectric contrast between PS/air after the PI block was etched. As a high refractive index contrast (more than 3) is needed to open the bandgap, the authors pointed to the possibility of enhancing the dielectric contrast of constituent material as well as employing other polymer materials to define single gyroid structures. Importantly, in 2018, Chiang and co-workers reported the use of an ethanol swollen gyroid PS-*b*-P2VP BCP template towards visible wavelength PhCs (see Fig. 13 for overall scheme).[173] Whilst the gyroid film was initially colorless in the solid state, exposure to ethanol that increases the lattice spacing turns the films a red hue color, *i.e.* a shift to the visible range, which remained upon drying in the solid state due to a kinetically frozen structure.

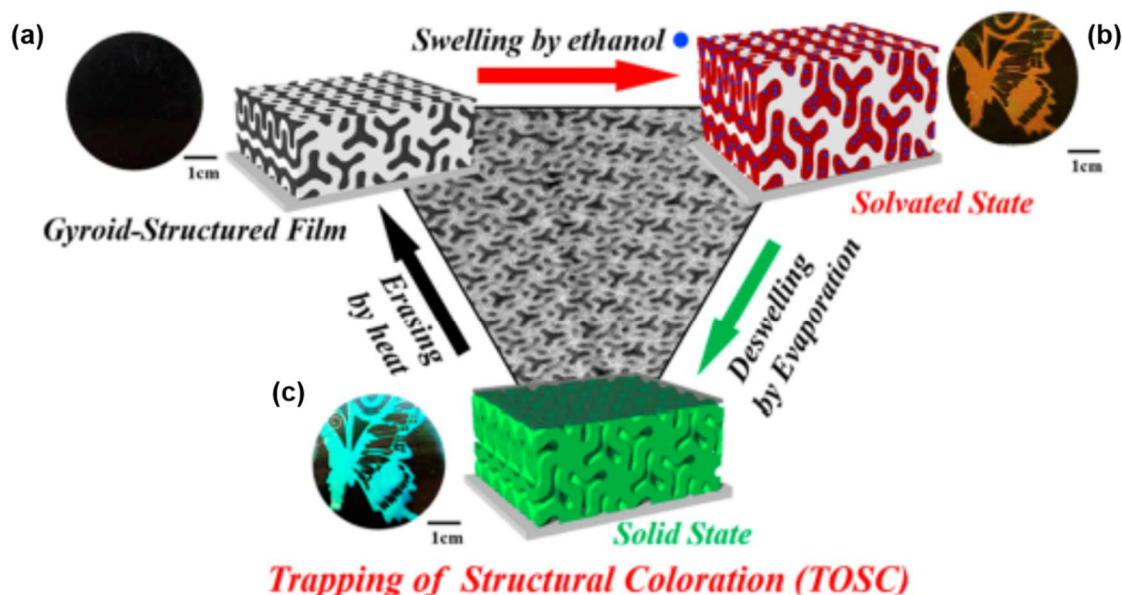


**Figure 13.** Scheme shows route to visible wavelength structural coloration PhC films using PS-*b*-P2VP BCPs. (a) Due to small gyroid unit lattice, the initial PS-*b*-P2VP gyroid film is colorless for visible regime. (b) After swelling in ethanol, and thereby expanding the unit lattice, a red color is induced. (c) Following deswelling after ethanol evaporation, a porous network is formed and maintained with a green coloration. The solid state morphological structure can be returned to its initial state via thermal annealing at 110°C and the decrease of the unit lattice. Figure reproduced with permission from American Chemical Society.[173]

Optical metamaterials have drawn considerable interest due to the fascinating optical phenomena exhibited and their theoretical predictions to design cloaking or super lensing devices.[174],[175] Metamaterial research was instigated by the realization of a negative index material using a split ring resonator by Pendry and co-workers.[176] Given that nanoresonators (also referred to as “meta-atoms” in the field)[177] are the building blocks of metamaterials, BCPs present a framework to tailor desired artificial material surfaces. The subwavelength nature of meta-atoms defines the dielectric permittivity and magnetic permeability,  $\epsilon$  and  $\mu$ , respectively.[178] BCPs are unique soft materials as exquisite precision can be exhibited where geometry, feature size, and alignment can be directly manipulated for tailoring artificial materials as highlighted of late by Gabinet and Osuji.[179] Metamaterials fabricated using BCPs have also garnered significant research interest in recent years. Nanoresonators cause the unnatural properties of propagation or scattering of light obtained with metamaterials, and are at the basis of fabricating artificial media with controlled electromagnetic interactions. Unlike for PhCs, this requires characteristic sizes of the nanostructures significantly smaller than visible wavelengths to avoid diffractive phenomena and rely on effective properties. Such subwavelength dimensions (30-200 nm) are conveniently provided by BCP self-assembled structures, while being challenging for more traditional “top-down” nanofabrication techniques. As for all optical metamaterials, BCP-based structures usually rely on resonant effects such as surface plasmon or cavity resonances, thus requiring noble metal or high index dielectrics, respectively. The composite nature of the final material dictates the choice of a BCP being able to either be partially cleaved away to leave space for a solid component, or have a strong differential affinity for metals or oxides. One should note that Au is an element that features prominently in reports owing to its strong resonance after incident light interactions, *i.e.* SPR (surface plasmon resonance) and LSPR (localized surface plasmon resonance) at the nanoscale. Au is also an attractive element since it is considered a non-toxic highly stable metal[180], particularly against surface oxidation. Au nanoparticles have easily polarized conduction electrons for preferential interaction with electromagnetic waves and production of nonlinear optical phenomena.

The combination of BCP organized nanostructures and plasmonic nanoparticles offers the ability to tailor both real (refractive index  $n$ ) and imaginary (absorption coefficient  $k$ ) optical index of the composite, or equivalently modulate the dielectric permeability  $\epsilon$  and the

magnetic permeability  $\mu$ . Modulating  $n_{eff}$  can lead in some cases to so-called topological darkness, first introduced by Kravet *et al.*, [181] which corresponds to the existence of a dark point in the reflection of a film of the material deposited on a substrate, and enables extreme phase-sensitive plasmonic detection. [182], [183] Other nanostructure-induced properties were demonstrated using materials templated from BCP gyroid phases have been shown to produce nanoporous gold materials presenting enhanced transmission, [184] or linear and circular dichroism. [185]

A surface plasmon is an electron oscillating phenomenon arising from the interaction of light waves with a metal/dielectric interface. Materials exhibiting collective oscillation of electrons (*i.e.* coupled surface plasmons) at the multiple interfaces in a metal/dielectric lamellar stack are colloquially referred to as hyperbolic metamaterials. [182] In hyperbolic metamaterials, two components of the dielectric permittivity tensor  $\epsilon$  possess opposite signs, as if a metal-like behavior was observed in one direction and dielectric-like behavior in another direction, producing a unique extremely anisotropic material. These intrinsic characteristics have seen hyperbolic metamaterials become a burgeoning area with potentially alluring applications in super-resolution imaging, as well as spontaneous and thermal emission engineering. Two architectures for achieving hyperbolic properties currently exist with the required uniaxial symmetry; (i) alternating stacked metal/dielectric layers that exhibit propagating surface plasmons and (ii) assemblies of parallel nanowires displaying collective surface plasmon behavior. They present specific light propagation properties due to a coupling between propagative surface plasmons in adjacent layers/cylinders. An innovative report by Wang *et al.* addressed the stacked metal/dielectric strategy using parallel oriented PS-*b*-P2VP lamellar sheets (center-to-center spacing 28 nm) embedded with 7 nm Au nanoparticles to produce a bulk hyperbolic metamaterial. [186] Their original fabrication methodology allows one to reach well controlled and very high concentration of embedded Au particles and, therefore, tailor the optical anisotropy of the metamaterial.

### 3.3 Metasurfaces

Metasurfaces are the 2D equivalent of metamaterials, and consist of assemblies of resonators (meta-atoms) with a subwavelength total thickness. They are designed to control the phase and amplitude of the transmitted light using the tailored light scattering of the resonators in the thin film. For example, Kim and co-workers reported an original technique to enhance the

effective optical index  $n_{\text{eff}}$  of a thin polymer/gold composite layer via Au nanodot film shrinkage generated from a hexagonal forming PS-*b*-PMMA BCP.[187] After shrinkage, Au nanoparticles possessed an interparticle distance of  $\sim 2.8$  nm (see Fig. 14) with an  $n_{\text{eff}}$  of 5.1 (@ 709 nm) in comparison to the original Au features that exhibited a  $n_{\text{eff}}$  of 1.43 (@ 583 nm) from an interparticle distance of  $\sim 33$  nm.

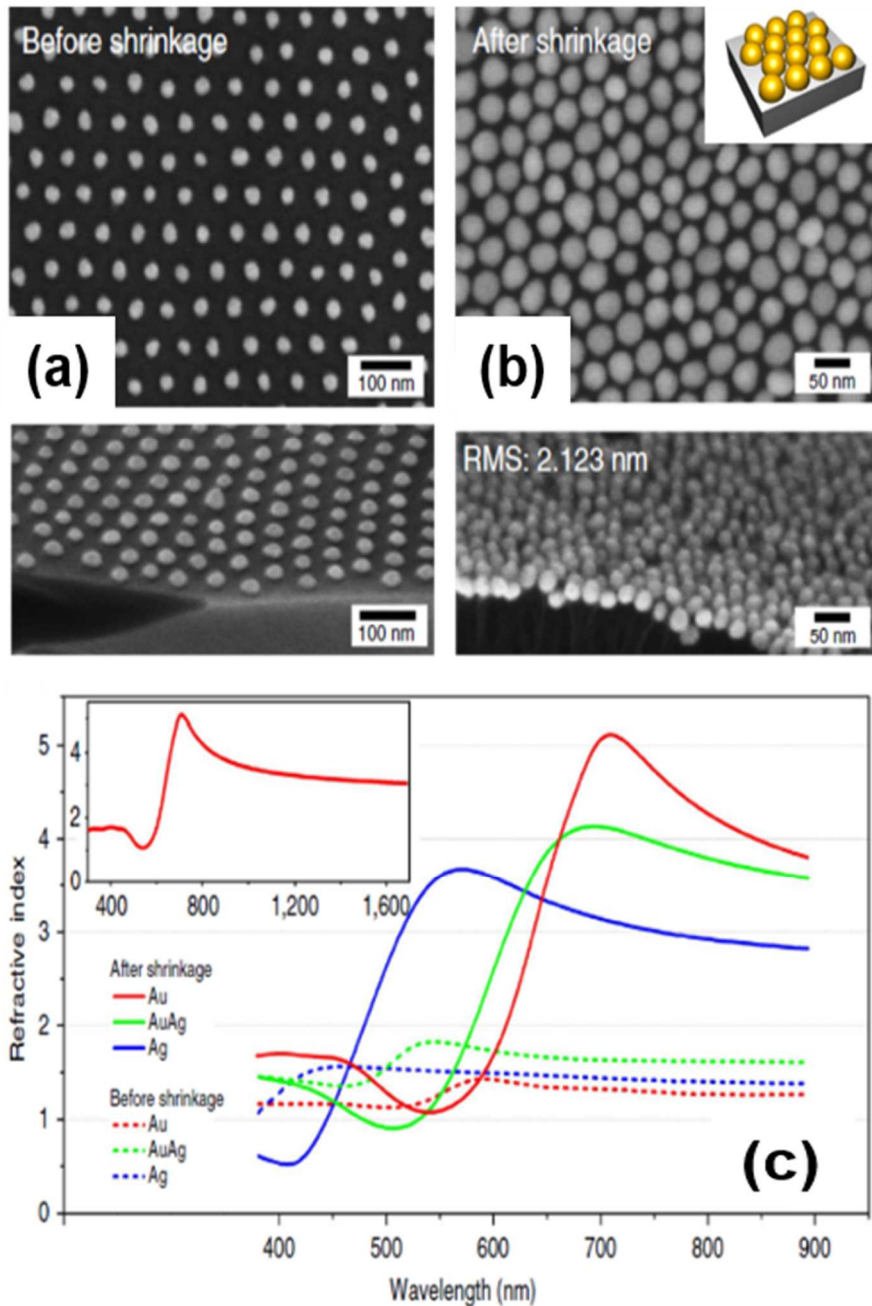


**Figure 14.** (a) Top-down scanning electron micrograph image of Au nanodot pattern from a hexagonal PS-*b*-PMMA BCP before shrinkage. (b) SEM image of Au nanodot pattern after film shrinkage. Cross-section SEM images of both are shown below. (c) Optical spectra of Au, AuAg, and Ag refractive index before and after shrinkage. Images reproduced with permission from Nature Publishing Group.[187]

Their process highlighted the use of metal particles from BCP templates that increased Au density in an effective manner to dictate  $n_{\text{eff}}$ . In a similar vein, Ponsinet and co-workers showed the versatility of a large PS-*b*-P2VP lamellar system with center-to-center spacing of 64 nm to fabricate isolated Au nanoparticle arrays via an immersion process.[188] Well-defined Au features with low metal content (16%) exhibited  $n_{\text{eff}}$  above 3 in the visible range, due to the controlled shape anisotropy of the particles within an otherwise azimuthally isotropic film. Hulkkonen *et al.* have also shown excellent control using PS-*b*-P2VP BCP etch masks to demonstrate porous silicon[189] as a means to tune  $n_{\text{eff}}$  and to template Au nanodomains for perfect absorption.[190] These works illustrated the possibility to induce significant optical effects owing to the nanoscopic structural control inherently associated with BCP templating. Moreover, the structural uniformity derived from BCP templating has been exploited in order to define specific structures of use for surface-enhanced Raman spectroscopy (SERS) substrates. Notable works include the fabrication of Au nanospheres (with SPR observed from 520 to 1000 nm),[191] Au@Ag core-shell nanoparticle arrays capable of tunable broadband enhancement with an enhancement factor greater than 270 compared to Au nanoparticles,[192] and more recently sub-10-nm Au plasmonic nanogap arrays were shown to significantly increase (greater than  $\sim 10^4$ ) the detection of thiophenol.[193]

From these examples, we see that structures of interest lie in a narrow size range, avoiding both the proximity to the visible wavelength, where diffractive effects occur, and dimensions at which metal or dielectric particles are too minute to interact significantly with light (tens of nanometers). In terms of BCP properties, this window corresponds to rather large molecular weights. As mentioned earlier in this section, one existing issue of large molecular weight BCPs is that reptation restricts rapid self-assembly and therefore limits access to large domain and period sizes that are attractive for visible light frequencies. However, recent evidence suggests that large feature sizes in neat BCPs can be accessed in relatively short time scales, *e.g.* less than 60 minutes. Critically, small molecules or polymers, and inorganic or nanoparticle inclusion are not required to speed up kinetics. Patterning large neat BCPs in such short periods are extremely attractive for nanomanufacturing purposes as such materials are at a mature stage from a scientific and technical standpoint. Whilst widely remarked that high molecular weight BCPs are problematic due to kinetic barriers associated with reptation slowing self-assembly, Mokarian *et al.* demonstrated a relatively facile process to pattern a large molecular weight lamellar PS-*b*-P2VP BCP.[194],[195] Notably, the high molecular



BCP required solvent annealing to plasticize the polymer thereby reducing kinetic limitations, but such a process may be undesirable for nanomanufacturing. However, remarkably, they showed that dot patterns that were subsequently used to create silicon nanopillars (with periods  $> 150$  nm and diameters  $> 100$  nm) could reduce reflectivity to almost 0 on the spectral range 400-900 nm, and reflection was  $\sim 1.75$  % at incident angles as high as  $75^\circ$ . Other researchers have also shown great promise self-assembling large neat BCPs,[196] but the obvious scarcity of approaches clearly emphasizes the need to further investigate ways to understand assembly to access large periods and domains for addressing nanomanufacturing concerns. Finally, we stress that polymer-based metasurfaces have the benefit of being easily mass produced over large areas, involve low cost of fabrication infrastructure, and can be deposited on nonplanar surfaces.

### 3.4 Summary

This section has exemplified the assets of BCPs in terms of characteristic sizes and nanopatterning capabilities that now exists for PhC and metamaterial formation that is pertinent for next-generation nanodevices. The reports of lamellar BCP sheets and gyroidal morphologies discussed above have shown extraordinary performance in their ability to manipulate light via both structural tailoring as well as material inclusion *e.g.* metals, dielectrics, *etc.* Moreover, later work examined in this section reflect research interest moving towards metasurfaces from metamaterials. Two key reasons exist for this paradigm shift. Firstly, 2D metasurface nanodevice fabrication is considered more facile than 3D metamaterial fabrication. And secondly, the associated high losses due to the attenuation of light at the output following light travelling through plasmonic metamaterials are highly undesirable. Thus, metasurfaces represent a very appealing means to explore light-matter interactions without considerable losses. Given the existing intricacy of the BCP self-assembly toolbox, *e.g.* alignment of features, multilayer patterning, we foresee many more intriguing optical advances using BCPs in the near future for metasurface fabrication and potentially further exploitation depending on 3D structures, *e.g.* hyperbolic metamaterials. While immense progress has been achieved using BCP materials to manipulate light-matter interactions in the IR and visible regime, functionality in the NIR range has been quite elusive for the most part. Thus, we envisage this as a major challenge to be overcome as our understanding and design of BCP-nanocomposite architectures continues to grow. Also, it is encouraging to see the emerging use of 3D printed and ink-jet printed tools with BCP

materials that integrates nanomaterials with low-cost accepted technologies, which will be a significant platform for nanomanufacturing.

## **Section 4. Environmental**

### **4.1 Background**

The versatility (size, shape, chemistry) of BCP membranes offers excellent capability to address environmental issues. Our environment is continually subjected to forms of waste, *e.g.* solvents causing biological damage in fish life, air pollution harming human health, and more recently discovered “microplastics” and “nanoplastics” that are present in many areas of daily life along with oceans and aquatic ecosystems.[197] Microplastics and nanoplastics are plastic fragments considered smaller than 5 mm and 100 nm respectively. Many studies suggest that microplastics themselves undergo fast nano-fragmentation into particles of micron and smaller sizes.[198] Such waste, present in drinking water, the food chain and the atmosphere is causing inordinate and long-term damage to human and animal life as well as inhabited ecosystems. In order to avoid such outcomes, methods to reduce or eliminate current issues and prevent further waste damage are critical. Nanoscale based technologies have enormous potential to solve certain environmental problems and are poised to make further breakthroughs.[199] Below, we discuss BCP membranes with a view to their implementation in environmental situations and nanomanufacturing.

Membrane separation technologies are increasingly being applied to address pollution of aquatic environments and potable water scarcity *i.e.* water purification and desalination. Desalination of seawater is necessary in many arid regions of the world and even applications such as artificial kidneys rely on polymer-based hollow fiber membranes. Such diverse applications drive continued demand for new membranes with tuneable properties including pore size and morphology, narrow size distribution and stimuli-response properties, critical features that are not offered by homopolymer membranes.[200] Many conventional membrane purification systems suffer inherent limitations attributed to current fabrication methods *e.g.* lack of control over water and solute permeability.[201] The scalability, low-

cost, flexible feature size and the wide range of material choice offered by BCPs makes them promising candidates for use as effective filtration devices in environmental based applications. Ultrafiltration membranes for water purification should address several demands such as high mechanical strength, high permeability and selectivity and resistance to fouling. This section focuses on progress over the last few decades where BCPs have been applied as filtration media and as surfactants to facilitate water purification, desalination and remediation. The two general BCP based separation techniques are: 1) Surfactant based separation (micelle capture of solute). 2) Non-porous and porous BCP rigid membranes.

#### **4.2 Surfactant separation**

Non-volatile pollutants originating from industrial activities that enter water streams are challenging for liquid-liquid (L-L) based extractions. Using BCPs in aqueous solution can overcome two main drawbacks commonly associated with L-L extraction: (i) difficulty in regeneration of the effective extractant liquid and (ii) the presence of an equilibrium concentration of extractant liquid dissolved in the water stream being treated. Early experiments showed that BCP aggregation behaviour in water increases the solubility of hydrocarbons.[202] A micelle-forming di-BCP in solution consists of a segregated core region consisting entirely of the *A* block and a shell region consisting of the solvent and the solvent compatible *B* block. Hurter and Hatton demonstrated that the effective solubilizing potential of BCP micellar solutions can be exploited to remove and recover non-halogenated, halogenated, polyaromatic and aromatic hydrocarbons from contaminated groundwater sources and industrial effluents.[203] Linear block copolymers capable of forming tight micelle structures were found to be the most effective for solubilization, with the solutes being concentrated in the hydrophobic micelle core (see Fig. 15 a). BCP micelles based on PEO-*b*-PO and PS-*b*-PVP are effective for solubilization of aromatics but ineffective for aliphatic based compounds.[204] It was found that the solubilize that is more compatible with the polymer block that constitutes the core of the micelle is selectively solubilized. Solubilizates that are good solvents for the block constituting the micellar core are solubilized in large quantities. For example, BCP micelles in mixtures of benzene and hexane will selectively solubilize benzene. Therefore, tuning of the BCP block chemistry allows easy separation of polar and non-polar species to separate various kinds of mixtures and represents a key advantage compared with non-BCP based surfactants.

An effective separation approach that retains the BCP while remaining permeable to small molecules is however required from a practical separation standpoint. The micellar enhanced ultrafiltration (MEUF) technique combines the extraction properties of BCP aggregates with the capability of ultrafiltration membranes.[205] Similarly, the use of hollow fiber membranes allows a semi-permeable barrier between the BCP solution and the polluted stream, a process known as pertraction *i.e.* permeable to compounds being extracted but impermeable to BCPs (as shown in Fig. 15 b). Work by Keurentjes[206] studied various molecular weights of tri-BCPs for exploring the extraction properties on organic pollutants from aqueous streams. For example, extraction of naphthalene, a polycyclic aromatic hydrocarbon and known carcinogen, was performed using PEO-*b*-PPO-*b*-PEO (L64, P103, P104) with the effect of temperature and concentration on the molecules investigated. Creating a solution that consists entirely of micelles can maximize extraction potential and is performed by controlling the critical micelle temperature (CMT) and the critical micelle concentration (CMC).[207] This is imperative for applications where solubilization occurs at room temperature. P104 forms stable micelles capable of solubilizing significant quantities of hydrocarbon at room temperature (see Fig. 15 c). Crystallization of the naphthalene occurs when the saturated solution is cooled from 30<sup>0</sup>C to 10<sup>0</sup>C and following simple filtration > 99% of the naphthalene was recovered from the polymer without any measurable loss of the BCP.

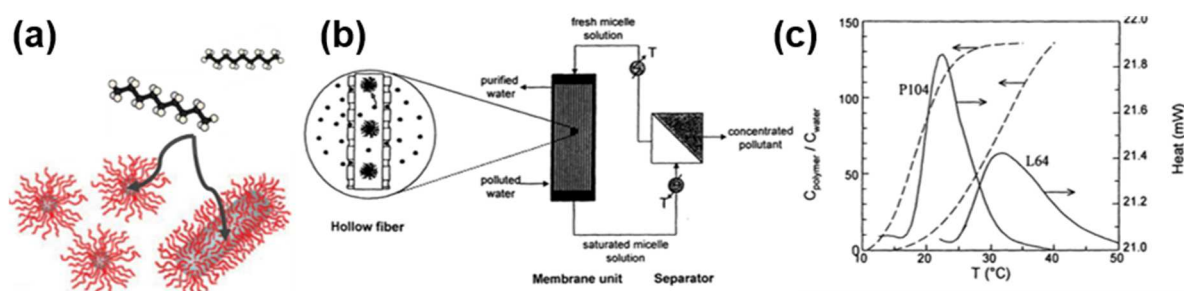


**Figure 15.** (a) BCPs forming tightly packed micelle structures with the pollutant concentrated in the hydrophobic core. (b) Pertraction based separation process that utilises BCP micelles embedded in hollow fiber membranes allowing effective recovery and reuse of the polymer. (c) Solubilization transition for BCP based on micelle concentration and size. Pollutant extraction and recovery of the polymer is easily achieved by tuning solution temperature. Panel (b) and (c) of figure are reproduced with permission from American Chemical Society.[206]

Tuning temperature of BCPs to form micelles in this way allows extraction of organics within hollow fiber membranes. The molecular weight of the hollow fiber membrane should be smaller than the molecular weight of the BCP surfactant but significantly larger than the pollutant. Thus, the pollutant has easy passage through the hollow fiber membrane, while the

BCP is contained within. Regeneration of the pollutant-free micelle solution is easily achieved by cooling the loaded micelle solution which forces the organic pollutant to separate from the BCP (Fig. 15 c). The pollutant phase can easily be removed using a simple separator unit. PEO-*b*-PPO-*b*-PEO BCPs (P104) have been used effectively for extraction of organic pollutants. Above a critical transition temperature, the solubilization of naphthalene in solution can increase up to 135 times the solubility in water due to an increase in micelle radius.

The use of BCP surfactants can also be implemented where removal of organics from soil and aquifers is important. Pump and treat remediation methods are relatively ineffective for cleaning soils and aquifers that contain hydrophobic nonaqueous phase liquids. In 2001, Lee *et al.* demonstrated effective removal of toluene (80% removal after 5 washes) from sand with no emulsion present and full recovery of surfactant solution using poly(oxypropylene)-*b*-poly(oxyethylene) (POP-*b*-POE).[208] BCP recovery was performed using hexane to remove the toluene. Reuse of surfactant is essential for cost-effective use of the technique. The results demonstrated that a BCP surfactant can be more effective than other non-BCP surfactants tested. In 2015, Langer and co-workers reported photoinduced precipitation of amphiphilic BCPs for extraction of pollutants from water and contaminated soil.[209] The research shows UV irradiation will alter the BCP colloidal stability to rapidly convert from nanoparticles to stable macroscopic aggregates which can readily capture pollutants. This novel method produced efficient removal of hydrophobic pollutants in small-scale experiments on wastewater and contaminated soil.

In recent years emerging sources of organic contamination including pharmaceuticals, food additives, industrial compounds, *etc.*, in aquatic ecosystems are an ever-increasing issue. In 2019 a novel technique using P4VP-*b*-PEO was applied for coating cellulose nanofibers where the BCP is dispersed to act as an adsorption film.[210] The method allows removal of any pollutant with electron deficient aromatic structures such as antibiotics, *e.g.* sulfamethoxazole (SMX). Adsorption is achieved by  $\pi$ - $\pi$  interactions between the pyridine and the electron deficient phenyl group of the SMX. Release of the adsorbed contaminant is performed by simple elution process (ethanol wash) allowing reuse of the films. BCP block selection can be exploited in this way to remove a wide range of these emerging contaminants in aquatic systems. This is a promising application of BCPs which have shown to be of substantial importance for water remediation due to their reusability and direct

application in the adsorption of hydrocarbons extending even to electron deficient aromatic compounds. However, further research is required to engineer novel BCP systems capable of large-scale water remediation which require extraction of a myriad of organic pollutants for nanomanufacturing.

### 4.3 BCP rigid membranes

Recent perspectives by Nunes and co-workers[211],[212] summarise some of the advantages and versatility endowed through using BCPs as membranes in water based applications. The two main techniques used for BCP pore generation are (i) film casting with selective block sacrifice and (ii) self-assembly and nonsolvent induced phase separation (SNIPS) – a promising, fast and scalable manufacturing technique due to its production alignment with industrial membrane fabrication. The type of membranes widely used in water purification and chemical processing suffer an omnipresent trend, high permeability results in low selectivity and vice versa.[213] Filtration technologies involving nonporous membranes (Ångström scale separations) such as water desalination[214] and gas separations[215] function via the solution diffusion mechanism.[216] However, the variable size of the free volume elements through which diffusion occurs hampers membrane performance. For non-porous membranes, charged BCPs have shown potential use in fabricating charge-mosaic membranes (CMM) which consist of oppositely charges alternating nanosize domains. This permits greater permeability to dissolved ions than small neutral molecules. Work by Ishizu *et al.* used AB and BAB PS-*b*-P4VP BCPs to create CMMs.[217],[218] The membrane was prepared by casting the BCP to form lamellar and spherical templates and reactions performed to quaternize the P4VP and sulfonate the PS domains to produce cationic and anionic domains. PS-*b*-poly(butadiene)-*b*-P4VP (PS-*b*-PB-*b*-P4VP) fabricated CMMs have shown substantial cation-exchange and anion-exchange capacities with the membranes highly permeable to electrolyte ( $J_{KCl} = 2.10 \times 10^{-8} \text{ mol/cm}^2\text{s}$ ).[219] Pentablock copolymers[220],[221] have been used to prepare CMMs in a similar fashion and are available commercially (NEXAR polymers). Research on CMMs has been very limited since these studies in the late 1980's and early 1990's and have been described in review.[222]

BCPs have recently shown promise for use in another type of non-porous membrane that combines aquaporins with BCPs (see Fig. 16 a and b). The aquaporin (or water channel) is a protein-based membrane that acts as a “plumbing system for cells”, allowing water to rapidly move into and out of a cell while preventing the passage of other solutes including ions and

protons. Aquaporins are responsible for urinary concentration in the kidney and control water balance in the body.[223] The use of these biomimetic membranes is attractive due to the possibility of realizing the large water fluxes available to biological systems. Work by Stoenescu *et al.* in 2004 was the first approach to induce a directed insertion of aquaporin proteins into ABC tri-BCPs.[224] A finding of the study is that orientation of the proteins could be tuned in the ABC membrane, producing directional functionality in BCP vesicles. Aquaporins have been demonstrated to work in an analogous manner to those present in biological membranes. An account of the interactions between aquaporin proteins and BCP matrixes can be found in the literature.[225] This continues to be an active area of research and improvements over the past decade have been reviewed.[201],[226] A study by Shen *et al.* in 2018 produced high permeability, with sharp selectivity, artificial water channel-based BCP membranes.[227] The fabricated membranes have a molecular weight cut-off of ~500 Da, a size range that is challenging in current commercial membranes. The design, inspired by the aquaporin found in the cell membranes of mangrove roots, uses peptide-appended pillar[5]arene (PAP) artificial water channels with a pore size of ~5 Å (as shown in Fig. 16 c). The PAP channels are embedded in amphiphilic BCPs (PB-*b*-PEO) forming lipid-like bilayer structures, as displayed in Fig. 16 d. The BCP supported structures offer superior chemical and mechanical stability[228] compared with techniques that embed PAP channels in lipid bilayers which are unsuitable for large scale applications.[229] This state-of-the-art technique can produce membranes with permeability an order of magnitude better than commercial membranes while maintaining close to the ideal selectivity from a membrane with 5 Å pores ( $65 \text{ Lm}^{-2}\text{h}^{-1}\text{bar}^{-1}$  vs  $4\text{-}7 \text{ Lm}^{-2}\text{h}^{-1}\text{bar}^{-1}$ ). Nanomanufacturing of PAP based BCP materials may solve various current fabrication challenges. The use of PAP artificial water channels embedded in BCPs addresses cost and availability issues with aquaporin that are required for large scale membrane integration. This emerging technology utilizing protein infiltrated BCP systems is both exciting and has potential for realizing a route towards a commercial high performance membrane filtration device.

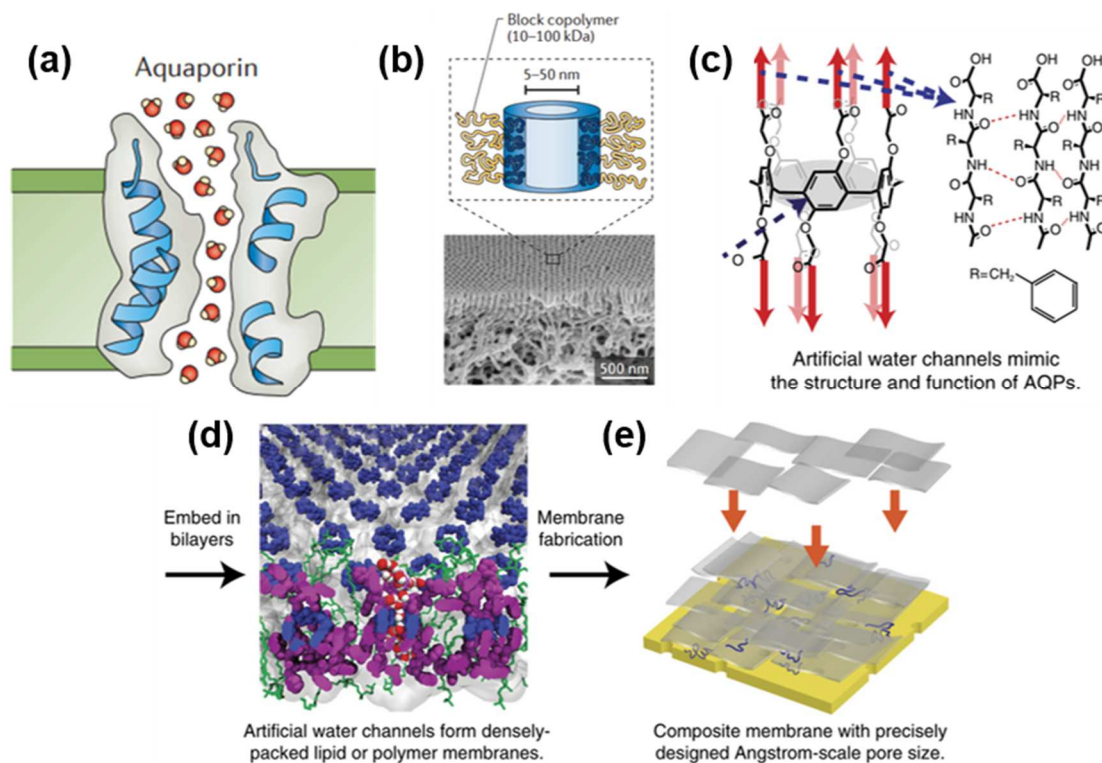


**Figure 16.** (a) Aquaporin is a protein-based membrane that acts as a “plumbing system for cells”, allowing water to rapidly pass through. (b) BCPs template for aquaporin incorporation. (c) Peptide-appended pillar channel is an artificial protein that mimics functionality of aquaporin’s with 5 Å pores. (d) PAP embedded in amphiphilic BCP bilayer and (e) large scale membrane integration. (a) and (b) are reproduced with permission from Macmillan Publishers Limited[201] and (c) - (e) reproduced with permission from Nature Publishing Group[227]

SNIPS is a very promising approach to generate porous BCP membranes due to its industry ready integration - *i.e.*: if the desired BCPs are available with narrow molecular weight distribution at competitive costs, scaling-up will not be problematic since the technology requires the same equipment currently used to produce commercial asymmetrically porous membranes. The SNIPS process was recently reviewed in the literature and interested readers are referred to references [200],[211]. Ultrafiltration membranes manufactured using the SNIPS technique are typically in the 20 - 70 nm range, see Fig. 17 a. Compared to the standard fabricated homopolymer membranes as shown in Fig. 17 b, BCP membranes have the potential to advance water treatment technologies due to their ordered nanostructures and myriad of chemical functionalities. A BCP nano-filtration membrane has been obtained with pore sizes as small as 1.5 nm, rejecting solutes of 600 g/mol at neutral pH with remarkably high flux of  $432 \text{ Lm}^{-2}\text{h}^{-1}\text{bar}^{-1}$ . [211] The SNIPS process may be the process with the fastest development and possesses the most potential for early industrial implementation since the process uses classical instrumentation of commercial membrane manufacture with innovative materials. The state of the art, developed by Nunes and Peinemann[230] using the SNIPS fabrication approach has achieved water fluxes of over  $3200 \text{ Lm}^{-2}\text{h}^{-1}\text{bar}^{-1}$ , an order of



magnitude higher than commercially available membranes with similar pore sizes. The work uses PS-*b*-P4VP to generate a membrane for selective separation of proteins. Further, the membrane is not limited to size-based separation but is also sensitive to different charge states. This is achieved by block quaternization to allow pores in the membrane to act like “on-off” gates. The potential here is considerable as these membranes can be extended to applications that demand both size-selective and charge based separation. Abetz and co-workers have pioneered a SNIPS approach for fabricating thin isoporous membranes.[231],[232],[233] By implementing a highly diluted one solvent system to reduce BCP consumption and minimize production costs compared to standard blade casting with a 6-fold increase in water flux (vs conventional membranes). The roll to roll process is capable of accommodating any conceivable membrane dimension. Other SNIPS approaches demonstrate pore size in the range of 3-4 nm with a molecular weight cut-off of 1.5 kg/mol, outstanding fouling resistance and high water permeance.[234] Wang and co-workers have demonstrated a ‘green’ selective swelling membrane fabrication process by using less aggressive solvents assisted by microwave swelling of polysulfone-based BCPs.[235] Importantly, they have shown the scalability of the process at pilot scale. Wang’s group have developed a spray coating deposition technique combined with selective swelling to tune thickness, pore size and hydrophilicity of membranes.[236]

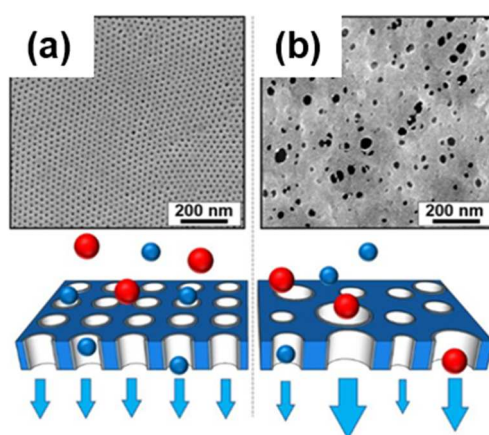


**Figure 17.** (a) Self-assembled BCP membrane and (b) commercial membrane fabricated using standard phase separation process. The blue and red spheres represent solutes of varied size filtered from solution. Image reproduced with permission from Nature Partner Journals.[200]

Cussler and co-workers have highlighted the potential that BCP derived nanoporous membranes have for commercial ultrafiltration.[237] Their work describes quantitatively how gas and liquid water are transported through BCP derived nano-channels. Liquid water flow in a cylindrical BCP nano-channel is laminar and consistent with the Hagen-Poiseuille law, while diffusion of gases is quantitatively consistent with Knudsen diffusion. Consequently,

both large hydraulic permeability and sharp molecular weight cut-off can be realized for a commercial BCP derived membrane. These membranes can be readily engineered to exhibit stability and robustness for high pressure applications or use in solvent media. Improving robustness in membranes can be done by a simple selective crosslinking process via UV irradiation and may allow membrane deployment in harsh filtration conditions such as high temperature, pressure and strong acidic or basic solutions.[238] Hillmyer and co-workers developed mechanically robust dicyclopentadiene BCP-derived nanoporous membranes by selective solvent etching of polylactide containing BCPs.[239],[240] Combining polymerization-induced self-assembly (PISA) with a “doubly reactive” block copolymer created a nanoporous membrane with both a percolating pore structure and substantial mechanical strength. The resulting porous structure (40 % void made of 14 nm pores) is isotropic meaning that permeability is independent of alignment – features which allow good selectivity and fast fluxes. In other work by Hillmyer, bicontinuous polyethylene membrane structures were fabricated using a BCP precursor.[241] The polyethylene membranes are chemically and thermally robust with very high porosity. Recent work in 2019 by Yang *et al.* developed a cheap, safe, reproducible, one-pot synthesis process using PISA synthesis on a series of BCPs to produce highly porous inverse bicontinuous phase membranes.[242] Tuning the degree of polymerization of the core-forming styrene (St) with N-phenylmaleimide (NMI) P(St-*alt*-NMI) block can achieve highly asymmetric copolymer compositions and allow a simple route to an inverse bicontinuous phase. Other researchers have used PEG-*b*-PI to generate inverse bicontinuous cubic mesophases.[243] Cross-linking of the PI chains via UV irradiation (365 nm) realized high structural membrane integrity in organic solvents. We note that the bicontinuous membrane approach remains attractive due to less stringent phase segregation demands compared to anisotropic BCP derived membranes. A route to produce robust reinforced water filtration membranes (24 nm pores) has also been reported by casting the BCP derived templates on rigid poly(ether sulfone) support membrane, see Fig. 18 a and b.[244] Fig. 15c shows the superior selectivity of the PS-*b*-PLA templated filtration membrane with a sharper rejection curve than for traditional phase inversion membranes.[240] BCP templating on support membranes is an active area of research with recent work demonstrating micellar forming PMMA-*b*-PSBMA cast and self-assembled on top of a commercial poly(vinyl difluoride) membrane.[245] Mean pore size of the membrane was ~ 26 nm with stability up to an applied pressure of 4 bar.

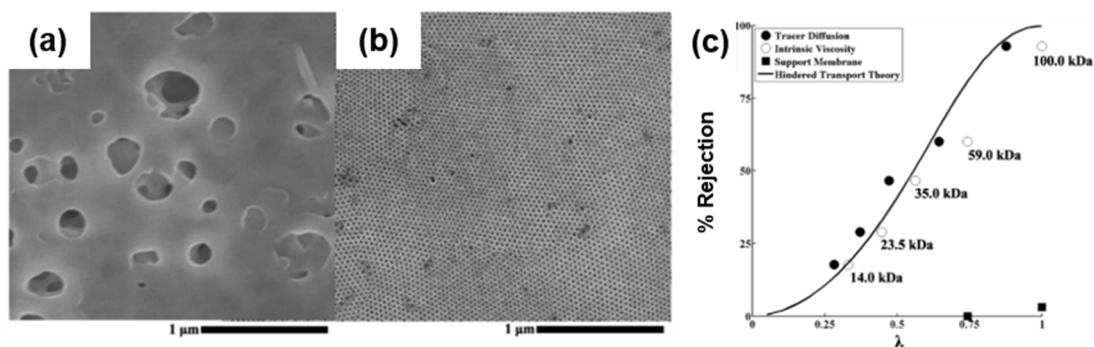


**Figure 18.** (a) Poly(ether sulfone) support membrane with (b) thin nanoporous (~24 nm pores) PS-*b*-PLA templated selective layer coated on top of the membrane support. (c) The resulting rejection curve for single solute PEO solutions used to challenge the membrane. The membrane has a sharper rejection curve than traditional phase inversion membranes. Images reproduced with permission from American Chemical Society.[244]

Siegel and co-workers demonstrated a clever approach to fabricate a composite ultrafiltration membrane by combining a thin (100  $\mu\text{m}$ ) silicon support membrane layer with a nanoporous BCP film (see Fig. 19). [246] The method uses well established fabrication processes to create microchannels in the silicon support. This technique affords both nanoscale size exclusion and fast transport. The authors reported a ~50-fold increase in selectivity compared with a commercial anodized alumina membrane (that possessed 200 nm pore sizes). Given the rigid support layer of these composite nanoporous membranes, we would expect robustness for a myriad of filtration applications. In particular, the microfabrication process for the support membrane makes deployment of these composite membrane amenable to scale-up through nanomanufacturing and integration for a range of devices.

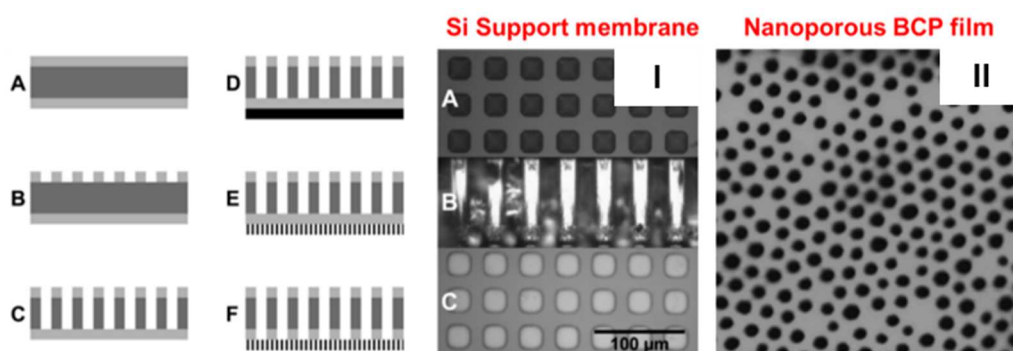


**Figure 19.** Fabrication scheme for a composite membrane (left hand side). The dark grey represents a 100  $\mu\text{m}$  thick silicon wafer with micro sized pores etched through the wafer via photolithography and reactive ion etch. A BCP is coated on the etched wafer (black line), phase segregated and etched (via reactive ion etch). (I) SEM images of the microporous silicon support showing top, cross section, bottom view and (II) the nanoporous BCP film with 40 nm pore diameter (image is 1  $\mu\text{m}$  square). Images reproduced with permission from American Chemical Society.[246]

Russell and co-workers developed a simple approach to tuning pore size in a BCP membrane.[247] Selective swelling of the PMMA block in a film of PS-*b*-PMMA resulted in

rapid contraction of the PMMA microdomain to generate uniform well defined pores. Thick films of the BCP (200 nm) were thermally annealed to produce PMMA cylinders (21 nm diameter) in a PS matrix. The pore size was readily tuned by swelling in acetic acid over various timescales (PMMA selective). Hexagonally packed pores formed in the PS matrix with size varying from 8 - 18 nm over exposure times of 30s - 60 min. The membrane showed excellent ultrafiltration performance when tested using Au nanoparticles (5 - 60 nm) dispersed in DI water at a pressure of 1 bar. Impressively, all nanoparticles over 30 nm were rejected by the membrane by all the BCP membranes tested. Most methods we have discussed thus far involve direct use of the phase segregated BCP as the main filtration media. We believe an industry ready approach for converting a phase segregated BCP template to form an inorganic ultrafiltration membrane is required for many applications *i.e.* a membrane structure that is robust in thermally, chemically or mechanically demanding environments. In this regard, Greil *et al.* demonstrated the use of sequential infiltration synthesis (SIS), an atomic layer deposition process, to modify PS-*b*-PMMA BCPs and replicate the neat structure to produce well-defined ultrathin (< 50 nm) alumina membranes.[248] Interestingly, in their study of saturated vapors permeating through the alumina membrane, they observed a deviation from Knudsen diffusion that became more pronounced with smaller pore sizes. The designed alumina template demonstrated selectivities as high as 7:1 for vapors of acetone and ethyl acetate. Nealey and co-workers also used the SIS strategy for converting cylinder forming PS-*b*-PMMA templates into alumina ultrafiltration membranes.[249] Selective metallization of the PMMA block across large areas was achieved (16 nm pore size demonstrated). The nonhomogeneous depth profile (gradient in Al<sub>2</sub>O<sub>3</sub> content through pore depth) of the fabricated membrane is ideal for separation applications. Protein separation with high flux and high selectivity was demonstrated by combining the SIS fabricated alumina membrane with an AAO support structure. Developing inorganic membranes, as described in these latter two cases, could broaden the prospects of advanced functionality integrated in a single design.

Fouling resistance is fundamental to longevity of an ultrafiltration. Various approaches by Hillmyer for tuning hydrophilicity in the membrane have been used to reduce pore blocking. For example, a PS-*b*-PDMA-*b*-PLA terpolymer was used to fabricate membranes and etching of the PLA block exposed the PDMA to produce a structure with hydrophilic pore walls rendering the membranes more fouling resistant.[250],[251] Other approaches involved blending PS-*b*-PEO and PS-*b*-PLA and etching the PLA to fabricate the hydrophilic

wall,[252],[253] or by annealing PEG-*b*-poly(sulfone)-*b*-PEG membranes to produce anti-fouling properties.[254] A very recent strategy demonstrated zwitterion-functionalized membranes with excellent fouling resistance.[255] The poly(2-dimethylaminoethyl methacrylate)-*b*-PS BCP membranes were soaked in ethanol and 1, 3-propanesultone exhibited several times higher water permeance than non-zwitterionized membranes. The excellent fouling resistance was attributed to the creation of a zwitterion-functionalized membrane surface that improved hydrophilicity.

#### 4.4 Summary

The progress highlighted in this section represents the considerable promise for using BCPs to nanomanufacture both surfactant and rigid membrane separation and filtration nanodevice technologies. By exploiting BCP morphology, a wide array of technologies can be realized for surfactant and rigid membranes. Surfactant based separation techniques are typically driven by BCP micelle capture of a solute and are advantageous for non-volatile pollutants and L-L based extractions. A myriad of pollutants can be selectively extracted by tuning the chemistry of the core forming block. The ease of separating polar and non-polar species represents a key advantage compared with standard surfactants. The BCP can also be readily recovered for reuse by altering the CMT. Given these advantages, BCP surfactants are well positioned to assist purification of small-scale aquifers, ground water systems, industrial effluents and aquatic ecosystems however we envisage upscaling to large water sources as currently prohibitive. There is immense potential for rigid membrane filtration applications afforded by the scalability, low-cost, flexible feature size and the wide range of material choice offered by BCPs. Extraordinary performance has been made in nano-filtration by implementing intricate design philosophies that combine BCP nano templates with aquaporin inspired artificial proteins. To be competitive in the ultrafiltration area, membranes typically require high selectivity and permeability, mechanical integrity, and resistance to fouling.[244] BCP defined membranes possess enormous potential to achieve all of these requirements owing to their versatility for high porosity, pore size distribution, high selectivity and tunable chemical and physical properties.[256] Recent progress utilizing the SNIPS process is encouraging for nanomanufacturing with state-of-the-art membranes achieving water fluxes over  $3000 \text{ Lm}^{-2}\text{h}^{-1} \text{ bar}^{-1}$ , an order of magnitude higher than commercially available membranes with similar pore sizes. Given the enormous challenge required for upscaling nanofiltration technologies to address environmental restoration, we envisage bottom-up fabrication processes like SNIPS as key to realizing large scale

deployment. Cost-effective manufacture of innovative BCP derived filtration membranes is possible due to compatibility with existing instrumentation used for commercial membrane manufacture. A white paper by the International Food Policy Research Institute describes a model predicting water quality deterioration through 2050 and shows the effects of drier climates, with 1 in 5 people at high risk of water pollution.[257] Given impending climate change scenarios, and considering economic and population growth projections,[258] further research to develop BCP derived separation technologies for securing many of the worlds future water supplies are needed now more than ever.

## **Section 5. Biological**

### **5.1 Background**

Soft-templating strategies capable of defining encapsulated materials in solution as well as nanoscale features serve as viable paths for enhanced sensitivity and performance for biological applications. In this section, BCPs in solution are examined initially, with a particular focus on materials for targeted drug delivery, wound healing and tissue engineering. Considering the possible permutations of BCP species in solution, *e.g.* micelles, vesicles (also referred to as polymersomes, readers are directed to reference [259] for a detailed review on same), spheres, *etc.* (see introduction), this section does not aim to be comprehensive but rather a guide to the field and extensive literature. Thus, we provide the reader with a cognizant view of BCP structures in solution (including injectable BCP hydrogels that are of particular interest given that they avoid surgical procedures[260]) with biological uses, thereby emphasizing the role BCP chemistry plays to endow specific functionality.

Following the BCP solution centred work we focus on BCP derived thin films with templated features and etched structures that have been utilized as biosensors, membranes for drug delivery, and antimicrobial surfaces are described. The latter section provides an insight into the myriad of bio-related applications that are now achievable with BCP materials in thin films. Moreover, with the increased focus on developing point-of-care diagnostic[261] and wearable technologies[262], creating tailored physiochemical nanoreactors hold significant value for drug delivery and high performance sensors. Thin film BCPs offer a low-cost and wafer scale templating methodology to define materials to sense a range of biochemical analytes.[263] BCP features (~ 5-50 nm) are similar to the dimensions of gas and biological

species thereby increasing detection limits. Additionally, the diverse material sets that can be patterned from BCP templates provide broad scope for sensing specific analytes. Nanostructuring features at substrate surfaces allows one the creation of label-free sensors where surface plasmon interactions can be used to identify analytes. The inherent sizes accessed through BCP self-assembly also open a promising route to dictate biomolecule interactions at surfaces with nanomanufacturing use.

## 5.2 Biorelated solution based BCPs

BCP solution based bioapplications embody one of the strongest areas to witness polymer synthesis progress and applicability. The polymerization toolset available to uniquely “dial-in” specific BCP geometries and dimensions with contemporary synthetic approaches combined with diverse chemical block functionality enables the formation of various objects with controlled size and shape. This is critical, especially for nanomedicine or nanocarrier uses where the complex interplay of drugs with the human body’s temperature, pH, and ion makeup must be evaluated.[264],[265],[266] Thus, polymers with distinct pH/temperature dependent phase transitions are advantageous.

Biocompatible thermoresponsive copolymers *i.e.* polymers that undergo a drastic physico-chemical behavior with moderate temperature changes in aqueous solutions are well-studied for biomedical uses.[267] Fig. 20 displays an example of such a transition in a study reported by Armes and co-workers on the ability to sterilize poly(glycerol monomethacrylate)-*b*-2-poly(hydroxypropyl methacrylate) BCP structures. This was made possible since the BCPs thermoresponsive behavior allowed ultrafiltration of micrometer sized bacteria in their spherical form (at 4°C, see Fig. 20 b).[268] This process has profound implications for tissue engineering to decrease the possibility of patient infections. (Note that thermoresponsive brush polymers are beyond the scope of this review but are a flourishing area of interest for “smart” surface fabrication and are detailed in reference[269]). Furthermore, two typical behaviors are observed with thermoresponsive copolymers; one where the polymer is miscible in a solvent with increased temperature (upper critical solution temperature, UCST), and the other where polymers that become insoluble with increasing temperature, *i.e.* lower critical solution temperature (LCST).[270] Poly(N-isopropylacrylamide) (PNIPAm) based copolymers represent the most studied LCST thermoresponsive copolymers[271] since the polymer’s LCST is ~ 32°C (below human body temperature, 36.5°C – 37.5°C), they undergo a well-defined coil-to-globule transition and can be rendered cationic or anionic.

Moreover, the ability to precisely tune and understand macromolecular PNIPAm structures has seen much focus on their use for drug delivery at site specific areas. In this vein, Ta *et al.* described the use of copolymers of PNIPAm-*co*-propylacrylic acid to modify liposomes in order to stabilize doxorubicin (a chemotherapy drug used to treat various cancers) in serum and to limit drug leakage over time.[272] A pivotal study by Li *et al.* showed the innate ability of a mussel inspired catecholfunctionalized PNIPAm based ABA terpolymer to exhibit a rapid thermo-responsive sol-to-gel transition, heal autonomously after repeated damage, and possessed excellent antifouling property (see Fig. 20 e and f).[273] The development of this hydrogel demonstrated a promising solution to the issue of degradation of hydrogels in-situ that can trigger inflammation. Moreover, in 2012, Lodge and co-workers reported the unique ability of an ABC terpolymer [poly(ethylenealt-propylene)-*b*-PEO-*b*-PNIPAm] to undergo sharp gelation at low polymer concentration.[274] Their work harnessed the innate ability of modifying BCP chemistry to effect structure-property relationships. This progress inspired several further critical works including that of Gupta *et al.* who reported the application of poly[(propylenesulfide)-*b*-(N,N-dimethylacrylamide)-*b*-NIPAm] triblock terpolymers to successfully overcome PNIPAm syneresis, and exhibited degradation and drug release initiated by reactive oxygen species, as shown in Fig. 20.[275]

Apart from the above mentioned works, immense research efforts have targeted polyester based BCPs owing to their ability to degrade without harmful by-products. For example, extensive literature exists on poly(lactide) (PLA), poly(caprolactone) (PCL), and poly(glycolide) (PGA) based BCPs for sustained as well as controlled drug release purposes.[276],[277],[278] Likewise, a plethora of polypeptide based BCPs have also been reported for hydrogel and drug delivery uses.[279],[280] Attention has centred on polypeptide BCPs since they can be made to possess both pH and temperature responsive properties. In addition, modification of polypeptides can be achieved in a simple fashion, and critically they readily degrade to amino acids in the body after their intended function. In 2018, Turabee *et al.* showcased the non-toxicity and efficacy of polypeptide BCPs to treat embryonic kidney cells even at high concentrations (2000  $\mu\text{g mL}^{-1}$ ).[281] Importantly, they illustrated the ability to deliver proteins to specific sites without inflammation and found the gels were bioresorbable in 6 weeks. Hammond and co-workers used click chemistry to incorporate a pH responsive polypeptide block in order to drive nanoparticle assembly for standard chemotherapy delivery of doxorubicin treatment of cancer cells.[282] The authors



used a folic acid conjugated PEG block to target the folate-receptor cancer cells to precisely engineer the accumulation of therapeutic doxorubicin. The above literature makes clear the level of complexity existing to address the issues surrounding our ability to engineer site-specific drugs and other therapeutic agents in a safe, biocompatible manner whilst still retaining high efficacy.

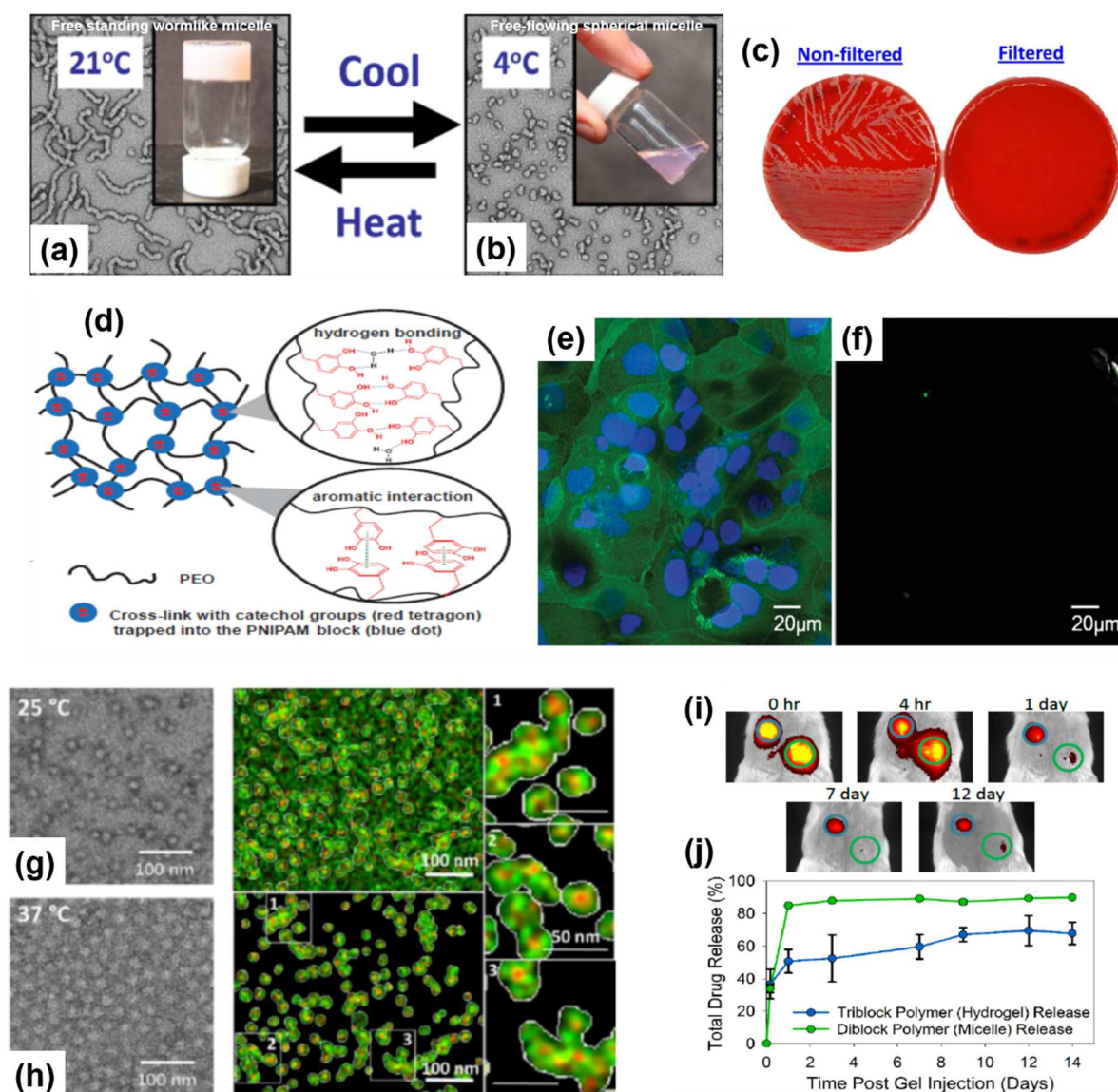


**Figure 20.** (a,b) TEM images and photographs of vials show reversible morphological transition of a thermoresponsive BCP from wormlike at 21°C to spherical at 4°C, where the transition at 4°C degrees makes it possible to filter microsized bacteria (c). Images reproduced with permission from American Chemical Society.[268] (d) Schematic and chemical characteristic of mussel engineered hydrogel with anti-fouling property. (e) Fluorescence microscopy images of uncoated and (f) mussel engineered hydrogel coated microwell dishes after exposure to Caco-2 cells for 48 h. Images reproduced with permission from Wiley.[273] (g,h) TEM

images of poly[(propylenesulfide)-*b*-(*N,N*-dimethylacrylamide)-*b*-NIPAm] micelles at 25 °C and 37 °C respectively used for controlled drug release. Corresponding STEM-EDS element maps for sulfur (red) and oxygen (green) at 37 °C with image thresholding and background subtraction. (i) In-vivo imaging after subcutaneous injection of 50  $\mu$ L of dye-loaded triBCP solution (blue circle, top left) and dye-loaded diblock copolymer solution (green circle, bottom right). Micelles of di-BCPs were observed to diffuse away rapidly while robust hydrogels which slowly released the model drug over 14 days were observed for the tri-BCP. (j) Graph illustrating the comparison between the di-BCP and tri-BCP solutions drug release described in (i). Images reproduced with permission from American Chemical Society.[275]

### 5.3 Biorelated BCP thin film features

In 2008, Ross and co-workers presented a method illustrating the effectiveness that BCPs possess to pattern active functional materials.[283] The authors used cylinder forming PS-*b*-PDMS features to pattern functional poly(3,4-ethylenedioxythiophene):poly(styrenesulfonate) (PEDOT:PSS) nanowires possessing 15 nm width and 35 nm period (see Fig. 21 a). A typical device setup is shown in Fig. 21 b. The resulting PEDOT:PSS nanowires were employed to act as an ethanol vapor sensor surpassing the performance of unpatterned films (tested at various thicknesses) due to increased surface-to-volume ratio. Note that this process utilized BCP patterns as an etch mask to pattern the underlying film/substrate.

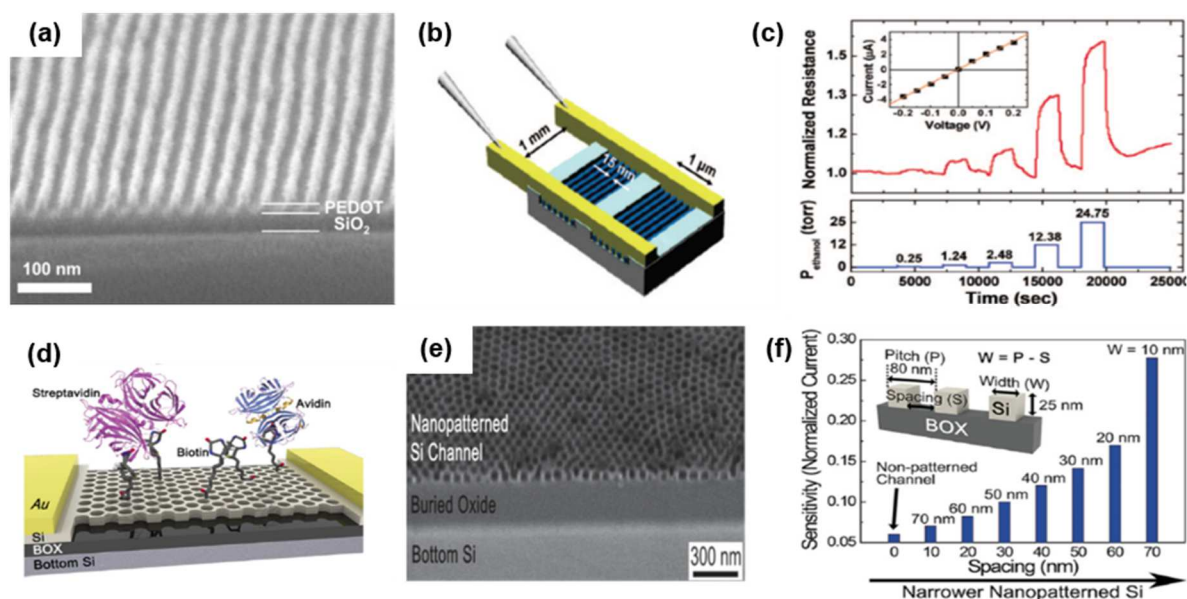


**Figure 21.** (a) Poly(3,4-ethylenedioxythiophene):poly(styrenesulfonate) (PEDOT:PSS) nanowires fabricated using a PS-*b*-PDMS BCP, subsequently used to sense ethanol vapor. (b) Illustration of chemiresistor using PEDOT:PSS nanowires. (c) Graph showing resistance change when exposed to ethanol vapor. Images reproduced with permission from American Chemical Society.[283] (d) Si nanomesh developed using PS-*b*-PMMA BCP, functionalized with biotin molecules enabling detection of streptavidin or avidin. (e) Side view SEM image of Si nanohole array. (f) Graph showing sensitivity versus spacing between two Si nanomesh pillars. Images reproduced with permission from Wiley.[284]

The process by Ross co-workers was one of the first of its kind and exemplified the potential of using BCPs to pattern functional material to fabricate sensor devices surpassing conventional processes. Notable sensor examples include silicon nanomesh functionalized

with biotin to detect streptavidin and avidin (see Fig. 21 d-f) with 1 nM sensitivity[284], and an ethanol sensor developed using patterned Si nanowires.[285] Both processes were developed from etching PS-*b*-PMMA BCP features into the underlying silicon substrates. In 2017, Borsali[286] and co-workers showed that  $\beta$ -cyclodextrin/ferrocene modified PS-*b*-PMMA templates could also be used to detect streptavidin. Moreover, the systems reversibility to change linkers *i.e.* changing ferrocene to  $\beta$ -cyclodextrin allowed new target molecule detection via cyclic voltammogram measurements. The associated processing of the above mentioned works involve well-understood and semiconductor compatible deposition and etching steps, which may accelerate the uptake of the methods in nanomanufacturing of biosensors. A more recent report has shown the use of a poly(3-hexylthiophene) based BCP, more commonly used in photovoltaics, to form helical nanofibrils to sense ammonia.[287] The report highlights the advantages of employing unique BCP chemistry for chemical sensing where size tunability of features, differing block chemistry can induce distinct and desired substrate surface chemistries. Moreover, the designed BCP allows for a one step process towards a sensor without any complex etching procedures or requirement for block removal.

On the other hand, infiltrating established BCP systems to create inorganic nanodots and nanowires provides a useful platform to design functional surfaces. For example, Kim and co-workers[288] reported a process to deposit Ag nanodots within a nanoporous PS-*b*-PMMA BCP film on a transparent substrate to create a label-free sensor with sub-ng ml<sup>-1</sup> level detection limit (0.01~0.1 ng ml<sup>-1</sup>). The Ag evaporated nanodots were functionalized with a self-assembled monolayer to allow for antigen binding. This was then followed by binding between antigen and the antibody that were analyzed using UV-vis. Ordered patterns of iron oxide nanofeatures infiltrated using metal salts in PS-*b*-PEO and PS-*b*-P4VP BCPs have also been used to electrochemically sense ethanol and/or hydrogen peroxide that demonstrate high sensitivity, detection limits, and strong anti-interference ability.[289],[290] Likewise, PS-*b*-PEO patterns infiltrated to produce Ag nanodots have shown promise as antimicrobial packaging as delays were observed in *Pseudomonas fluorescens* and *Staphylococcus aureus* growth, *i.e.* both Gram-positive and Gram-negative bacteria.[291] Notable reports using PS-*b*-P4VP BCP materials include their use as porous templates for the rapid detection (2s) of glucose with a low detection limit (0.05  $\mu$ M),[292] templating CuO nanodots for selective dopamine determination (with a sensitivity of 326.91  $\mu$ A and detection limit of 0.03  $\mu$ M),[293] and also the templating of Au nanoparticles for localized surface

plasmon resonance biosensors that was 3 fold better than traditional deposition processes, *e.g.* use of (3-aminopropyl)-trimethoxysilane or polyelectrolytes.[294] A more recent study by Olsen and co-workers has shown the potential of a thin film biosensor based on a protein-polymer BCP.[295] In their work, they emphasized the capability of analyte to be trapped in protein lamellar areas only, reporting excellent performance for analyte detection even when using small analyte sizes (15.6 kDa) or when analysing blood or urine samples.

Implantable controlled release devices could potentially offer convenience for patients over injections as mentioned in section 5.2.[256] Innovative techniques to capture excess drug molecules are required to limit side effects in healthy tissues where tumor selectivity is low in chemotherapy treatments. Developing implantable devices that can reliably and controllably release a drug molecule over extended periods will also be a major step forward for patients managing chronic diseases *e.g.* rheumatoid arthritis, diabetes, Crohn's disease. In 2009, Lo *et al.*[296] reported on the use of a PS-*b*-PLLA BCP to derive a nanoporous PS template to use as a coating on implantable devices for drug delivery. Specifically, the porous template was loaded with sirolimus (an immunosuppressive agent) to allow slow release, *i.e.* greater than hours to release the drug, in an effort to overcome limitations of previously reported methods. Sirolimus loaded cylindrical and lamellar features are shown in Fig. 22a and b, while Fig. 22c represents the cumulative release of sirolimus with respect to original film thickness. Uehara *et al.*[297] demonstrated the use of a nanoporous membrane from a PE-*b*-PS BCP for the size selective diffusion of glucose and albumin molecules. The authors showed the superiority of their PE membrane (over conventional alumina membranes) to allow the passing of glucose molecules while retaining bovine serum albumin (BSA) molecules.

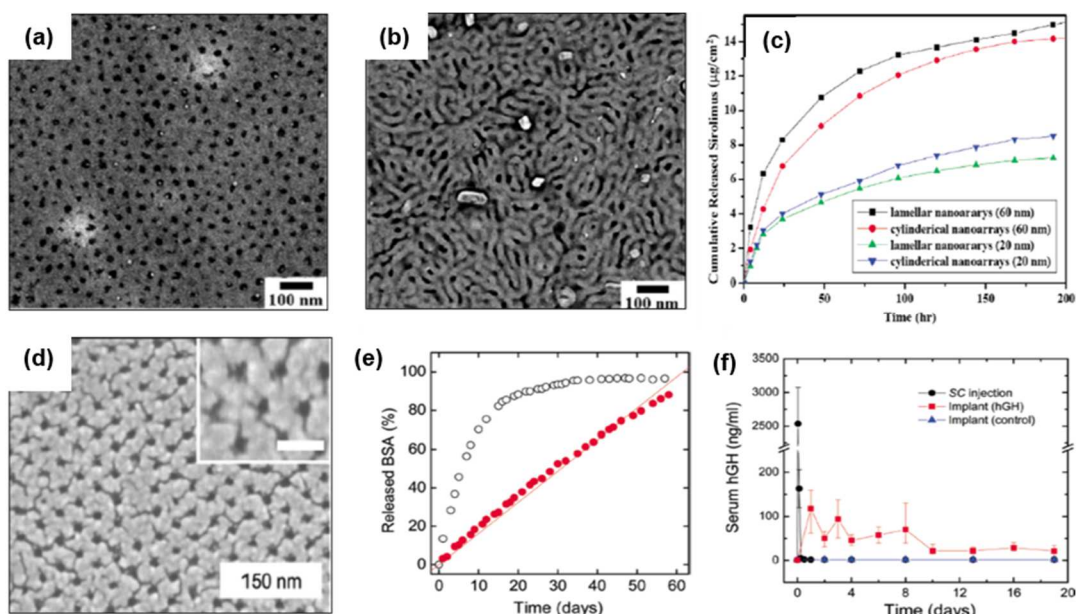


**Figure 22.** (a) SEM image of sirolimus infilled porous PS-*b*-PLLA cylindrical template. (b) SEM image of sirolimus infilled porous PS-*b*-PLLA lamellar template. (c) Graph showing increase in total release of sirolimus with respect to thickness of cylindrical or lamellar films. Images reproduced with permission from American Chemical Society.[296] (d) Porous PS-*b*-PMMA template with 7 nm Au evaporated on top of film for controlled protein drug delivery. (e) Graph of released bovine serum albumin over course of 60 days, white circles indicate a supporting membrane with nominal pore thickness of 200 nm, while red circles show nanoporous PS-*b*-PMMA template with 15 nm pore size. (f) *In vivo* release of human growth hormone (hGH) over 3 weeks. Au coated nanoporous BCP template (see structure in (d)) studied shows controlled release over course of 3 weeks (red squares) in comparison to subcutaneous injection of hGH (black circle) and control (blue triangle). Images reproduced with permission from American Chemical Society.[298]

In 2010, Yang *et al.*[298] described a drug delivery device based upon cylindrical PS-*b*-PMMA nanochannels to release BSA and human growth hormone (hGH) by single file diffusion. Au coated nanoporous PS-*b*-PMMA patterns were developed as shown in Fig. 22 d possessing 7 nm of Au and pore size of ca. 10 nm. Interestingly, zero-order release of the proteins *in vitro* was observed for up to 2 months without denaturation (see Fig. 22 e for BSA released) while a nearly constant release *in vivo* of hGH occurred for as long as 3 weeks in implanted devices in Sprague Dawley rats (see Fig. 22 f). More recently, Balsara and co-workers[299] utilized a tri-BCP copolymer possessing sulfonated polystyrene end blocks and a poly(ethylene) middle block (S-SES) to capture Doxorubicin. As the author's noted, chemotherapy drugs can have "deleterious interactions between unused drug molecules and human tissue", and therefore, there is significant scope to develop membrane technologies to enhance implantable device performance to meet these crucial demands for nanomanufacturing. The S-SES membrane performed best to capture doxorubicin in the presence of water rich channels in a lamella forming morphology in aqueous environment.

Studies have also suggested that surfaces possessing nanotopographies defined by BCPs could be beneficial to cell adhesion and cell fate.[300],[301],[302] In contrast to expensive optical lithography, BCP templating offers a low-cost alternative to accessing such nanoscale dimensions, in particular for addressing neuroprosthetic technology requirements. Mokarian *et al.*[303] exemplified the use of BCP lithography using a pattern transferred nanotopography of silicon nanowires to limit cell proliferation and increase focal adhesion of human neuroblastoma SH-SY5Y cells. The authors observed this using vertical silicon nanowires fabricated from metal ion infiltrated PS-*b*-PEO BCP dot patterns. The etched Si nanowires, possessed feature sizes of 20 nm (with 92 nm height), managed to reduce electrical impedance and increase conductivity.

The capability of BCP materials to pattern nanoscale features has also led to the pursuit of ways to precisely dictate protein adsorption[304] and affinity[305] at surfaces, in order to mimic the intricate behavior of living cells.[306],[307],[308] For example, in 2010, Composto and co-workers[309] functionalized UV/O<sub>3</sub> etched PS-*b*-PMMA channels with 3-aminopropyltriethoxysilane (APTES) in order to attach filamentous actin (F-actin). While selectivity of F-actin was limited, the study demonstrated a broader use of BCPs to organise biomolecules. More recently, diverse studies have expanded our knowledge of protein adsorption including the investigation of zwitterionic BCP micelles and their effect on protein adhesion and antibacterial behavior,[310] while Stel *et al.* elucidated the effects of surface BCP heterogeneity to confine bacterial surface layers and thus subsequent proteins and nanoparticles (see Fig 23 below).[311] Others have demonstrated the excellent performance of porous BCP films such as PS-*b*-PMMA to chemically attach lysozyme with heterogeneous elasticity,[312] porous PS-*b*-PLLA to increase the adsorption of lysozyme and BSA.[313] and isoporous PS-*b*-P4VP membranes (developed using SNIPS) with pore sizes of ~ 8.6 nm to separate proteins of sub-10 nm.[314] In 2017, a more elaborate and robust process, which avoids expensive lithography processing was reported by Choi and co-workers to selectively separate biomolecules.[315] They fabricated a 5 nm thin reduced graphene oxide nanosieve from a PS-*b*-PMMA template, which could withstand mechanical pressures up to 1 atm, and was employed to selectively separate the common human blood protein haemoglobin from a mixture of haemoglobin and immunoglobulin G. As outlined in the above examples, expanding our understanding and toolkit to design such surfaces could lead to new diagnostic detection methods and ways to improve patient recovery.[316]

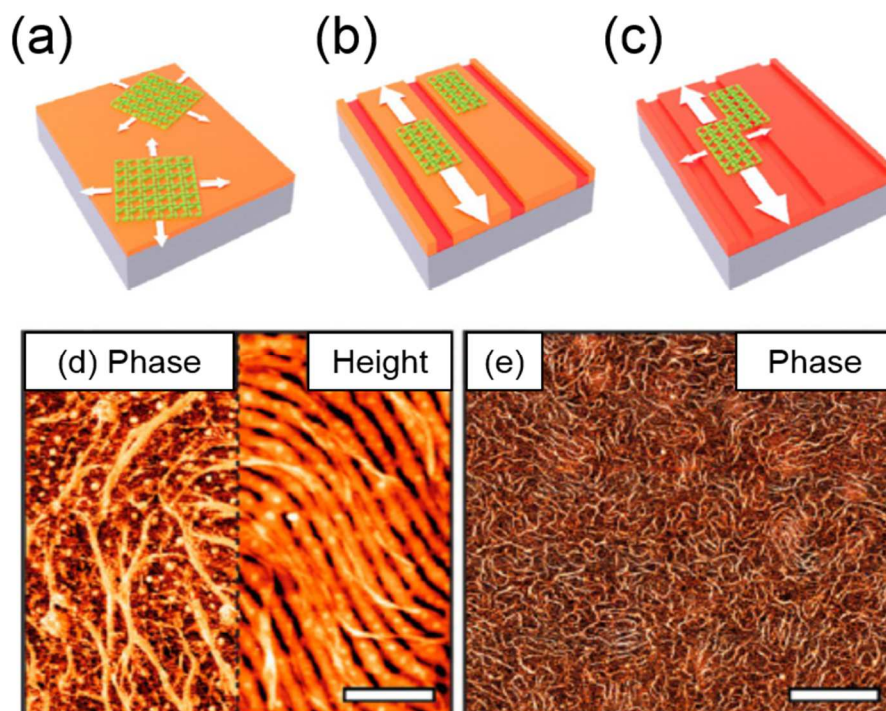


**Figure 23.** Behavior shown in schematic of bacterial surface layers on (a) a uniform substrate exhibiting isotropic nucleation and growth, (b) a patterned substrate with hydrophobic (orange) and hydrophilic (red) areas, where the surface layers nucleate and grow specifically along the hydrophobic regions, and (c) on a hydrophilic substrate with different topographic dimensions, surface layers nucleate on both areas but grow faster along the trench region. Extending process beyond proteins with pattern alignment to longer molecules like collagen as shown in AFM images in (d) and (e). (d,e) Respective phase and height images of long collagen bundles aligned along PS-*b*-PEO BCP stripe pattern underneath. Scale bar is 200 nm in (d) and 2  $\mu$ m in (e). Images reproduced with permission from American Chemical Society.[311]

#### 5.4 Summary

The broad scope of BCP based solution and thin films described in this section shows clearly the progress in respective fields to precisely engineer both macromolecule structures and chemistry. This has played a pivotal role in the progress of hydrogels and drug nanocarriers, and future progress on drug delivery devices will be expedited by control and design of BCPs for nanomanufacturing. Furthermore, the applications of BCPs as thin films to incorporate functional material or their use as etch masks to fabricate nanostructures as described reveals the possible avenues towards on-chip diagnostic devices. The latter field is less well-researched in comparison to solution based applications and thus space to explore new materials and BCP structures will be critical for future nanodevice developments.

#### 6. Conclusions

Nanomanufacturing of devices and associated processes hold the key to unlocking future technological advances that will allow society to progress. Such developments to minimize waste, and importantly to allow sustainability of materials depends on our understanding and

processing of nanomaterials. This review has highlighted the extensive use of BCP materials

Block Copolymer	Ref.	Role of BCP, Morphological	Application	Performance	Nanomanufacturing	Additional Comment(s)
-----------------	------	----------------------------	-------------	-------------	-------------------	-----------------------

for use across energy, photonic, environmental, and biological areas. The attractive characteristics, *e.g.* tuneable chemistry, tailored nanoscale dimensions, high porosity, exotic morphologies, to name a few, of BCPs has immensely impacted the nanotechnological field to achieve long life cycle performing Li-O<sub>2</sub> batteries, flexible color-responsive sensors, and large-area membrane fabrication for highly selective separation (see table 2 below for recent examples of BCPs employed and their broad uses). Moreover, the rich nature of BCP morphologies possible in solution have enhanced device performance in catalysis and enabled new drug delivery techniques. Overall, the diverse applications outlined in this review endowed through BCP structural materials re-enforces their flexibility, and thus illustrates their important position in the nanomaterials toolbox that can significantly contribute to future nanomanufacturing. Continuing to advance our macromolecular engineering knowledge of new BCPs and their interactions will lead the way for more far-reaching applications.



		Description, & Material Formed		Remark	Advantages to SOA	
PEO- <i>b</i> -PPO- <i>b</i> -PEO (F108)	[78]	F108 acts as surfactant. TiO <sub>2</sub> powder synthesized.	<b>Energy</b> Molecular hydrogen generation for fuel cells.	High photocatalytic H <sub>2</sub> evolution rates (1.22 mmol.h. <sup>-1</sup> .g <sup>-1</sup> ) compared to commercial products.	Mild conditions compared to sol-gel processes.  Co-catalyst free.	Used Evaporation-Induced Self-Assembly (EISA) technique
PDMAEMA- <i>b</i> -PEGMA	[108]	Mo-doped PdPt@Pt core-shell octahedral, with an ionic BCP and reduced graphene oxide.	<b>Energy</b> Oxygen reduction reactions with potential application in fuel cells	Initial mass activity 31-fold higher than commercial Pt/C.  200-fold higher mass activity after 10, 000 cycles of durability testing.	PDMAEMA- <i>b</i> -PPEGMA, functionalized graphene facilitates intermolecular charge transfer.	PDMAEMA- <i>b</i> -PPEGMA is an ionic BCP that promotes stability of metal NPs.
PI- <i>b</i> -PS- <i>b</i> -PEO	[112]	Host for electroplating of material. Double gyroidal 3D network. Composed of carbon, poly(phenylene oxide) and a composite of sulfur and poly(3,4-ethylenedioxythiophene)	<b>Energy</b> Solid-state nano-3-D Li-ion/sulfur system.	Capacity was 3 orders of magnitude higher compared to similar 2D architecture.  45 times higher capacity than previously reported 3D system.	Nanosized electrodes that allows efficient use of space.	Smaller dimensions (> 50 nm) than used in composite or thin-film batteries.  Smaller overall footprint to conventional processing.
PS- <i>b</i> -P2VP	[153]	1D periodic in-plane lamellae formed for visualisation. 3 vertically stacked components of PDMS-BCP-IG-PDMS [see section 2 for further details]	<b>Photonic</b> Stretchable capacitive sensor based on strain-responsive structural color.	Fast response times (~80 msec).  Reliable capacitance and structural color changes over 1000 cycles.	Versatility of BCP allows stacked lamellae architecture.  Potential for wearable electronics and real-time monitoring.	Possible to observe recognition of finger, knee and elbow bending, localized pressure and the shape of a strained object.
PS- <i>b</i> -P2VP	[194]	Template for metal ion inclusion. PS- <i>b</i> -P2VP hexagonal etch mask. Si nanopillars generated.	<b>Photonic</b> Absorbing nanosurface.	Reduced reflectivity by a factor of 100.  <0.16% between 400 and 900 nm at 30°.	Based on BCP self-assembly and the use of traditional deposition and plasma treatments for high aspect ratio Si nanosurfaces.	Ultra large domain sizes and periods formed.  Demonstrated on planar and curved surfaces.
PS- <i>b</i> -PMMA	[187]	Template for Au deposition. Hexagonally packed nanodots. Au features. Ag also shown.	<b>Photonic</b> High refractive index metasurface.	Effective refractive index of 5.10 demonstrated.  Spatially graded and anisotropic refractive indices shown.	Vacuum deposition and etching processes facilitate large scale wafer processing.	Strategy enables pattern shrinkage.
PEG- <i>b</i> -PLA	[209]	BCP is photocleavable. Macroscopic aggregates. BCP stabilises nanoparticle in core, corona acts as protection. Photosensitive core-shell nanoparticles.	<b>Environmental</b> Extraction of pollutants from water and soil.	Nanoparticles reduce the teratogenicity of bisphenol A, triclosan and 17 $\alpha$ -ethinyl estradiol.	Scalable process with precise nanoparticle control.	Process carried out without generating toxic byproducts.  Experiments using wastewater, thermal printing paper and contaminated soil showed the versatility of the process.
PB- <i>b</i> -PEO	[227]	Membrane used for functionalization. Peptide channels with pore size of ~ 5 Å. Pillar[5]arene artificial water channels embedded in BCP.	<b>Environmental</b> Highly permeable and selective polymer membrane.	Permeability (~65 L m <sup>-2</sup> h <sup>-1</sup> bar <sup>-1</sup> )	Angstrom-scale pore sizes fabricated.	Inspired by biological water channel proteins, aquaporins, which can be found in mangrove tree roots.

PS- <i>b</i> -P2VP	[236]	PS- <i>b</i> -P2VP BCP used as membrane. Membrane is formed atop macroporous nylon support.	<b>Environmental</b> Formation of BCP composite membranes for ultrafiltration.	Rejections to 22-nm SiO <sub>2</sub> and 15 nm Au nanospheres was ~99 % and 98.2 % respectively.	Spray coating technique is used. Pore size and surface hydrophilicity can be tuned based upon hot ethanol swelling conditions that generate porous structure. Possible to scale-up.	Defect-free and uniform dense membranes formed.  BCP thickness can be controlled within ~ micrometers (~2.8-6.8 μm).
PS- <i>b</i> -PE- <i>b</i> -PS	[299]	BCP is used as a membrane to capture chemotherapy drug. Membrane consists of sulfonated PS end blocks. PE middle block provides membrane integrity.	<b>Biological</b> Doxorubicin removal from bloodstream	31 mins required to remove 90% of doxorubicin.	Process was integrated with new class of biomedical devices, referred to as ChemoFilter.	The water rich channels in the membrane of lamellar forming systems favour rapid doxorubicin capture.
PS- <i>b</i> -P4VP BCPs	[314]	BCP is used as a membrane separate proteins. Micron thick films with < 10 nm pore sizes. Sulfonated polyethylene glycol was used as an additive.	<b>Biological</b> Protein separation.	97% rejection of proteins with molecular size of 6.4×5.5×5 nm  Pore density up to 1.3×10 <sup>15</sup> /m <sup>2</sup>	SNIPS approach employed. Reproducible and tunable pore sizes can be accessed.	Pore sizes as small as 8.6 nm generated.  Exceptional separation demonstrated with regard to mixtures of proteins of similar size (6.4×5.5×5 vs 7×3.8×3.8 nm).
PEG- <i>b</i> -AMP BCPs	[317]	BCP contains antimicrobial and antibiofilm properties. Grafted onto silicone rubber.	<b>Biological</b> Antimicrobial surfaces for biomedical devices.	After in vitro cytotoxicity study, confirmed that coating is biocompatible with mammalian cells. High antimicrobial activity against range of pathogenic bacteria.	Bottlebrush-like coating is easily grafted to surfaces, e.g. silicone, that is commonly employed as a catheter.	Increasing PEG chain length improved hemolytic activity.  Excellent antifouling behavior due to reduced protein adsorption and platelet adhesion.  PEG's biocompatibility reduced AMP Cytotoxicity.

**Table 2.** Examples of application areas and rationale for BCP material choice discussed herein.

## 7. Perspective

### 7.1 Future directions of BCP materials for nanomanufacturing

Future directions in the field of BCPs will lay the foundation for nanomanufacturing and progress in our ability to control BCP structural complexity is all-important. This will afford an access to a greater variety of structures beyond simple di-BCP morphologies. As witnessed in Nature, hierarchical structures at various length scales are a prerequisite toward novel functionalities.[318],[319] To fulfil this objective, recent advances in macromolecular engineering such as the development of sequence-controlled copolymers,[320],[321] offer tremendous opportunities to code macromolecules for specific nanotechnology applications. As of today, the translation from fully-artificial coded macromolecules[322] to complex three-dimensional structures such as the ones found in proteins is still in its infancy. In the BCP field, such a challenge translates in the controlled expression of secondary structures

induced by crystallinity or weak interactions such as hydrogen bonding.[323],[324] This first step will grant access to chiral arrangement with controllable handedness which is a prerequisite for complex nanomanufacturing in biology and optics. A second challenge is related to the precise registration of self-assembled structures in relation to each other via directed self-assembly methods.[325] Progress has to be made regarding control of interfaces in order to build on-demand 3D structures with an accurate positioning of both primary and secondary structures obtained from BCP self-assembly. Fig. 24 a shows an example of how stacking various morphologies of di-BCPs can be used to access more exotic features,[326] and “non-native” morphologies are now of significant interest in an effort to realize new device concepts.[326],[327] Moreover, tri-BCPs can form unique patterns with various symmetries and up to 30 morphologies have been predicted theoretically.[328], [329] Other intricate patterns have also been reported in recent years by the groups of Yager and Black[330],[331] as well as Ross and Berggren (see Fig. 24 b) [332],[333].

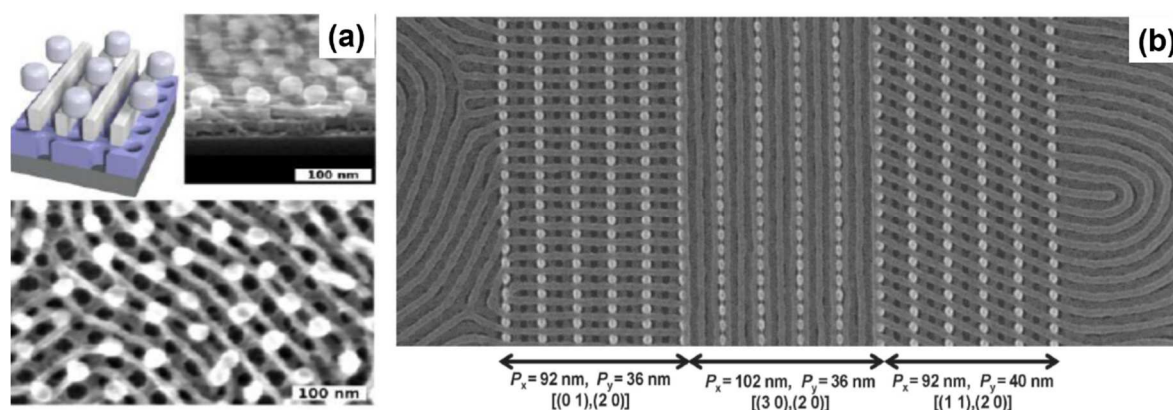


**Fig. 24.** (a) Design of non-native BCP morphologies using various stacked di-BCP morphologies. Reprinted with permission from Royal Society of Chemistry.[326] (b) 3D templated structures from bilayer PS-*b*-PDMS BCP films formed within e-beam lithographic guiding patterns.[333] Reprinted with permission from American Association for the Advancement of Science.

Finally, nanomanufacturing for advanced technologies requires access to a panoply of functional materials from metal to oxides in the form of nano-objects or continuous materials. The hybridization of the structures formed by BCP self-assembly is critical for the advent of BCP nanomanufacturing in order to convert the BCP template into highly functional structures.

## 7.2 Transition of BCP materials towards functional devices

This article has centred on the application of BCPs for advanced technologies. It must be remembered that styrene BCPs are widely used in rubber compositions especially automotive and aeronautical industries and is one of the reasons for the long-life and properties of modern tyres.[334] We also cannot forget the DuPont product Lycra (spandex, elastane), a polyurethane BCP patented in 1958 and now the basis of all sportswear.[335] Many people may quote the cost of BCPs being a barrier to commercial uptake, but the above applications give lie to this. BCP materials can be made cost effectively and in bulk; scale-up is considered practical for most systems. It is worth exploring why these systems have not been used widely and commercially in the fields described herein.

Firstly, many of the examples discussed are based on thin film applications. Taking the example of processor fabrication, the volume of BCP needed for a 30 cm wafer is the order of  $2 \times 10^{-9} \text{ m}^3$ . Currently the worldwide production is around 100 million wafers or a total volume of  $0.2 \text{ m}^3$  and it is questionable if the capital expenditure required to scale would be commensurate with this volume. Of course, small agile processing equipment could be used but the profitability for the product manufacturer is questionable for a single product. Another barrier to widespread use is that existing technology platforms exist. Switching to an alternative patterning technology, even to expensive photolithography, requires considerable changes in practice. This would require, method development, regulation change, capital investment, people training *etc.* Changing technology might eventually precipitate improved or cheaper products, but there is a high initial cost. A further barrier is that in many cases there is no convergence of the science. No one material solution that has been demonstrated at scale.

Of course, all of the above bottlenecks are common barriers for implementation of new technologies. However, things will change. As more applications are found, there will be enough systems to warrant synthesis at scale. As applications develop more will be precipitated. The future remains bright because BCPs give unrivalled properties, particularly for surface engineering and tuning the energy of any surface towards a desired application. They may have important use in defining the future of plastics where we can render any surface property using an inexpensive, readily recyclable bulk system. The question is not if these will be brought to market, it is when.

## Acknowledgements

The authors are sincerely grateful for financial support from the University of Bordeaux and the LabEx AMADEus (ANR-10-LABEX-0042-AMADEUS), and the financial support of Science Foundation Ireland (SFI) under grant number 12/RC/2278 and 16/SP/3809. This research is also co-funded by the European Regional Development Fund and Science Foundation Ireland under Ireland's European Structural and Investment Fund.

## 8. References

- [1] J.A. Liddle, G.M. Gallatin, *ACS Nano*, 10 (2016) 2995-3014.
- [2] W. Huang, X. Yu, Y. Liu, W. Qiao, L. Chen, *Frontiers of Mechanical Engineering*, 12 (2017) 99-109.
- [3] C.A. Ross, K.K. Berggren, J.Y. Cheng, Y.S. Jung, J.-B. Chang, *Advanced Materials*, 26 (2014) 4386-4396.
- [4] J. Bang, U. Jeong, D.Y. Ryu, T.P. Russell, C. J Hawker, *Advanced Materials*, 21 (2009) 4769-4792.
- [5] Y.-C. Tseng, S.B. Darling, *Polymers*, 2 (2010) 470-489.
- [6] I. Botiz, S.B. Darling, *Materials Today*, 13 (2010) 42-51.
- [7] M.A. Morris, S.C. Padmanabhan, M.C. Cruz-Romero, E. Cummins, J.P. Kerry, *Meat Science*, 132 (2017) 163-178.
- [8] S. Moritomi, T. Watanabe, S. Kanzaki, "SUMITOMO KAGAKU", vol. 2010-I.
- [9] S. Biswas, P. Kumari, P.M. Lakhani, B. Ghosh, *European Journal of Pharmaceutical Sciences*, 83 (2016) 184-202.
- [10] F.H. Schacher, P.A. Rugar, I. Manners, *Angewandte Chemie - International Edition*, 51 (2012) 7898-7921.
- [11] Y. Mai, A. Eisenberg, *Chemical Society Reviews*, 41 (2012) 5969-5985.
- [12] F.S. Bates, M.A. Hillmyer, T.P. Lodge, C.M. Bates, K.T. Delaney, G.H. Fredrickson, *Science*, 336 (2012) 434-440.
- [13] H. Feng, X. Lu, W. Wang, N.-G. Kang, W.J. Mays, *Polymers*, 9 (2017).
- [14] G.R. Whittell, I. Manners, *Advanced Materials*, 19 (2007) 3439-3468.
- [15] N.J.W. Penfold, J. Yeow, C. Boyer, S.P. Armes, *ACS Macro Letters*, 8 (2019) 1029-1054.
- [16] J.-L. Six, K. Ferji, *Polymer Chemistry*, 10 (2019) 45-53.
- [17] V. Ponsinet, *Nanopatterns Produced by Directed Self-Assembly in Block Copolymer Thin Films*, in: J. Rodríguez-Hernández, C. Drummond (Eds.) *Polymer Surfaces in Motion: Unconventional Patterning Methods*, Springer International Publishing, Cham, 2015, pp. 73-97.
- [18] P. Mansky, P. Chaikin, E.L. Thomas, *Journal of Materials Science*, 30 (1995) 1987-1992.
- [19] P. Mansky, C.K. Harrison, P.M. Chaikin, R.A. Register, N. Yao, *Applied Physics Letters*, 68 (1996) 2586-2588.
- [20] C. Cummins, M.A. Morris, *Microelectronic Engineering*, 195 (2018) 74-85.
- [21] J.H. Kim, H.M. Jin, G.G. Yang, K.H. Han, T. Yun, J.Y. Shin, S.-J. Jeong, S.O. Kim, *Advanced Functional Materials*, n/a (2019) 1902049.
- [22] R.A. Farrell, N.T. Kinahan, S. Hansel, K.O. Stuen, N. Petkov, M.T. Shaw, L.E. West, V. Djara, R.J. Dunne, O.G. Varona, P.G. Gleeson, S.J. Jung, H.Y. Kim, M.M. Kolečnik, T. Lutz,

- C.P. Murray, J.D. Holmes, P.F. Nealey, G.S. Duesberg, V. Krstić, M.A. Morris, *Nanoscale*, 4 (2012) 3228-3236.
- [23] D. Borah, C. Cummins, S. Rasappa, R. Sentharamaikkannan, M. Salaun, M. Zelsmann, G. Lontos, K. Ntetsikas, A. Avgeropoulos, A.M. Morris, *Nanomaterials*, 8 (2018).
- [24] C. Cummins, D. Borah, S. Rasappa, R. Sentharamaikkannan, C. Simao, A. Francone, N. Kehagias, C.M. Sotomayor-Torres, M.A. Morris, *ACS Omega*, 2 (2017) 4417-4423.
- [25] C. Cummins, A.P. Bell, M.A. Morris, *Nanomaterials (Basel, Switzerland)*, 7 (2017) 304.
- [26] S. Ji, L. Wan, C.-C. Liu, P.F. Nealey, *Progress in Polymer Science*, 54 (2016) 76-127.
- [27] H. Hu, M. Gopinadhan, C.O. Osuji, *Soft Matter*, 10 (2014) 3867-3889.
- [28] X. Chevalier, C. Nicolet, R. Tiron, A. Gharbi, M. Argoud, J. Pradelles, M. Delalande, G. Cunge, G. Fleury, G. Hadziioannou, C. Navarro, *Scaling-down lithographic dimensions with block-copolymer materials: 10nm-sized features with PS-b-PMMA*, SPIE2013.
- [29] R.A. Farrell, N. Petkov, M.T. Shaw, V. Djara, J.D. Holmes, M.A. Morris, *Macromolecules*, 43 (2010) 8651-8655.
- [30] P.A.R. Delgadillo, R. Gronheid, C.J. Thode, H. Wu, Y. Cao, M. Neisser, M. Somervell, K. Nafus, P.F. Nealey, *MOEMS*, 11 (2012) 031302.
- [31] C. Sinturel, F.S. Bates, M.A. Hillmyer, *ACS Macro Letters*, 4 (2015) 1044-1050.
- [32] G.S. Doerk, R. Li, M. Fukuto, K.G. Yager, *Macromolecules*, 53 (2020) 1098-1113.
- [33] S. Woo, H.S. Wang, Y. Choe, J. Huh, J. Bang, *ACS Macro Letters*, 5 (2016) 287-291.
- [34] T. Ube, T. Kosaka, H. Okazaki, K. Nakae, T. Ikeda, *Journal of Materials Chemistry C*, 5 (2017) 1414-1419.
- [35] S.Y. Kim, J. Gwyther, I. Manners, P.M. Chaikin, R.A. Register, *Advanced Materials*, 26 (2014) 791-795.
- [36] A. Nunns, J. Gwyther, I. Manners, *Polymer*, 54 (2013) 1269-1284.
- [37] M.D. Rodwogin, C.S. Spanjers, C. Leighton, M.A. Hillmyer, *ACS Nano*, 4 (2010) 725-732.
- [38] F. Kayser, G. Fleury, S. Thongkham, C. Navarro, B. Martin-Vaca, D. Bourissou, *Macromolecules*, 51 (2018) 6534-6541.
- [39] N.A. Lynd, A.J. Meuler, M.A. Hillmyer, *Progress in Polymer Science*, 33 (2008) 875-893.
- [40] T. Segal-Peretz, J. Winterstein, M. Doxastakis, A. Ramírez-Hernández, M. Biswas, J. Ren, H.S. Suh, S.B. Darling, J.A. Liddle, J.W. Elam, J.J. de Pablo, N.J. Zaluzec, P.F. Nealey, *ACS Nano*, 9 (2015) 5333-5347.
- [41] T. Hashimoto, K. Tsutsumi, Y. Funaki, *Langmuir*, 13 (1997) 6869-6872.
- [42] R.A. Farrell, T.G. Fitzgerald, D. Borah, J.D. Holmes, M.A. Morris, *International Journal of Molecular Sciences*, 10 (2009) 3671-3712.
- [43] K. Brassat, J.K.N. Lindner, *Advanced Materials Interfaces*, 7 (2020) 1901565.
- [44] M. Kim, K.S. Schmitt, W.J. Choi, D.J. Krutty, P. Gopalan, *Polymers*, 7 (2015).
- [45] R. Lundy, S.P. Flynn, C. Cummins, S.M. Kelleher, M.N. Collins, E. Dalton, S. Daniels, M.A. Morris, R. Enright, *Physical Chemistry Chemical Physics*, 19 (2017) 2805-2815.
- [46] C. Jin, B.C. Olsen, E.J. Luber, J.M. Buriak, *Chemistry of Materials*, 29 (2017) 176-188.
- [47] C.M. Bates, M.J. Maher, D.W. Janes, C.J. Ellison, C.G. Willson, *Macromolecules*, 47 (2013) 2-12.
- [48] C. Sinturel, M. Vayer, M. Morris, M.A. Hillmyer, *Macromolecules*, 46 (2013) 5399-5415.
- [49] C.T. Black, C. Forrey, K.G. Yager, *Soft Matter*, 13 (2017) 3275-3283.
- [50] K. Brassat, D. Kool, C.G.A. Nallet, J.K.N. Lindner, *Advanced Materials Interfaces*, 7 (2020) 1901605.
- [51] C. Cummins, T. Ghoshal, J.D. Holmes, M.A. Morris, *Advanced Materials*, 28 (2016) 5586-5618.

- [52] T. Smart, H. Lomas, M. Massignani, M.V. Flores-Merino, L.R. Perez, G. Battaglia, *Nano Today*, 3 (2008) 38-46.
- [53] R.L.N. Hailes, A.M. Oliver, J. Gwyther, G.R. Whittell, I. Manners, *Chemical Society Reviews*, 45 (2016) 5358-5407.
- [54] A. Pavía-Sanders, S. Zhang, J.A. Flores, J.E. Sanders, J.E. Raymond, K.L. Wooley, *ACS Nano*, 7 (2013) 7552-7561.
- [55] H. Qiu, Z.M. Hudson, M.A. Winnik, I. Manners, *Science*, 347 (2015) 1329.
- [56] S.J. Holder, N.A.J.M. Sommerdijk, *Polymer Chemistry*, 2 (2011) 1018-1028.
- [57] D. Bendejacq, V. Ponsinet, M. Joanicot, *The European physical journal. E, Soft matter*, 13 (2004) 3-13.
- [58] D.D. Bendejacq, V. Ponsinet, *The Journal of Physical Chemistry B*, 112 (2008) 7996-8009.
- [59] F. Dutertre, O. Boyron, B. Charleux, C. Chassenieux, O. Colombani, *Macromolecular Rapid Communications*, 33 (2012) 753-759.
- [60] D. Maysinger, J. Lovrić, A. Eisenberg, R. Savić, *European Journal of Pharmaceutics and Biopharmaceutics*, 65 (2007) 270-281.
- [61] U. Tritschler, S. Pearce, J. Gwyther, G.R. Whittell, I. Manners, *Macromolecules*, 50 (2017) 3439-3463.
- [62] M. Ramanathan, Y.-C. Tseng, K. Ariga, S.B. Darling, *Journal of Materials Chemistry C*, 1 (2013) 2080-2091.
- [63] T. Ito, G. Ghimire, *ChemElectroChem*, 5 (2018) 2937-2953.
- [64] Y. Zou, X. Zhou, Y. Zhu, X. Cheng, D. Zhao, Y. Deng, *Accounts of Chemical Research*, 52 (2019) 714-725.
- [65] Y. Zou, X. Zhou, J. Ma, X. Yang, Y. Deng, *Chemical Society Reviews*, 49 (2020) 1173-1208.
- [66] H.L. Tan, F.F. Abdi, Y.H. Ng, *Chemical Society Reviews*, 48 (2019) 1255-1271.
- [67] M.A. Fox, M.T. Dulay, *Chemical Reviews*, 93 (1993) 341-357.
- [68] M. Morsella, N. d'Alessandro, A.E. Lanterna, J.C. Scaiano, *ACS Omega*, 1 (2016) 464-469.
- [69] H.C. Winkler, M. Suter, H. Naegeli, *Journal of nanobiotechnology*, 14 (2016) 44.
- [70] A. Mills, G. Hill, S. Bhopal, I.P. Parkin, S.A. O'Neill, *Journal of Photochemistry and Photobiology A: Chemistry*, 160 (2003) 185-194.
- [71] S. Usai, J.J. Walsh, *Journal of Electroanalytical Chemistry*, 815 (2018) 86-89.
- [72] T. Busani, R.A.B. Devine, *Semiconductor Science and Technology*, 20 (2005) 870-875.
- [73] N. Rahimi, R.A. Pax, E.M. Gray, *Progress in Solid State Chemistry*, 44 (2016) 86-105.
- [74] V.A. Lebedev, D.A. Kozlov, I.V. Kolesnik, A.S. Poluboyarinov, A.E. Becerikli, W. Grünert, A.V. Garshev, *Applied Catalysis B: Environmental*, 195 (2016) 39-47.
- [75] J. Schneider, M. Matsuoka, M. Takeuchi, J. Zhang, Y. Horiuchi, M. Anpo, D.W. Bahnemann, *Chem Rev*, 114 (2014) 9919-9986.
- [76] Y.C. Lin, S.H. Liu, H.R. Syu, T.H. Ho, *Spectrochimica acta. Part A, Molecular and biomolecular spectroscopy*, 95 (2012) 300-304.
- [77] M.L. Carreon, H.G. Carreon, J. Espino-Valencia, M.A. Carreon, *Materials Chemistry and Physics*, 125 (2011) 474-478.
- [78] Y. AlSalka, A. Hakki, J. Schneider, D.W. Bahnemann, *Applied Catalysis B: Environmental*, 238 (2018) 422-433.
- [79] F.M. Pesci, G. Wang, D.R. Klug, Y. Li, A.J. Cowan, *The journal of physical chemistry. C, Nanomaterials and interfaces*, 117 (2013) 25837-25844.
- [80] Y. Li, S. Cao, A. Zhang, C. Zhang, T. Qu, Y. Zhao, A. Chen, *Applied Surface Science*, 445 (2018) 350-358.

- [81] T. Zhao, Y. Ren, J. Yang, L. Wang, W. Jiang, A.A. Elzatahry, A. Alghamdi, Y. Deng, D. Zhao, W. Luo, *Journal of Materials Chemistry A*, 4 (2016) 16446-16453.
- [82] A. Trapalis, N. Todorova, T. Giannakopoulou, N. Boukos, T. Speliotis, D. Dimotikali, J. Yu, *Applied Catalysis B: Environmental*, 180 (2016) 637-647.
- [83] S. Yin, L. Song, S. Xia, Y. Cheng, N. Hohn, W. Chen, K. Wang, W. Cao, S. Hou, P. Müller-Buschbaum, *Small Methods*, 4 (2020) 1900689.
- [84] N. Hohn, S.J. Schlosser, L. Bießmann, S. Grott, S. Xia, K. Wang, M. Schwartzkopf, S.V. Roth, P. Müller-Buschbaum, *Nanoscale*, 10 (2018) 5325-5334.
- [85] E.C. Giraud, P. Mokarian-Tabari, D.T.W. Toolan, T. Arnold, A.J. Smith, J.R. Howse, P.D. Topham, M.A. Morris, *ACS Applied Nano Materials*, 1 (2018) 3426-3434.
- [86] Z. Wang, S. Liu, J. Zhang, J. Yan, Y. Zhao, C. Mahoney, R. Ferebee, D. Luo, J. Pietrasik, M.R. Bockstaller, K. Matyjaszewski, *Langmuir*, 33 (2017) 12276-12284.
- [87] B. Liu, C.-H. Kuo, J. Chen, Z. Luo, S. Thanneeru, W. Li, W. Song, S. Biswas, S.L. Suib, J. He, *Angewandte Chemie*, 127 (2015) 9189-9193.
- [88] P. Yang, D. Zhao, D.I. Margolese, B.F. Chmelka, G.D. Stucky, *Chemistry of Materials*, 11 (1999) 2813-2826.
- [89] G. Velegraki, J. Miao, C. Drivas, B. Liu, S. Kennou, G.S. Armatas, *Applied Catalysis B: Environmental*, 221 (2018) 635-644.
- [90] L. Kuai, J. Wang, T. Ming, C. Fang, Z. Sun, B. Geng, J. Wang, *Sci Rep*, 5 (2015) 9923.
- [91] W. Wei, L. Samad, J.W. Choi, Y. Joo, A. Way, M.S. Arnold, S. Jin, P. Gopalan, *Chemistry of Materials*, 28 (2016) 4017-4023.
- [92] J. Liu, Y. Liu, N. Liu, Y. Han, X. Zhang, H. Huang, Y. Lifshitz, S.T. Lee, J. Zhong, Z. Kang, *Science*, 347 (2015) 970-974.
- [93] J.J. Walsh, C. Jiang, J. Tang, A.J. Cowan, *Physical Chemistry Chemical Physics*, 18 (2016) 24825-24829.
- [94] Y. Wang, M.F. Ibad, H. Kosslick, J. Harloff, T. Beweries, J. Radnik, A. Schulz, S. Tschierlei, S. Lochbrunner, X. Guo, *Microporous and Mesoporous Materials*, 211 (2015) 182-191.
- [95] L. Li, R.G. Hadt, S. Yao, W.-Y. Lo, Z. Cai, Q. Wu, B. Pandit, L.X. Chen, L. Yu, *Chemistry of Materials*, 28 (2016) 5394-5399.
- [96] T. Skaltsas, N. Karousis, S. Pispas, N. Tagmatarchis, *Nanotechnology*, 25 (2014) 445404.
- [97] R. Wang, R. Qu, C. Jing, Y. Zhai, Y. An, L. Shi, *RSC Advances*, 7 (2017) 10100-10107.
- [98] D.H. Lee, D.O. Shin, W.J. Lee, S.O. Kim, *Advanced Materials*, 20 (2008) 2480-2485.
- [99] D.O. Shin, D.H. Lee, H.S. Moon, S.J. Jeong, J.Y. Kim, J.H. Mun, H. Cho, S. Park, S.O. Kim, *Advanced Functional Materials*, 21 (2011) 250-254.
- [100] Q. Feng, X.Z. Yuan, G. Liu, B. Wei, Z. Zhang, H. Li, H. Wang, *Journal of Power Sources*, 366 (2017) 33-55.
- [101] B.C. Ong, S.K. Kamarudin, S. Basri, *International Journal of Hydrogen Energy*, 42 (2017) 10142-10157.
- [102] Z.W. Seh, J. Kibsgaard, C.F. Dickens, I. Chorkendorff, J.K. Nørskov, T.F. Jaramillo, *Science*, 355 (2017).
- [103] J.Y. Kim, J. Lim, H.M. Jin, B.H. Kim, S.-J. Jeong, D.S. Choi, D.J. Li, S.O. Kim, *Advanced Materials*, 28 (2016) 1591-1596.
- [104] M. Sun, Y. Chen, G. Tian, A. Wu, H. Yan, H. Fu, *Electrochimica Acta*, 190 (2016) 186-192.
- [105] D. Chandra, N. Abe, D. Takama, K. Saito, T. Yui, M. Yagi, *ChemSusChem*, 8 (2015) 795-799.
- [106] X. Zhong, J. Tang, J. Wang, M. Shao, J. Chai, S. Wang, M. Yang, Y. Yang, N. Wang, S. Wang, B. Xu, H. Pan, *Electrochimica Acta*, 269 (2018) 55-61.



- [107] E.-G. Jung, Y. Shin, M. Lee, J. Yi, T. Kang, *ACS Applied Materials & Interfaces*, 7 (2015) 10666-10670.
- [108] K.Y. Cho, Y.S. Yeom, H.Y. Seo, P. Kumar, A.S. Lee, K.-Y. Baek, H.G. Yoon, *ACS Applied Materials & Interfaces*, 9 (2017) 1524-1535.
- [109] D.A. Boyd, Y. Hao, C. Li, D.G. Goodwin, S.M. Haile, *ACS Nano*, 7 (2013) 4919-4923.
- [110] Y. Guo, J. Tang, J. Henzie, B. Jiang, W. Xia, T. Chen, Y. Bando, Y.-M. Kang, M.S.A. Hossain, Y. Sugahara, Y. Yamauchi, *ACS Nano*, (2020).
- [111] Y. Choi, S.K. Cha, H. Ha, S. Lee, H.K. Seo, J.Y. Lee, H.Y. Kim, S.O. Kim, W. Jung, *Nature Nanotechnology*, 14 (2019) 245-251.
- [112] J.G. Werner, G.G. Rodríguez-Calero, H.D. Abruña, U. Wiesner, *Energy & Environmental Science*, 11 (2018) 1261-1270.
- [113] M.G. Fischer, X. Hua, B.D. Wilts, I. Gunkel, T.M. Bennett, U. Steiner, *ACS Applied Materials & Interfaces*, 9 (2017) 22388-22397.
- [114] C. Jo, Y. Kim, J. Hwang, J. Shim, J. Chun, J. Lee, *Chemistry of Materials*, 26 (2014) 3508-3514.
- [115] B.G. Kim, C. Jo, J. Shin, Y. Mun, J. Lee, J.W. Choi, *ACS Nano*, 11 (2017) 1736-1746.
- [116] J. Hwang, C. Jo, M.G. Kim, J. Chun, E. Lim, S. Kim, S. Jeong, Y. Kim, J. Lee, *ACS Nano*, 9 (2015) 5299-5309.
- [117] S.A. Cho, Y.J. Jang, H.-D. Lim, J.-E. Lee, Y.H. Jang, T.-T.H. Nguyen, F.M. Mota, D.P. Fenning, K. Kang, Y. Shao-Horn, D.H. Kim, *Advanced Energy Materials*, 7 (2017) 1700391.
- [118] S. Liu, C. Wang, S. Dong, H. Hou, B. Wang, X. Wang, X. Chen, G. Cui, *RSC Advances*, 8 (2018) 27973-27978.
- [119] A. Vuorema, J.J. Walsh, M. Sillanpää, W. Thielemans, R.J. Forster, F. Marken, *Electrochimica Acta*, 73 (2012) 31-35.
- [120] A. Mills, N. Elliott, G. Hill, D. Fallis, J.R. Durrant, R.L. Willis, *Photochemical & Photobiological Sciences*, 2 (2003) 591-596.
- [121] P. Hartmann, D.-K. Lee, B.M. Smarsly, J. Janek, *ACS Nano*, 4 (2010) 3147-3154.
- [122] S.T. Kochuveedu, Y.H. Jang, Y.J. Jang, D.H. Kim, *Journal of Materials Chemistry A*, 1 (2013) 898-905.
- [123] L. Shen, C. He, J. Qiu, S.-M. Lee, A. Kalita, S.B. Cronin, M.P. Stoykovich, J. Yoon, *ACS Applied Materials & Interfaces*, 7 (2015) 26043-26049.
- [124] B. O'Regan, M. Grätzel, *Nature*, 353 (1991) 737-740.
- [125] A. Sarkar, N.J. Jeon, J.H. Noh, S.I. Seok, *The Journal of Physical Chemistry C*, 118 (2014) 16688-16693.
- [126] M. Zúkalová, A. Zúkal, L. Kavan, M.K. Nazeeruddin, P. Liska, M. Grätzel, *Nano Letters*, 5 (2005) 1789-1792.
- [127] J. Massin, M. Bräutigam, N. Kaeffer, N. Queyriaux, M.J. Field, F.H. Schacher, J. Popp, M. Chavarot-Kerlidou, B. Dietzek, V. Artero, *Interface Focus*, 5 (2015) 20140083-20140083.
- [128] D. Adak, S. Ghosh, P. Chakraborty, K.M.K. Srivatsa, A. Mondal, H. Saha, R. Mukherjee, R. Bhattacharyya, *Solar Energy Materials and Solar Cells*, 188 (2018) 127-139.
- [129] T. Uekert, M.F. Kuehnel, D.W. Wakerley, E. Reisner, *Energy & Environmental Science*, 11 (2018) 2853-2857.
- [130] M.I. Stockman, *Physics Today*, 64 (2011) 39-44.
- [131] P. Dong, Y.-K. Chen, G.-H. Duan, T. Neilson David, *Nanophotonics* 2014, pp. 215.
- [132] D. Thomson, A. Zilkie, J.E. Bowers, T. Komljenovic, G.T. Reed, L. Vivien, D. Marris-Morini, E. Cassan, L. Virost, J.-M. Fédéli, J.-M. Hartmann, J.H. Schmid, D.-X. Xu, F. Boeuf, P. O'Brien, G.Z. Mashanovich, M. Nedeljkovic, *Journal of Optics*, 18 (2016) 073003.

- [133] P. Cheben, R. Halir, J.H. Schmid, H.A. Atwater, D.R. Smith, *Nature*, 560 (2018) 565-572.
- [134] M. Lipson, *Nanotechnology*, 15 (2004) S622-S627.
- [135] M. Lipson, *J. Lightwave Technol.*, 23 (2005) 4222.
- [136] S.A. Miller, Y.-C. Chang, C.T. Phare, M.C. Shin, M. Zadka, S.P. Roberts, B. Stern, X. Ji, A. Mohanty, O.A. Jimenez Gordillo, U.D. Dave, M. Lipson, *Optica*, 7 (2020) 3-6.
- [137] F. Monticone, A. Alù, *Reports on Progress in Physics*, 80 (2017) 036401.
- [138] A. Baron, A. Aradian, V. Ponsinet, P. Barois, *Optics & Laser Technology*, 82 (2016) 94-100.
- [139] J. Yoon, W. Lee, E.L. Thomas, *MRS Bulletin*, 30 (2011) 721-726.
- [140] Y.A. Vlasov, X.-Z. Bo, J.C. Sturm, D.J. Norris, *Nature*, 414 (2001) 289-293.
- [141] H. Wang, K.Q. Zhang, *Sensors (Basel)*, 13 (2013) 4192-4213.
- [142] C. Fenzl, T. Hirsch, O.S. Wolfbeis, *Angewandte Chemie International Edition*, 53 (2014) 3318-3335.
- [143] G. Pitruzzello, T.F. Krauss, *Journal of Optics*, 20 (2018) 073004.
- [144] P. Lova, G. Manfredi, D. Comoretto, *Advanced Optical Materials*, 6 (2018) 1800730.
- [145] A.L. Liberman-Martin, C.K. Chu, R.H. Grubbs, *Macromolecular Rapid Communications*, 38 (2017) 1700058.
- [146] R. Verduzco, X. Li, S.L. Pesek, G.E. Stein, *Chemical Society Reviews*, 44 (2015) 2405-2420.
- [147] Y. Kang, J.J. Walsh, T. Gorishnyy, E.L. Thomas, *Nature Materials*, 6 (2007) 957-960.
- [148] H.S. Lim, J.-H. Lee, J.J. Walsh, E.L. Thomas, *ACS Nano*, 6 (2012) 8933-8939.
- [149] M. Poutanen, G. Guidetti, T.I. Gröschel, O.V. Borisov, S. Vignolini, O. Ikkala, A.H. Gröschel, *ACS Nano*, 12 (2018) 3149-3158.
- [150] Y. Ahn, E. Kim, J. Hyon, C. Kang, Y. Kang, *Advanced Materials*, 24 (2012) OP127-OP130.
- [151] H.S. Kang, J. Lee, S.M. Cho, T.H. Park, M.J. Kim, C. Park, S.W. Lee, K.L. Kim, D.Y. Ryu, J. Huh, E.L. Thomas, C. Park, *Advanced Materials*, 29 (2017) 1700084.
- [152] Y.-W. Chiang, C.-Y. Chou, C.-S. Wu, E.-L. Lin, J. Yoon, E.L. Thomas, *Macromolecules*, 48 (2015) 4004-4011.
- [153] T.H. Park, S. Yu, S.H. Cho, H.S. Kang, Y. Kim, M.J. Kim, H. Eoh, C. Park, B. Jeong, S.W. Lee, D.Y. Ryu, J. Huh, C. Park, *NPG Asia Materials*, 10 (2018) 328-339.
- [154] A. Noro, Y. Tomita, Y. Shinohara, Y. Sageshima, J.J. Walsh, Y. Matsushita, E.L. Thomas, *Macromolecules*, 47 (2014) 4103-4109.
- [155] B.R. Sveinbjörnsson, R.A. Weitekamp, G.M. Miyake, Y. Xia, H.A. Atwater, R.H. Grubbs, *Proceedings of the National Academy of Sciences*, 109 (2012) 14332.
- [156] B.R. Sveinbjörnsson, R.A. Weitekamp, G.M. Miyake, Y. Xia, H.A. Atwater, R.H. Grubbs, *Proceedings of the National Academy of Sciences of the United States of America*, 109 (2012) 14332-14336.
- [157] G.M. Miyake, R.A. Weitekamp, V.A. Piunova, R.H. Grubbs, *Journal of the American Chemical Society*, 134 (2012) 14249-14254.
- [158] Y. Qiao, Y. Zhao, X. Yuan, Y. Zhao, L. Ren, *Journal of Materials Science*, 53 (2018) 16160-16168.
- [159] D.-P. Song, T.H. Zhao, G. Guidetti, S. Vignolini, R.M. Parker, *ACS Nano*, 13 (2019) 1764-1771.
- [160] D.P. Song, C. Li, W. Li, J.J. Watkins, *ACS Nano*, 10 (2016) 1216-1223.
- [161] D.-P. Song, G. Jacucci, F. Dundar, A. Naik, H.-F. Fei, S. Vignolini, J.J. Watkins, *Macromolecules*, 51 (2018) 2395-2400.
- [162] T. Zhang, J. Yang, X. Yu, Y. Li, X. Yuan, Y. Zhao, D. Lyu, Y. Men, K. Zhang, L. Ren, *Polymer Chemistry*, 10 (2019) 1519-1525.

- [163] B.M. Boyle, T.A. French, R.M. Pearson, B.G. McCarthy, G.M. Miyake, *ACS Nano*, 11 (2017) 3052-3058.
- [164] X. Jia, H. Tan, J. Zhu, Responsive Photonic Crystals with Tunable Structural Color, in: Z. Lin, Y. Yang, A. Zhang (Eds.) *Polymer-Engineered Nanostructures for Advanced Energy Applications*, Springer International Publishing, Cham, 2017, pp. 151-172.
- [165] H.-Y. Hsueh, C.-T. Yao, R.-M. Ho, *Chemical Society Reviews*, 44 (2015) 1974-2018.
- [166] L. Wu, W. Zhang, D. Zhang, *Small*, 11 (2015) 5004-5022.
- [167] J.A. Dolan, B.D. Wilts, S. Vignolini, J.J. Baumberg, U. Steiner, T.D. Wilkinson, *Advanced Optical Materials*, 3 (2015) 12-32.
- [168] V. Saranathan, C.O. Osuji, S.G. Mochrie, H. Noh, S. Narayanan, A. Sandy, E.R. Dufresne, R.O. Prum, *Proc Natl Acad Sci U S A*, 107 (2010) 11676-11681.
- [169] I. Vukovic, G.t. Brinke, K. Loos, *Polymer*, 54 (2013) 2591-2605.
- [170] V. Luzzati, P.A. Speg, *Nature*, 215 (1967) 701-704.
- [171] S. Peng, R. Zhang, V.H. Chen, E.T. Khabiboulline, P. Braun, H.A. Atwater, *ACS Photonics*, 3 (2016) 1131-1137.
- [172] A.M. Urbas, M. Maldovan, P. DeRege, E.L. Thomas, *Advanced Materials*, 14 (2002) 1850-1853.
- [173] E.L. Lin, W.L. Hsu, Y.W. Chiang, *ACS Nano*, 12 (2018) 485-493.
- [174] N. Yu, F. Capasso, *Nat Mater*, 13 (2014) 139-150.
- [175] P. Lalanne, P. Chavel, *Laser and Photonics Reviews*, 11 (2017).
- [176] J.B. Pendry, A.J. Holden, D.J. Robbins, W.J. Stewart, *IEEE Transactions on Microwave Theory and Techniques*, 47 (1999) 2075-2084.
- [177] A. Baron, A. Aradian, V. Ponsinet, P. Barois, *Comptes-Rendus-de-l'Academie-des-Sciences*, (2019).
- [178] V. Ponsinet, A. Baron, E. Pouget, Y. Okazaki, R. Oda, P. Barois, *EPL*, 119 (2017).
- [179] U.R. Gabinet, C.O. Osuji, *Nano Research*, 12 (2019) 2172-2183.
- [180] B. Kang, M.M. Afifi, L.A. Austin, M.A. El-Sayed, *ACS Nano*, 7 (2013) 7420-7427.
- [181] V.G. Kravets, F. Schedin, R. Jalil, L. Britnell, R.V. Gorbachev, D. Ansell, B. Thackray, K.S. Novoselov, A.K. Geim, A.V. Kabashin, A.N. Grigorenko, *Nature Materials*, 12 (2013) 304-309.
- [182] J. Toudert, X. Wang, C. Tallet, P. Barois, A. Aradian, V. Ponsinet, *ACS Photonics*, 2 (2015) 1443-1450.
- [183] F. Aubrit, F. Testard, A. Paquirissamy, F. Gobeaux, X. Wang, F. Nallet, P. Fontaine, V. Ponsinet, P. Guenoun, *Journal of Materials Chemistry C*, 6 (2018) 8194-8204.
- [184] S. Salvatore, A. Demetriadou, S. Vignolini, S.S. Oh, S. Wuestner, N.A. Yufa, M. Stefik, U. Wiesner, J.J. Baumberg, O. Hess, U. Steiner, *Advanced Materials*, 25 (2013) 2713-2716.
- [185] S. Vignolini, N.A. Yufa, P.S. Cunha, S. Guldin, I. Rushkin, M. Stefik, K. Hur, U. Wiesner, J.J. Baumberg, U. Steiner, *Advanced Materials*, 24 (2012) OP23-OP27.
- [186] X. Wang, K. Ehrhardt, C.m. Tallet, M. Warengem, A. Baron, A. Aradian, M. Kildemo, V. Ponsinet, *Optics and Laser Technology*, 88 (2017) 85-95.
- [187] J.Y. Kim, H. Kim, B.H. Kim, T. Chang, J. Lim, H.M. Jin, J.H. Mun, Y.J. Choi, K. Chung, J. Shin, S. Fan, S.O. Kim, *Nature Communications*, 7 (2016) 12911.
- [188] A. Alvarez-Fernandez, K. Aissou, G. Pécastaings, G. Hadziioannou, G. Fleury, V. Ponsinet, *Nanoscale Advances*, 1 (2019) 849-857.
- [189] H.H. Hulkkonen, T. Salminen, T. Niemi, *ACS Applied Materials & Interfaces*, 9 (2017) 31260-31265.
- [190] H. Hulkkonen, A. Sah, T. Niemi, *ACS Applied Materials & Interfaces*, 10 (2018) 42941-42947.

- [191] W. Lee, S.Y. Lee, R.M. Briber, O. Rabin, *Advanced Functional Materials*, 21 (2011) 3424-3429.
- [192] S.K. Cha, J.H. Mun, T. Chang, S.Y. Kim, J.Y. Kim, H.M. Jin, J.Y. Lee, J. Shin, K.H. Kim, S.O. Kim, *ACS Nano*, 9 (2015) 5536-5543.
- [193] H.M. Jin, J.Y. Kim, M. Heo, S.-J. Jeong, B.H. Kim, S.K. Cha, K.H. Han, J.H. Kim, G.G. Yang, J. Shin, S.O. Kim, *ACS Applied Materials & Interfaces*, 10 (2018) 44660-44667.
- [194] P. Mokarian-Tabari, R. Sentharamaikkannan, C. Glynn, T.W. Collins, C. Cummins, D. Nugent, C. O'Dwyer, M.A. Morris, *Nano Letters*, 17 (2017) 2973-2978.
- [195] S.H. Mir, G. Rydzek, L.A. Nagahara, A. Khosla, P. Mokarian-Tabari, *Journal of The Electrochemical Society*, 167 (2020).
- [196] E. Kim, H. Ahn, S. Park, H. Lee, M. Lee, S. Lee, T. Kim, E.-A. Kwak, J.H. Lee, X. Lei, J. Huh, J. Bang, B. Lee, D.Y. Ryu, *ACS Nano*, 7 (2013) 1952-1960.
- [197] A. Cózar, F. Echevarría, J.I. González-Gordillo, X. Irigoien, B. Úbeda, S. Hernández-León, Á.T. Palma, S. Navarro, J. García-de-Lomas, A. Ruiz, M.L. Fernández-de-Puelles, C.M. Duarte, *Proceedings of the National Academy of Sciences*, (2014) 201314705.
- [198] M. Revel, A. Châtel, C. Mouneyrac, *Current Opinion in Environmental Science & Health*, 1 (2018) 17-23.
- [199] P. Samaddar, A. Deep, K.-H. Kim, *Chemical Engineering Journal*, 342 (2018) 71-89.
- [200] Y. Zhang, N.E. Almodovar-Arbelo, J.L. Weidman, D.S. Corti, B.W. Boudouris, W.A. Phillip, *npj Clean Water*, 1 (2018) 2.
- [201] J.R. Werber, C.O. Osuji, M. Elimelech, *Nature Reviews Materials*, 1 (2016) 16018.
- [202] R. Nagarajan, K. Ganesh, *The Journal of Chemical Physics*, 90 (1989) 5843-5856.
- [203] P.N. Hurter, T.A. Hatton, *Langmuir*, 8 (1992) 1291-1299.
- [204] R. Nagarajan, M. Barry, E. Ruckenstein, *Langmuir*, 2 (1986) 210-215.
- [205] E. Blaß, *Chemie Ingenieur Technik*, 62 (1990) 166-167.
- [206] J.T.F. Keurentjes, *Block Copolymer Micelles for Water Remediation, Surfactant-Based Separations*, American Chemical Society 1999, pp. 92-112.
- [207] Z. Zhou, B. Chu, *Journal of Colloid and Interface Science*, 126 (1988) 171-180.
- [208] D.-H. Lee, R.D. Cody, E.L. Hoyle, *Groundwater Monitoring & Remediation*, 21 (2001) 49-57.
- [209] F. Brandl, N. Bertrand, E.M. Lima, R. Langer, *Nature Communications*, 6 (2015) 7765.
- [210] J. Herrera-Morales, T.A. Turley, M. Betancourt-Ponce, E. Nicolau, *Materials (Basel)*, 12 (2019) 230.
- [211] S.P. Nunes, *Macromolecules*, 49 (2016) 2905-2916.
- [212] S.P. Nunes, P.Z. Culfaz-Emecen, G.Z. Ramon, T. Visser, G.H. Koops, W. Jin, M. Ulbricht, *Journal of Membrane Science*, (2019) 117761.
- [213] H.B. Park, J. Kamcev, L.M. Robeson, M. Elimelech, B.D. Freeman, *Science*, 356 (2017) eaab0530.
- [214] G.M. Geise, H.B. Park, A.C. Sagle, B.D. Freeman, J.E. McGrath, *Journal of Membrane Science*, 369 (2011) 130-138.
- [215] L.M. Robeson, *Journal of Membrane Science*, 320 (2008) 390-400.
- [216] B.D. Freeman, *Macromolecules*, 32 (1999) 375-380.
- [217] K. Ishizu, K. Inagaki, T. Fukutomi, *Journal of Polymer Science: Polymer Chemistry Edition*, 23 (1985) 1099-1108.
- [218] K. Ishizu, A. Murakami, T. Fukutomi, *Journal of Polymer Science Part A: Polymer Chemistry*, 24 (1986) 1441-1454.
- [219] L. Liang, S. Ying, *Journal of Polymer Science Part B: Polymer Physics*, 31 (1993) 1075-1081.
- [220] Y. Miyaki, H. Nagamatsu, M. Iwata, K. Ohkoshi, K. Se, T. Fujimoto, *Macromolecules*, 17 (1984) 2231-2236.

- [221] Y. Isono, H. Ito, K. Hirahara, T. Fujimoto, Y. Miyaki, *Journal of Membrane Science*, 43 (1989) 205-216.
- [222] S.P. Nunes, A. Car, *Industrial & Engineering Chemistry Research*, 52 (2013) 993-1003.
- [223] S. Nielsen, J. Frokiaer, D. Marples, T.H. Kwon, P. Agre, M.A. Knepper, *Physiological reviews*, 82 (2002) 205-244.
- [224] R. Stoenescu, A. Graff, W. Meier, *Macromolecular bioscience*, 4 (2004) 930-935.
- [225] A. Abdelrasoul, H. Doan, A. Lohi, *Interactions between Aquaporin Proteins and Block Copolymer Matrixes, Biomimetic and Bioinspired Membranes for New Frontiers in Sustainable Water Treatment Technology* 2017.
- [226] J. Zhao, X. Zhao, Z. Jiang, Z. Li, X. Fan, J. Zhu, H. Wu, Y. Su, D. Yang, F. Pan, J. Shi, *Progress in Polymer Science*, 39 (2014) 1668-1720.
- [227] Y.-x. Shen, W. Song, D.R. Barden, T. Ren, C. Lang, H. Feroz, C.B. Henderson, P.O. Saboe, D. Tsai, H. Yan, P.J. Butler, G.C. Bazan, W.A. Phillip, R.J. Hickey, P.S. Cremer, H. Vashisth, M. Kumar, *Nature Communications*, 9 (2018) 2294.
- [228] D.E. Discher, A. Eisenberg, *Science*, 297 (2002) 967.
- [229] K. Kita-Tokarczyk, J. Grumelard, T. Haefele, W. Meier, *Polymer*, 46 (2005) 3540-3563.
- [230] X. Qiu, H. Yu, M. Karunakaran, N. Pradeep, S.P. Nunes, K.-V. Peinemann, *ACS Nano*, 7 (2013) 768-776.
- [231] J. Hahn, J.I. Clodt, C. Abetz, V. Filiz, V. Abetz, *ACS Applied Materials & Interfaces*, 7 (2015) 21130-21137.
- [232] V. Abetz, *Macromolecular Rapid Communications*, 36 (2015) 10-22.
- [233] T. Bucher, V. Filiz, C. Abetz, V. Abetz, *Membranes*, 8 (2018).
- [234] S. Qavi, A.P. Lindsay, M.A. Firestone, R. Foudazi, *Journal of Membrane Science*, 580 (2019) 125-133.
- [235] J. Zhou, Y. Wang, *Macromolecules*, 53 (2020) 5-17.
- [236] D. Ma, J. Zhou, Z. Wang, Y. Wang, *Journal of Membrane Science*, 598 (2020) 117656.
- [237] W.A. Phillip, J. Rzayev, M.A. Hillmyer, E.L. Cussler, *Journal of Membrane Science*, 286 (2006) 144-152.
- [238] S.Y. Yang, J. Park, J. Yoon, M. Ree, S.K. Jang, J.K. Kim, *Advanced Functional Materials*, 18 (2008) 1371-1377.
- [239] L. Chen, W.A. Phillip, E.L. Cussler, M.A. Hillmyer, *Journal of the American Chemical Society*, 129 (2007) 13786-13787.
- [240] W.A. Phillip, M. Amendt, B. O'Neill, L. Chen, M.A. Hillmyer, E.L. Cussler, *ACS Applied Materials & Interfaces*, 1 (2009) 472-480.
- [241] L.M. Pitet, M.A. Amendt, M.A. Hillmyer, *Journal of the American Chemical Society*, 132 (2010) 8230-8231.
- [242] P. Yang, Y. Ning, T.J. Neal, E.R. Jones, B.R. Parker, S.P. Armes, *Chemical Science*, 10 (2019) 4200-4208.
- [243] J. Kim, M. Yoon, S.-M. Jin, J. Lee, Y. La, E. Lee, K.T. Kim, *Polymer Chemistry*, 10 (2019) 3778-3785.
- [244] W.A. Phillip, B. O'Neill, M. Rodwogin, M.A. Hillmyer, E.L. Cussler, *ACS Applied Materials & Interfaces*, 2 (2010) 847-853.
- [245] H. Thankappan, G. Bousquet, M. Semsarilar, A. Venault, Y. Chang, D. Bouyer, D. Quemener, *Membranes*, 9 (2019).
- [246] E.E. Nuxoll, M.A. Hillmyer, R. Wang, C. Leighton, R.A. Siegel, *ACS Appl Mater Interfaces*, 1 (2009) 888-893.
- [247] H. Ahn, S. Park, S.W. Kim, P.J. Yoo, Y. Ryu du, T.P. Russell, *ACS Nano*, 8 (2014) 11745-11752.

- [248] S. Greil, A. Rahman, M. Liu, C.T. Black, *Chemistry of Materials*, 29 (2017) 9572-9578.
- [249] C. Zhou, T. Segal-Peretz, M.E. Oruc, H.S. Suh, G. Wu, P.F. Nealey, *Advanced Functional Materials*, 27 (2017) 1701756.
- [250] J. Rzyayev, M.A. Hillmyer, *Macromolecules*, 38 (2005) 3-5.
- [251] J. Rzyayev, M.A. Hillmyer, *Journal of the American Chemical Society*, 127 (2005) 13373-13379.
- [252] H. Mao, P.L. Arrechea, T.S. Bailey, B.J.S. Johnson, M.A. Hillmyer, *Faraday Discussions*, 128 (2005) 149-162.
- [253] H. Mao, M.A. Hillmyer, *Soft Matter*, 2 (2006) 57-59.
- [254] X. An, Y. Hu, N. Wang, T. Wang, Z. Liu, *NPG Asia Materials*, 11 (2019) 13.
- [255] C. Zhang, C. Yin, Y. Wang, J. Zhou, Y. Wang, *Journal of Membrane Science*, 599 (2020) 117833.
- [256] E.A. Jackson, M.A. Hillmyer, *ACS Nano*, 4 (2010) 3548-3553.
- [257] Veolia/IFPRI (International Food Policy Research Institute), [www.ifpri.org/publication/murky-future-global-water-quality-new-global-study-projects-rapid-deterioration-water](http://www.ifpri.org/publication/murky-future-global-water-quality-new-global-study-projects-rapid-deterioration-water) Accessed 2020.
- [258] A. Boretti, Rosa, L. , *npj Clean Water*, 2 (2019).
- [259] Y. Zhu, B. Yang, S. Chen, J. Du, *Progress in Polymer Science*, 64 (2017) 1-22.
- [260] C.T. Huynh, M.K. Nguyen, D.S. Lee, *Macromolecules*, 44 (2011) 6629-6636.
- [261] V. Gubala, L.F. Harris, A.J. Ricco, M.X. Tan, D.E. Williams, *Analytical Chemistry*, 84 (2012) 487-515.
- [262] A.K. Yetisen, H. Qu, A. Manbachi, H. Butt, M.R. Dokmeci, J.P. Hinstroza, M. Skorobogatiy, A. Khademhosseini, S.H. Yun, *ACS Nano*, 10 (2016) 3042-3068.
- [263] H.G. Yoo, M. Byun, C.K. Jeong, K.J. Lee, *Advanced Materials*, 27 (2015) 3982-3998.
- [264] D. Niu, Y. Li, J. Shi, *Chemical Society Reviews*, 46 (2017) 569-585.
- [265] S. Czarnęcki, A. Bertin, *Chemistry – A European Journal*, 24 (2018) 3354-3373.
- [266] X. Hu, Y. Zhang, Z. Xie, X. Jing, A. Bellotti, Z. Gu, *Biomacromolecules*, 18 (2017) 649-673.
- [267] A. Bordat, T. Boissenot, J. Nicolas, N. Tsapis, *Adv Drug Deliv Rev*, 138 (2019) 167-192.
- [268] A. Blanz, R. Verber, O.O. Mykhaylyk, A.J. Ryan, J.Z. Heath, C.W.I. Douglas, S.P. Armes, *Journal of the American Chemical Society*, 134 (2012) 9741-9748.
- [269] K. Nagase, T. Okano, H. Kanazawa, *Nano-Structures & Nano-Objects*, 16 (2018) 9-23.
- [270] R. Liu, M. Fraylich, B.R. Saunders, *Colloid and Polymer Science*, 287 (2009) 627-643.
- [271] S. Lanzalaco, E. Armelin, *Gels*, 3 (2017) 36.
- [272] T. Ta, A.J. Convertine, C.R. Reyes, P.S. Stayton, T.M. Porter, *Biomacromolecules*, 11 (2010) 1915-1920.
- [273] L. Li, B. Yan, J. Yang, L. Chen, H. Zeng, *Advanced Materials*, 27 (2015) 1294-1299.
- [274] C. Zhou, M.A. Hillmyer, T.P. Lodge, *Journal of the American Chemical Society*, 134 (2012) 10365-10368.
- [275] M.K. Gupta, J.R. Martin, T.A. Werfel, T. Shen, J.M. Page, C.L. Duvall, *J Am Chem Soc*, 136 (2014) 14896-14902.
- [276] Y. Yi, G. Lin, S. Chen, J. Liu, H. Zhang, P. Mi, *Materials Science and Engineering: C*, 83 (2018) 218-232.
- [277] K.E. Washington, R.N. Kularatne, V. Karmegam, M.C. Biewer, M.C. Stefan, *WIREs Nanomedicine and Nanobiotechnology*, 9 (2017) e1446.
- [278] T. Urbánek, E. Jäger, A. Jäger, M. Hrubý, *Polymers*, 11 (2019).

- [279] A. Shah, M.S. Malik, G.S. Khan, E. Nosheen, F.J. Iftikhar, F.A. Khan, S.S. Shukla, M.S. Akhter, H.-B. Kraatz, T.M. Aminabhavi, *Chemical Engineering Journal*, 353 (2018) 559-583.
- [280] Z. Song, Z. Han, S. Lv, C. Chen, L. Chen, L. Yin, J. Cheng, *Chemical Society Reviews*, 46 (2017) 6570-6599.
- [281] M.H. Turabee, T. Thambi, H.T.T. Duong, J.H. Jeong, D.S. Lee, *Biomaterials Science*, 6 (2018) 661-671.
- [282] M.A. Quadir, S.W. Morton, L.B. Mensah, K. Shopsowitz, J. Dobbelaar, N. Effenberger, P.T. Hammond, *Nanomedicine: Nanotechnology, Biology and Medicine*, 13 (2017) 1797-1808.
- [283] Y.S. Jung, W. Jung, H.L. Tuller, C.A. Ross, *Nano Letters*, 8 (2008) 3776-3780.
- [284] C.K. Jeong, H.M. Jin, J.-H. Ahn, T.J. Park, H.G. Yoo, M. Koo, Y.-K. Choi, S.O. Kim, K.J. Lee, *Small*, 10 (2013) 337-343.
- [285] R. Sozaraj, B. Dipu, C.F. Colm, L. Tarek, T.S. Matthew, D.H. Justin, A.M. Michael, *Nanotechnology*, 24 (2013) 065503.
- [286] S.J. Fayad, E. Minatti, V. Soldi, S. Fort, P. Labbé, R. Borsali, *Polymer*, 123 (2017) 128-136.
- [287] S. Wei, F. Tian, F. Ge, X. Wang, G. Zhang, H. Lu, J. Yin, Z. Wu, L. Qiu, *ACS Applied Materials & Interfaces*, 10 (2018) 22504-22512.
- [288] D.O. Shin, J.-R. Jeong, T.H. Han, C.M. Koo, H.-J. Park, Y.T. Lim, S.O. Kim, *Journal of Materials Chemistry*, 20 (2010) 7241-7247.
- [289] S. Rasappa, T. Ghoshal, D. Borah, R. Senthamaraiannan, J.D. Holmes, M.A. Morris, *Scientific Reports*, 5 (2015) 13270.
- [290] S.Z. Bas, C. Cummins, D. Borah, M. Ozmen, M.A. Morris, *Analytical Chemistry*, 90 (2018) 1122-1128.
- [291] S. Azlin-Hasim, M.C. Cruz-Romero, T. Ghoshal, M.A. Morris, E. Cummins, J.P. Kerry, *Innovative Food Science & Emerging Technologies*, 27 (2015) 136-143.
- [292] T. Guo, J. Gao, X. Qin, X. Zhang, H. Xue, *Polymers*, 10 (2018) 723.
- [293] S.Z. Bas, C. Cummins, A. Selkirk, D. Borah, M. Ozmen, M.A. Morris, *ACS Applied Nano Materials*, (2019).
- [294] M. Lu, H. Zhu, C.G. Bazuin, W. Peng, J.-F. Masson, *ACS Sensors*, 4 (2019) 613-622.
- [295] J.M. Paloni, X.-H. Dong, B.D. Olsen, *ACS Sensors*, 4 (2019) 2869-2878.
- [296] K.-H. Lo, M.-C. Chen, R.-M. Ho, H.-W. Sung, *ACS Nano*, 3 (2009) 2660-2666.
- [297] H. Uehara, M. Kakiage, M. Sekiya, D. Sakuma, T. Yamonobe, N. Takano, A. Barraud, E. Meurville, P. Ryser, *ACS Nano*, 3 (2009) 924-932.
- [298] S.Y. Yang, J.-A. Yang, E.-S. Kim, G. Jeon, E.J. Oh, K.Y. Choi, S.K. Hahn, J.K. Kim, *ACS Nano*, 4 (2010) 3817-3822.
- [299] X.C. Chen, H.J. Oh, J.F. Yu, J.K. Yang, N. Petzetakis, A.S. Patel, S.W. Hetts, N.P. Balsara, *ACS Macro Letters*, 5 (2016) 936-941.
- [300] N. Anh Tuan, R.S. Sharvari, K.F.Y. Evelyn, *Journal of Physics: Condensed Matter*, 28 (2016) 183001.
- [301] M.J. Dalby, N. Gadegaard, R.O.C. Oreffo, *Nature Materials*, 13 (2014) 558.
- [302] E.K.F. Yim, E.M. Darling, K. Kulangara, F. Guilak, K.W. Leong, *Biomaterials*, 31 (2010) 1299-1306.
- [303] P. Mokarian-Tabari, C. Vallejo-Giraldo, M. Fernandez-Yague, C. Cummins, M.A. Morris, M.J.P. Biggs, *Journal of Materials Science-Materials in Medicine*, 26 (2015).
- [304] T. Xie, J. Chatteraj, P.J. Mulcahey, N.P. Kelleher, E. Del Gado, J.-i. Hahn, *Nanoscale*, 10 (2018) 9063-9076.
- [305] M. Vuoriluoto, H. Orelma, B. Zhu, L.-S. Johansson, O.J. Rojas, *ACS Applied Materials & Interfaces*, 8 (2016) 5668-5678.

- [306] J. Malmström, J. Travas-Sejdic, *Journal of Applied Polymer Science*, 131 (2014).
- [307] O.S. Rabotyagova, P. Cebe, D.L. Kaplan, *Biomacromolecules*, 12 (2011) 269-289.
- [308] B. Bhushan, S.R. Schricker, *Journal of biomedical materials research. Part A*, 102 (2014) 2467-2480.
- [309] J.H. Park, Y. Sun, Y.E. Goldman, R.J. Composto, *Langmuir*, 26 (2010) 10961-10967.
- [310] S. Uluhan, V. Bütün, S. Banerjee, I. Erel-Goktepe, *Langmuir*, 35 (2019) 1156-1171.
- [311] B. Stel, I. Gunkel, X. Gu, T.P. Russell, J.J. De Yoreo, M. Lingenfelder, *ACS Nano*, 13 (2019) 4018-4027.
- [312] H. Wang, C.T. Black, P. Akcora, *Langmuir*, 32 (2016) 151-158.
- [313] X.-B. Wang, T.-C. Lin, H.-Y. Hsueh, S.-C. Lin, X.-D. He, R.-M. Ho, *Langmuir*, 32 (2016) 6419-6428.
- [314] G.-d. Zhu, Y.-r. Ying, X. Li, Y. Liu, C.-y. Yang, Z. Yi, C.-j. Gao, *Journal of Membrane Science*, 566 (2018) 25-34.
- [315] D.-S. Lee, S. Park, Y.D. Han, J.E. Lee, H.Y. Jeong, H.C. Yoon, M.Y. Jung, S.O. Kim, S.-Y. Choi, *Nanoscale*, 9 (2017) 13457-13464.
- [316] I. Firkowska-Boden, X. Zhang, K.D. Jandt, *Advanced healthcare materials*, 7 (2018) 1700995.
- [317] Q. Gao, M. Yu, Y. Su, M. Xie, X. Zhao, P. Li, P.X. Ma, *Acta Biomaterialia*, 51 (2017) 112-124.
- [318] P. Fratzl, R. Weinkamer, *Progress in Materials Science*, 52 (2007) 1263-1334.
- [319] P. Tseng, B. Napier, S. Zhao, A.N. Mitropoulos, M.B. Applegate, B. Marelli, D.L. Kaplan, F.G. Omenetto, *Nature Nanotechnology*, 12 (2017) 474-480.
- [320] J.-F. Lutz, M. Ouchi, D.R. Liu, M. Sawamoto, *Science*, 341 (2013) 1238149.
- [321] J.-F. Lutz, *Macromolecules*, 48 (2015) 4759-4767.
- [322] R. Arai, *Biophysical reviews*, 10 (2018) 391-410.
- [323] S. Shanmugam, J. Xu, C. Boyer, *ACS Central Science*, 3 (2017) 95-96.
- [324] X. Lu, J. Li, D. Zhu, M. Xu, W. Li, Q. Lu, *Angewandte Chemie International Edition*, 57 (2018) 15148-15152.
- [325] S.-J. Jeong, J.Y. Kim, B.H. Kim, H.-S. Moon, S.O. Kim, *Materials Today*, 16 (2013) 468-476.
- [326] G.S. Doerk, K.G. Yager, *Molecular Systems Design & Engineering*, 2 (2017) 518-538.
- [327] N. Demazy, C. Cummins, K. Aissou, G. Fleury, *Advanced Materials Interfaces*, n/a (2019) 1901747.
- [328] V. Abetz, R. Stadler, *Macromolecular Symposia*, 113 (1997) 19-26.
- [329] K. Aissou, W. Kwon, M. Mumtaz, S. Antoine, M. Maret, G. Portale, G. Fleury, G. Hadziioannou, *ACS Nano*, 10 (2016) 4055-4061.
- [330] P.W. Majewski, A. Rahman, C.T. Black, K.G. Yager, *Nat Commun*, 6 (2015).
- [331] A. Rahman, P.W. Majewski, G. Doerk, C.T. Black, K.G. Yager, 7 (2016) 13988.
- [332] A. Tavakkoli K. G, S.M. Nicaise, K.R. Gadelrab, A. Alexander-Katz, C.A. Ross, K.K. Berggren, *Nature Communications*, 7 (2016) 10518.
- [333] A. Tavakkoli K. G, K.W. Gotrik, A.F. Hannon, A. Alexander-Katz, C.A. Ross, K.K. Berggren, *Science*, 336 (2012) 1294.
- [334] T.C. Chung, W. Janvikul, R. Bernard, R. Hu, C.L. Li, S.L. Liu, G.J. Jiang, *Polymer*, 36 (1995) 3565-3574.
- [335] J.J.C. Shivers, United States Patent Office 3,023,192, Patented Feb. 27, 1962.





**Energy**

The top-left quadrant is orange and features four stylized sun icons with yellow centers and green rays. The word "Energy" is written in a large, red, serif font.



**Photonics**

The top-right quadrant is grey. A large red arrow points downwards from the top edge. Below the text "Photonics" is a black wavy line representing a light wave. A purple arrow points to the right from the right edge of this quadrant.

**Block  
copolymers**

A light pink rounded rectangular box containing the text "Block copolymers" in a bold, black, sans-serif font, positioned centrally between the four quadrants.



**Environmental**

The bottom-left quadrant is yellow and features six blue water droplets. Two of the droplets at the bottom have concentric circles around them, representing ripples in water.



**Biological**

The bottom-right quadrant is blue and features a yellow DNA double helix with red and green base pairs. The word "Biological" is written in a large, white, serif font.